THE MOLECULAR CONSEQUENCES OF VITAMIN B_{12} DEPRIVATION IN THE POLAR DIATOM, *FRAGILARIOPSIS CYLINDRUS*

by

Catalina Maria Albury

Submitted in partial fulfilment of the requirements
for the degree of Masters of Science

at

Dalhousie University
Halifax, Nova Scotia
March 2022

Dalhousie University is located in Mi'kma'ki, the ancestral and unceded territory of the Mi'kmaq. We are all Treaty people.

Dedication

For my ancestors. For my ancestors' ancestors.

For the Galicians who unfurled their sails on the mountainous Iberian coast.

For the West African diaspora who were trafficked shoulder to shoulder across the Atlantic with rice sewn into their braids.

For the Colombian inhabitants of the walled city overlooking the Caribbean Sea.

For the Bahamian people that made a livelihood on the archipelago's jagged islands, weathering hurricanes and plucking pink conch shells from the seafloor like jewels.

The ocean is intertwined with our lives, losses, triumphs, and travels. The same water that flows through them flows through me, just as it flows through the smallest living beings that sustain our world.

Por mis ancestros. Por los ancestros de mis ancestros.

Pos los Gallegos quien desplegaron sus velas en la costa montañosa de Iberia.

Por la diáspora Africana occidental quien fueron traficados hombro a hombre por el océano Atlántico con arroz sembrado en sus trenzas.

Por los Costeños de la cuidad amurallada con vista al Mar Caribe.

Por la gente Bahameña quien hizo un sustento en las islas dentadas del archipiélago, aguantando huracanes y desprendiendo conchas rosadas del fondo marino como joyas.

El océano es entrelazado con nuestras vidas, perdidas, triunfos, y viajes. La misma agua que fluye a través de ellos fluye por me, al igual que fluye por los seres vivos mas pequeños que sostienen nuestro mundo.

Table of Contents

List of Tables

List of Figures

Abstract

Fragilariopsis cylindrus is an ecologically significant diatom inhabiting sea ice and water column assemblages in the Southern Ocean (SO). Microbial growth in SO microbial communities has been demonstrated to be periodically limited or co-limited by vitamin B_{12}. In this dissertation, I examine the molecular consequences of B_{12} deprivation in *F. cylindrus*, with a focus on alterations to protein expression and metabolite production. Despite unchanged growth rates, B_{12}-deprived *F. cylindrus* cells display responses that can impact the production of growth stimulating compounds, including induction of a putative B_{12} remodeling pathway and differential production of DMSP and thiamine related compounds. My findings highlight that assessments of marine phytoplankton's responses to stressors beyond growth rate should be considered in order to generate accurate predictions of community interactions in micronutrient deprived environments. These results have implications for our understanding the relationship between B_{12} availability and community composition and nutrient cycling in a changing ocean.

List of Abbreviations

Ado-B_{12}: Adenosylcobalamin

AHCase: Adenosylhomocysteinase

APS: Ammonium persulfate

ATP: Adenosine 5'-triphosphate

B_1: Vitamin B_1; Thiamin

B_{12}: Vitamin B_{12}; Cobalamin

B_2: Vitamin B_2; Riboflavin

B_7: Vitamin B_7; Biotin

BLAST: Basic Local Alignment Search Tool

BMIS: Best Matched Internal Standard

CBA1: Cobalamin Acquisition Protein 1

CN-B_{12}: Cyanocobalamin

Chl-D: Mg-chelatase subunit D

CobN: Aerobic cobaltochelatase subunit N

CobS: Aerobic cobaltochelatase subunit S

CobT: Aerobic cobaltochelatase subunit T

CobW: Cobalamin biosynthesis protein W

cRAP: common Repository of Adventitious Proteins

cSHMT: cytosolic Serine Hydroxymethyltransferase

DAPI: 4′,6-diamidino-2-phenylindole

DE: Differentially Expressed

DMB: 5, 6-di-methylbenzimidazole

DMS: Dimethyl sulfide

DMSP: Dimethylsulfoniopropionate

DTT: 1,4-Dithiothreitol

FDR: False Discovery Rate

IRS: Internal Reference Scaling

IRMS: Isotope Ratio Mass Spectrometer

JGI: Joint Genome Institute

KEGG: Kyoto Encyclopedia of Genes and Genomes

LC-MS: Liquid Chromatography Mass Spectrometry

MCM: Methyl CoA Mutase

Me-B_{12}: Methylcobalamin

METase: monohydroxyethyl terephthalate hydrolase

MetE: B_{12}-independent methionine synthase

MetH: B_{12}-dependant methionine synthase

MetK: S-adenosylmethionine synthase

MS: Mass spectrometer

MTHFR: Methylenetetrahydrofolate reductase

MMT: methylthiohydroxybutryate methyltransferase

NCBI: National Center for Biotechnology Information

OH-B_{12}: Hydroxycobalamin

PCA: Principal Component Analysis

PBGS: Porphobilinogen Synthase

ChlD: protoporphyrin IX Mg-chelatase

PAM: Pulse-amplitude-modulated

QC: Quality Control

RFU: Relative Fluorescence Units

RNR: Ribonucleotide Reductase

SAH: S-Adenosyl Homocysteine

SAM: S-Adenosyl Methionine

SO: Southern Ocean

TEMED: Tetramethylethylenediamine

THF: Tetrahydrofolate

5,10-MTHF: 5,10-methylene tetrahydrofolate

ThiC: Thiamine biosynthesis protein C

TMT: Tandem Mass Tagging

UROD: uroporphyrinogen III decarboxylase

Acknowledgments

I am grateful to have been a guest on Mi'kmaw land whilst completing the research included in this dissertation. I would like to thank my family, especially my *abuela* for sparking my curiosity for the natural world, my mother for insisting that I not take "no" for an answer, my father for modeling selfless devotion and empathy as tenets for a fulfilling life, and my sister for lending me her strength and leadership in times of need. I am grateful to my partner, Tor, and my closest friends, Zanib, Aaron, and Araminta, for keeping me grounded throughout the course of completing this degree. I also have the extraordinary members of the Bertrand lab to thank for the input, support, and joy that they have provided during my 4 years as a lab member, from my time as an undergraduate student to today. This includes (in no particular order) Loay Jabre, Scott McCain, Cat Bannon, Gianpaolo Cardellini, Megan Roberts, Lena Beckley, and many others. I'd like to extend my dearest thanks to Dr. Elden Rowland for providing his technical expertise on all things mass spectrometry. Elden is ever available to share a laugh or song, which were needed throughout this experience at times. Lastly, this dissertation would have never been completed without the lasting dedication, innovation, and insight of my supervisor, Dr. Erin Bertrand. Having the privilege to work with her has shaped my worldview immensely. I have her to thank for skilfully shaping my research, especially as she undertook the joys of becoming a new mother whilst guiding me through the final stretch of this journey.

Chapter I: Introduction

1.1 Trace Nutrient Limitation in the Ocean – Marine phytoplankton are key players in the Earth's carbon cycle. An estimated 46% of global net primary productivity originates from the ocean, most of which is conducted by phytoplankton (Field *et al.,* 1998). In addition to forming the base of marine food webs, phytoplankton are responsible for export of carbon to the deep ocean, acting as a global sink for anthropogenic carbon dioxide inputs (Michaels & Silvers 1988). Abiotic factors such as light and nutrient availability are known to drive phytoplankton growth in the ocean (Pilson 2012). Nutrients required in trace concentrations for microbial growth, also known as micronutrients, include metals and vitamins. These often utilized in the active sites of critical enzymes. For example, the trace metal iron is required in enzymes that are crucial to the electron transport chain, which creates the required redox potential required for the generation of ATP, the main currency of energy for the cell. Iron availability is also critical for the function of many of the components of the photosynthetic apparatus (Ferreira and Straus 1994). Like iron, manganese is needed for photosynthetic processes as a core component of the oxygen-evolving complex of photosystem II (Yachandra *et al.,* 1996). Additional trace metals that are important for phytoplankton growth include zinc, copper, and cobalt (Sunda & Hunstman 1998). Another important class of micronutrients are vitamins. The vitamins are a heterogenous group of compounds characterized by being required in small amounts for life and metabolic integrity in animals (Bender 2003). The three main vitamins understood to be required by eukaryotic microalgae for growth are thiamin (vitamin B_1), cobalamin (vitamin B_{12}), and biotin (vitamin B_7) (Provasoli & Carlucci 1974).

Despite their small requirements in the cell compared to macronutrients in the ocean, trace metals and vitamins can disproportionally affect the growth and structure of microbial communities. Liebig's law of the minimum dictates that the nutrient that is in shortest supply relative to the cell's need is that which will limit an organisms' growth, and more widely, system productivity (de Baar 1994). This was expanded on by John Martin in the 1990's, who noticed that there were vast regions of the ocean where macronutrients were abundant and yet not yielding the expected amount of life. He described these areas of ocean as HNLC's (high nutrient; low chlorophyll areas), as at the time, chlorophyll was the chosen method for estimating phytoplankton biomass. Martin postulated the reason for this phenomenon and went on to discover that adding iron to seawater led to increased growth (Martin 1990; Martin *et al.,* 1994). Martin later declared that if he was provided with "half a tanker of iron", he could catalyze "an ice age" (Pilson 2012). Although the concept of utilizing iron additions to facilitate drawdown of carbon dioxide via increased growth is now understood to be far more nuanced, Martin's bravado emphasizes the sheer magnitude of consequences of trace nutrient availability on global biogeochemical processes. More recent works have examined the nature of micronutrient limitation on microbial communities with revised approaches, broader scopes, and improved technology. We now understand that differential availability of micronutrients has the possibility to fuel or inhibit the growth of various members of microbial communities, leading to alterations in community composition and structure (Provasoli 1963; Sañudo-Wilhelmy *et al.,* 2014). In particular, mounting evidence places vitamin B_{12} among important drivers of microbial ecology and biogeochemistry in the ocean, making its utilization and dynamics in significant species worthy of further examination. An estimated

half of all phytoplankton species have absolute vitamin B_{12} requirements (Croft *et al.,* 2005) and bottle incubation experiments have demonstrated that the addition of B_{12} to natural communities results in increased growth (Bertrand *et al.,* 2007). The link between B_{12} availability and community-level effects on oceanic microbes has been explored by several studies, which have demonstrated that B_{12} availability can alter community composition, net productivity, and growth in a variety of marine environments (Sañudo-Wilhelmy *et al.,* 2006; Gobler *et al.,* 2017; Koch *et al.,* 2011; Browning *et al.,* 2017).

1.2. Vitamin B_{12}: The History, Sources, and Sinks of an Enigmatic Metalloenzyme – Vitamin B_{12} was initially discovered as an anemia-causing factor by two doctors, Minot and Murphy, in 1926. Later work demonstrated that vitamin B_{12} deprivation reduces methionine synthase activity in humans, leading to disruptions in nucleic acid biosynthesis (Shane & Stokstad 1985). As researchers worked towards maintaining alga in culture on synthetic media, the importance of vitamin B_{12} to growth and physiology emerged. Remarkably, Hutner, noticed that he could use liver concentrates normally used to treat patients suffering from pernicious anemia to maintain cultures of *Euglena*. In 1949, Hutner discovered that these extracts, in fact, contained vitamin B_{12}, which was facilitating the growth of the cultures (Hutner *et al.,* 1949). Later, as vitamin B_{12} was increasingly studied in oceanographic circles as a micronutrient required for phytoplankton growth, investigations into B_{12} requirements and utilization in microalgae became more common. Droop studied how the uptake of vitamin B_{12} availability affected growth in the haptophyte *Monochrysis lutheri* (now recognized as *Pavlova lutheri)*. The results of his seminal work with vitamin B_{12} demonstrated that growth rate depended on intercellular

quota of the vitamin, rather than its concentration in the media (Droop 1968), which was contradictory to the prevailing perspective at the time. Droop's research established that intracellular vitamin B_{12} quotas correlate with growth rate, highlighting the coenzyme's importance as a potential controlling factor to primary productivity in microalgae. Vitamin B_{12}'s scarce concentrations in the ocean (picomolar to subpicomolar; Heal *et al.,* 2014) support the notion that B_{12} may limit growth. Additionally, the cofactor is only produced biogenically by certain bacterial and archaeal groups (Raux *et al.,* 2000). Yet, many eukaryotic microbes possess the genes for B_{12} biosynthesis despite not being able to produce the complete molecule *de novo* (Vancaester *et al.,* 2020).

Vitamin B_{12} is a remarkable molecule in that its biosynthesis is recognized as one of the most complex pathways known to humankind, utilizing a total of 30 enzyme-mediated steps. This process is reviewed in detail in Raux *et al.,* 2000. The biosynthetic pathway begins with a shared precursor, the tetrapyrrole ring, that also goes on to produce heme and chlorophyll-a. In the centre of the ring for each of these molecules is a metal ion: iron, magnesium, and cobalt, in heme, chlorophyll-a, and cobalamin respectively. In addition to the production of the ring, the lower ligand of the molecule must also be synthesized. In cobalamins, the lower ligand of the molecule is either DMB (5, 6-di-methylbenzimidazole) or adenine. Cobalamins with DMB as the lower ligand are readily utilized by B_{12}-dependent microalgal consumers, but evidence shows that cobalamins with adenine (pseudocobalamins) are orders of magnitude less bioavailable for their use (Helliwell *et al.,* 2016). Helliwell and colleagues have discovered that if DMB is provided to certain species along with pseudocobalamin, they are able to remodel the pseudocobalamin into cobalamin (Helliwell *et al.,* 2016). The upper ligand also has a few possible modifications.

Cobalamins with Ado-, CN-, OH-, and Me- groups as the upper ligand produce adenosyl-, cyano-, hydroxo- and methylcobalamin respectively. Cyanocobalamin is a product of the commercial synthesis of cobalamin (Obeid *et al.,* 2015). Adenosyl- and methyl-cobalamin are the biologically active forms of cobalamin but are rapidly highly photolabile and degrade to hydroxocobalamin upon exposure to light.

1.3 Vitamin B_{12} Utilization in Eukaryotic Microalgae – Vitamin B_{12} is required for growth by some photosynthetic eukaryotes for use as a cofactor in essential enzymes. The biologically active forms of cobalamin, adenosyl- and methylcobalamin, are utilized by eukaryotes as cofactors in MCM (methylmalonyl-CoA mutase) and the methionine synthase MetH, respectively. An alternate B_{12}-independent methionine synthase enzyme, MetE, can also be used to synthesize methionine in some organisms (Banjaree & Matthews 1990). Out of the recognized B_{12}-requiring enzymes in eukaryotes, MetH has been hypothesized to be the primary sink for B_{12} use, as MetE's presence is correlated with a lack of an absolute B_{12} requirement for growth (Helliwell *et al.,* 2011). The requirement of B_{12} for growth, also known as B_{12} auxotrophy, has arisen many times throughout the evolutionary history of photosynthetic microbes via the loss of genes encoding the MetE enzyme (Helliwell *et al.,* 2011). Notably, phytoplankton and land plants play the same trophic role as primary producers in their respective environments, yet land plants solely utilize MetE to produce methionine, and do not require exogenous B_{12}. It has thereby been hypothesized that eukaryotic algae are faced with a high selective pressure to maintain the B_{12}-dependent methionine synthase pathway (Bertrand *et al.,* 2013; Bertrand & Allen 2012; Helliwell *et al.,* 2011; Ellis *et al.,* 2017). Our understanding of the dynamics between

these two enzymes and the broader consequences of B_{12} limitation in biogeochemically significant regions of the ocean remains limited.

1.4 Vitamin B_{12} in a Southern Ocean Context – The Southern Ocean (SO) is a biogeochemically significant region responsible for distributing nutrients to the global ocean (Sarmiento *et al.,* 2004). The SO hosts some of the largest seasonal phytoplankton blooms in the world (Sallée J-B *et al.,* 2015). Evidence suggests that B_{12} utilization and cycling have far-reaching consequences for SO microbial assemblages as vitamin B_{12} can limit or co-limit phytoplankton growth there (Bertrand *et al.,* 2007). Ellis *et al.,* 2017 found that, compared to diatoms in other waters, a much higher proportion of Antarctic diatoms are able to produce MetE, allowing them to utilize both the B_{12} dependent and independent pathways for methionine synthesis. One such diatom, *Fragilariopsis cylindrus,* is a major component of sea ice and water column assemblages in the SO (Kang & Fryxell 1992; Mock & Hoch 2005). This psychrophile has been described as an emerging model diatom species (Falciatore *et al.,* 2020) and possesses the gene for production of MetE (Helliwell *et al.,* 2011). MetE transcripts in *F. cylindrus* have been demonstrated to decrease in the presence of B_{12}, but it exhibits no difference in growth rate due to vitamin starvation (Ellis *et al.,* 2017). We chose to study the effects of vitamin B_{12} deprivation in SO diatoms using *F. cylindrus* for these experiments due to its ecological significance and sequenced genome (Mock *et al.,* 2017).

1.5 Thesis Overview – This dissertation aims to characterize the molecular consequences of vitamin B_{12} deprivation in an ecologically significant polar diatom. We tackle this question by investigating the proteome and metabolite production of axenic *F. cylindrus* cultures grown in the absence of vitamin B_{12}. This dissertation aims to (1) explore the

interaction between protein expression, vitamin B_{12}, and elevated temperature and (2) characterize changes in production of potentially B_{12}-dependent metabolites and physiology in response to B_{12} deprivation in *F. cylindrus.*

In Chapter II, the interactive effects of B_{12} deprivation and heat stress on the proteome of *F. cylindrus* were examined. *F. cylindrus* was cultured with and without the addition of exogenous B_{12}, and then exposed to an elevated temperature treatment. We measured the expression of the methionine synthases MetH and MetE and conducted a proteomic discovery experiment to identify proteins that were differentially expressed in response to the individual and combined stressors. I designed and performed the culturing experiments with guidance from Dr. Erin Bertrand. I also performed cell count and photophysiological measurements and completed sample preparation for all protein measurements. Targeted and discovery protein samples were run on mass spectrometers in both the Bertrand lab and Dalhousie's MS core facility by Dr. Elden Rowland based on methods developed with Dr. Bertrand. The database search for our discovery proteomics experiment was also conducted by Dr. Rowland. The remaining data analysis was performed by me, including normalization procedures and differential expression analyses. Dr. Bertrand provided guidance and feedback on the ideas presented in the chapter.

Chapter III investigates the effects of vitamin B_{12} deprivation on diatom physiology and metabolite production, in addition to presenting the first direct measurements of cellular B_{12} quotas in *F. cylindrus.* We grew *F. cylindrus* cultures at an optimal growth temperature of 6 °C, with and without the addition of exogenous B_{12} and, using targeted metabolite quantification approaches, we monitored the abundance of cobalamin, in addition to a suite of metabolites previously shown to be affected by B_{12} deprivation in other organisms. For

this chapter, I also designed and performed the culturing experiments with guidance from Dr. Erin Bertrand. I performed cell count, particulate carbon and nitrogen, and cell size measurements, in addition to preparing protein samples for quantitative measurements of MetE and MetH. Dr. Elden Rowland and I extracted the samples for metabolite measurements together. Dr. Rowland performed the mass spectrometry and I performed the analysis of the protein and metabolite data, including selecting best matched internal standards using methods with advice from Cat Bannon. Dr. Bertrand also provided guidance and feedback on the ideas presented in this chapter.

Chapter II: Complex Proteomic Rearrangements in Response to Vitamin B_{12} Deprivation and Heat Stress in the Polar Diatom, *Fragilariopsis cylindrus*

2.1 Abstract

Vitamin B_{12} is a cobalt-containing micronutrient that periodically limits phytoplankton growth in the Southern Ocean (SO). B_{12} deprivation has been demonstrated to lead to metabolic consequences in diatoms, including methionine starvation and changes to osmolyte production. In this study, we examine the interactive effects of B_{12} deprivation and heat stress on the proteome of the ecologically significant SO diatom, *Fragilariopsis cylindrus*. *F. cylindrus* was grown in B_{12}-replete and B_{12}-deplete conditions and exposed to supra-optimal (12 °C) and control (4 °C) temperatures. Targeted and global proteomic analyses were then used to identify the combined molecular consequences of the two stressors. We found that growth was unaffected by B_{12} availability at supra-optimal temperatures, despite complex proteomic rearrangements in response to the combined stressors. Amongst these rearrangements, we identify proteins that may be used to remodel fragments of B_{12}. We also demonstrate that canonical B_{12} deprivation and elevated temperature responses persist at the intersection of the two stressors, suggesting that proteomic biomarkers used to survey B_{12} limitation in diatoms *in-situ* are reliable, even at lethal temperatures. The data provided in this study suggests that the physiological impacts of vitamin B_{12} in a non-auxotrophic diatom are multifaceted and complex, despite the absence of changes to growth rate. Additionally, *F. cylindrus* may increase the biologically labile B_{12} pool by remodelling fragments of B_{12}, improving their ability to thrive in the Southern Ocean's generally low B_{12} environment. The differential expression of proteins used to respond to B_{12} deprivation highlights the strong selective pressure that vitamin B_{12} imposes on Southern Ocean diatoms.

2.2 Introduction

Fragiliariopsis cylindrus is an ecologically significant pennate diatom which inhabits the Southern Ocean (SO). This region shapes the Earth's climate and biogeochemistry, supporting global primary productivity via the upwelling and circulation of nutrient-rich deep water to ocean basins (Sarmiento *et al.,* 2004). The ecological and biogeochemical landscape of this ocean hub is driven by large-scale seasonal phytoplankton blooms (Sallée J-B *et al.,* 2015). Controls on the composition and spatio-temporal extent and of these blooms are multifaceted, including both oceanographic conditions and biotic factors (Boyd 2002). The roles of B-vitamins have been increasingly explored as important regulators of blooms globally (Panzeca *et al.,* 2008; Sañudo-Wilhelmy *et al.,* 2006; Gobler *et al.,* 2017; Koch *et al.,* 2011; Bertrand *et al.,* 2007; Browning *et al.,* 2017). In the SO, bottle incubation experiments have found vitamin B_{12} to be limiting or colimiting to phytoplankton growth (Bertrand *et al.,* 2007; Taylor *et al.,* 2008; Bertrand *et al.,* 2015), suggesting that it plays a significant role as a regulator of primary productivity in the region. However, the individual molecular responses to B_{12} deprivation and other relevant environmental variables in important SO species have not been explored in detail.

Vitamin B_{12} (also known as cobalamin) is a cobalt-containing micronutrient found in the ocean in picomolar concentrations (Heal *et al.,* 2014; Suffridge *et al.,* 2017). It is only synthesized by select prokaryotes (Raux *et al.,* 2000) and tends to photodegrade upon exposure to UV light (Carlucci *et al.,* 1969). The cofactor is rapidly consumed by phytoplankton and bacteria in the surface ocean (Heal *et al.,* 2014). Vitamin B_{12} and its related cobamides are primarily required by photosynthetic eukaryotes for participation in methylation reactions and radical rearrangements (Bertrand & Allen 2012). In methylation reactions, methylcobalamin is used to catalyze the conversion of homocysteine and methyl-

tetrahydrofolate into methionine, an essential amino acid and cellular source of methylation capacity, via the methionine synthase MetH. Additionally, some eukaryotes can also utilize an alternative methionine synthase, MetE, which is B_{12}-independent (Banerjee and Matthews 1990). The absence of genes encoding the MetE enzyme in algal genomes has been linked to B_{12} auxotrophy, meaning that most organisms without the enzyme require the vitamin for survival (Helliwell *et al.,* 2011). MetE has a slower turnover rate than MetH, making it a more energetically costly and resource intensive method of methionine production (Banerjee and Matthews 1990; Bertrand *et al.,* 2013), which may be why MetE expression has been demonstrated to significantly decline in the presence of B_{12} in organisms that possess both enzymes (Croft *et al.,* 2005; Bertrand *et al.,* 2012). One such organism, *Fragilariopsis cylindrus,* is a major component of sea ice and pelagic seasonal ice zone assemblages at both poles (Kang & Fryxell 1992; Mock & Hoch 2005). Along with many other SO diatoms, *F. cylindrus* possesses genes to produce both methionine synthase enzymes (Ellis *et al.,* 2017). The B_{12} deprivation responses of *F. cylindrus* have been explored via transcriptomic observation of methionine synthases, demonstrating that MetE transcripts are enriched in the absence of B_{12} (Ellis *et al.,* 2017). Furthermore, genes for a cobalamin acquisition protein, CBA1, have also been identified in *F. cylindrus* (Bertrand *et al.,* 2012), but otherwise its responses to B_{12} deprivation have gone largely unexplored, and no direct measurements of these B_{12} deprivation proteins have been conducted to date in *F. cylindrus*.

Mass spectrometry-based proteomic approaches, applied to phytoplankton cultures, allow us to observe which proteins are enriched or depleted in response to a treatment, providing information about the production of enzymes and other proteins that mitigate the effects of

environmental stressors or respond to nutrient limitation. Experiments like these have been common for some time now, but they rarely examine the interactive effects of environmentally relevant factors. Multiple stressors can lead to unexpected responses, impacting an organism differently than the sum of their individual effects (Folt *et al.,* 1999). Whilst culture studies represent merely a simplification of an organisms' possible function in its environment, designing experiments that account for combined stressors provides the opportunity for a more complete understanding of organisms' responses to their dynamic environment.

In previous work examining interactions between B_{12} availability and heat stress, Xie *et al.,* 2013 found that the green alga, *Chlamydomonas reinhardtii*, was particularly sensitive to combined B_{12} deprivation and increased temperature. *C. reinhardtii* was rescued from heat stress at lethal temperatures in the presence of B_{12}-producing bacteria, or upon the addition of both exogenous B_{12} and methionine. This observation suggested that B_{12} use may confer heat stress tolerance in *C. reinhardtii* because of MetH's possible enhanced resistance to high temperatures when compared to MetE (Xie *et al.,* 2013). The prevalence of B_{12}-mediated heat resistance in this green alga also implies that a reduction in methionine synthesis activity has negative consequences in the face of heat stress, suggesting that this reaction may serve as a metabolic bottleneck. Is it possible that methionine synthesis also acts as a bottleneck to growth at normally lethal temperatures in *F. cylindrus*?

To tackle this question, we examined the effects of elevated temperature on *F. cylindrus* and how their mechanisms may affect the methionine synthase pathway. An in-depth analysis of *F. cylindrus'* proteomic responses to elevated temperature has not been

completed, but the transcriptomic effects of heat stress have been explored in Mock *et al.,* 2017. Interestingly, Mock and colleagues found that the temperature response to 11 °C (described as an "elevated temperature treatment") was much more subtle relative to the effects of darkness on the transcriptome. The molecular effects of supra-optimal temperatures in cold adapted organisms, also known as psychrophiles, are currently considered to reflect their cold-adapted states. There are two significant challenges to overcome for organisms to thrive in cold environments: decreased membrane fluidity and reduced reaction speeds (Feller 2013). Therefore, psychrophiles tend to upregulate proteins related to the synthesis of membrane components and osmolytes at cold temperatures (Collins & Margesin 2019). Psychrophiles are also known to modify their enzymes to increase specificity and binding or increase the quota of important proteins, such as those involved in photosynthesis and protein synthesis, in order to manage temperature-mediated decreases in reaction rates (Feller 2013). Increases in temperature past the temperature optima (T_{opt}) of an organism can lead to the reversal of these acclimations (Liang *et al.,* 2019). Given our lack of understanding related to how molecular responses to B_{12} deprivation vary with important environmental variables such as temperature in psychrophiles, we designed an experiment to explore the interactive effects of B_{12} deprivation and elevated temperature in *F. cylindrus*.

We conducted multifactorial culturing of *F. cylindrus*, depriving these cultures of B_{12} and applying an elevated temperature treatment of 12 °C, the lowest temperature that proved to be lethal. These conditions were comparable to Xie *et al.,* 2013's study design, chosen to allow us to investigate whether this psychrophile displays the same B_{12}-mediated heat stress response. It is important to note that we do not expect mean sea surface temperatures

in the SO to reach 12 °C in coming centuries. However, micro-environments like meltwater pools have been shown to create extreme temperature environments, leading to significant impacts for Antarctic microbes like *F. cylindrus* (Sackett *et al.* 2013). As such, these conditions can be considered extreme, but with environmental relevance. Twenty-four hours after exposure, we measured methionine synthase concentrations and conducted a global proteomic analysis. We hypothesized that the combined molecular effects of B_{12} deprivation and heat stress in *F. cylindrus* would be synergistic rather than additive, leading to differences in protein expression in cultures exposed to both stressors not seen in cells treated with each stressor individually. Upon completion of the experiment, we found that the expression of the B_{12}-independent methionine synthase pathways in *F. cylindrus* persisted at lethal temperatures, unlike that of *C. reinhardtii*, where a decline in *metE* transcripts was observed (Xie *et al.,* 2013). Furthermore, complex proteomic rearrangements occurred in response to the interactive effects of lethal temperatures and B_{12} deprivation, contrasting the responses to each stressor individually. It is critical to build a baseline understanding of how temperature can interactively affect the molecular consequences of important environmental variables such as vitamin B_{12} availability. Although no change in growth was observed in response to B_{12} availability, changes in protein expression demonstrated that *F. cylindrus* adopts varying strategies to deal with the combined stressors.

2.3 Materials and Methods

2.3.1 Semicontinous Culturing - Axenic cultures of *Fragilariopsis cylindrus* (strain CCMP1102) were obtained from the Provasoli-Guillard National Center for Marine Algae and Microbiota. The cells were inoculated into 250 mL vent-capped culture flasks and

maintained with sterile techniques at 4 °C, with a saturating irradiance of approximately 100 μE m^{-2} s^{-1} in a 12:12 hour light-dark cycle. 4 °C was chosen as a relevant control temperature for the pelagic Southern Ocean environment (Sackett *et al.*, 2013). Autoclaved SOW media (Sunda *et al.,* 2005; Price *et al.,* 1988/89) was used to prepare enriched f/2 medium (Guillard & Ryther 1962, Guillard 1975) to support the growth of the cultures. The linear relationship between fluorescence under our growth conditions and cell count was established with a Turner hand-held fluorometer and flow cytometer, respectively (Supporting Information Figure S2.1b,c). This preliminary culture was grown through exponential phase to determine which cell densities corresponded to early exponential growth (Supporting Information Figure S2.1a). Then, three biological replicates, both with and without the addition of 369 pM of vitamin B_{12} in the form of cyanocobalamin, were maintained at 4 °C and transferred every 48 hours to keep them within the range of RFU (Relative Fluorescence Units) corresponding with late exponential growth (between 60 and 120 RFU). This was done for approximately 3 months, as similar amounts of time have been utilized to acclimatize *F. cylindrus* to experimental conditions in previous experiments (Mock & Hock 2005, Petrou *et al.,* 2012). During the experiment, cell counts were obtained with a BD Accuri C6 Flow Cytometer. The cultures were regularly monitored for bacterial contamination with microscopy and 4′,6-diamidino-2-phenylindole (DAPI) stain.

After the acclimation period, each replicate was split in two and exposed to two temperature treatments at 0 hours (Figure 2.1). The control cultures were maintained at 4 °C, and the other half were exposed to the elevated temperature treatment of 12 °C. Subsequently, the cultures were sampled every 24 hours for a total of 72 hours. At each

time point, each culture's cell count was taken via flow cytometry and a measure of photosynthetic capacity, F_v/F_m, was measured with a PAM (Pulse Amplitude Modulated) fluorometer (DUAL-PAM-100; Heinz Walz GmbH) after a 20-minute dark acclimation period on ice. A secondary trial with a 10 °C elevated temperature treatment was also conducted to confirm that 12 °C is the lowest lethal temperature for *F. cylindrus* cells (Supporting Information Figure S2.2b). Targeted and global proteomic measurements (described below) were made on biomass from cultures vacuum filtered onto 2.0 μm isopore membrane filters (Millipore) after 24 hours of exposure to their respective temperature treatments and stored at -80 °C.

2.3.2 Sample Preparation for Proteomic Analyses – Protein was extracted from filters in 0.75 mL of protein extraction buffer (0.1 M Tris/HCl, pH: 7.5, 5mM EDTA, 2% SDS) for 10 minutes at room temperature and then heated on a thermomixer for 15 minutes at 95 ° C and 350 RPM. Then, the filters were sonicated on ice for 1 minute at 50% amplitude (120 W, QSonica microprobe). They were then incubated at room temperature for 30 minutes, with vortexing every 10-15 minutes. The samples were centrifuged at 15,000XG for 30 minutes at 20 °C. The supernatant and debris-containing cell pellet were then separated. A Micro BCA Protein Assay Kit (Thermo Scientific) was used to determine protein concentration in the supernatant.

30 μg of protein was then digested with trypsin with an in-gel procedure modified from Kachuk *et al.,* 2015. The protein solution was polymerized by making up the sample with 10 mM Tris to 100 μL. Then, 100 μL of 1 M Tris Buffer, 40% Acryl-Bis, TEMED was added to each sample, followed by 7 μL 1% APS. The samples were then incubated for 1

hour at 20 °C. 200 µL of gel fixing solution (10% acetic acid and 50% methanol in LC-MS water) was added and the samples were incubated at 20 °C for 30 minutes. Then, 1.6 mL gel fixing solution was added, followed by another 20 °C incubation overnight. The supernatant was discarded and 1 mL of milliQ water was added, and the samples were incubated once again at 20 °C and 350 RPM for 20 minutes. The resulting supernatant was then discarded, and each gel was cut into 8-12 pieces with a sterile blade in a glass petri dish. The gel slices were reduced, alkylated, and washed (Supporting Information, Table S2.1). The gels were rehydrated in trypsin (1:20 µg trypsin:µg protein) and suspended in 25 mM ammonium bicarbonate for 2 hours on ice. Then, they were incubated at 37 °C for 20 minutes and covered in 25 mM ammonium bicarbonate and incubated for 16 hours at 37 °C. Following digestion, samples were resuspended and acidified with 3.5µl formic acid on ice and desalted using 50 mg Strata C18-E (55 µm, 70 Å) SPE columns (Phenomonex) to remove any primary amines and then brought to dryness in a vacuum centrifuge (Eppendorf).

2.3.3 Targeted Proteomic Analysis – A Dionex Ult 3000 UPLC integrated to a TSQ Quantiva mass spectrometer was used for targeted proteomic analysis. This instrument was equipped with a heated, low flow capillary ESI probe (HES-II). Settings were as follows: spray voltage 35000 V, sheath gas 0.5, auxillary gas 0.2, ion transition tube temperature of 325 °C, vapor gas to 70 °C. Chrom filter was set to 10 seconds. Stock solutions of heavy isotope labelled standards for MetE and MetH peptides were prepared in acetic acid, acetonitrile, and HPLC-grade water and added to each sample in concentrations to give 20 and 40 femtomoles of each peptide on column after injection (Bertrand *et al.,* 2013). 0.3

µg of total protein was injected onto the column. Peak areas and retention times were exported to and processed with Skyline. The details of peptides analyzed can be found in Supporting Information, Table S2.2.

2.3.4 Global Proteomic Analysis via Tandem Mass Tagging (TMT) – The procedure for labeling and fractionating protein samples for TMT is adapted from Wu *et al.,* 2019. The digested protein samples were resuspended in 50 mM HEPES (pH 8.5) to give a protein concentration of 0.5 ug μL^{-1}. A pool, which was used in internal reference channels, was made by combining 10 µL aliquots from each sample (one pool for each TMT experiment). 44 µL of each resuspended sample was transferred to 2 mL tubes. Samples were labeled with TMT10plex™ Isobaric Label Reagent Set (Thermo Scientific). The 0.8 mg TMT reagents were suspended in 41 µL of anhydrous acetonitrile and 16 µL of this TMT reagent mixture was added to each sample or pool. A table with sample and pool matrixes for labeling can be found in Table S2.3. The samples were briefly vortexed and centrifuged, followed by a 1-hour incubation at room temperature. The labelling reaction was quenched with 2 µL 5% NH_4OH and the samples were stored at -80 °C until fractionation with a high pH C18 chromatography using an Onyx C18 100 x 4.6 mm column. A 30-minute linear gradient from 5% to 30% solvent B at a flow rate of 1 mL per minute (solvent A: 95% water, 5% acetonitrile, 10 mM ammonium formate pH 9; solvent B: 95% acetonitrile, 5% water, 10 mM ammonium formate pH 9) was applied during fractionation. 60 x 0.6 mL fractions were collected and concatenated (e.g. 1, 11, 21, 31, 41, 51) to give 10 fractions for each TMT set. Fractions were brought to dryness by vacuum centrifuge and re-suspended in 50 µl 0.5% formic acid, 3% acetonitrile.

A Dionex Ultimate 3000 UHPLC (Thermo-Scientific, San Jose, CA) interfaced to the Thermo nanosource of an Orbitrap Velos Pro (Themo Scientific) was used to conduct Nanoflow LC-MS/MS on the TMT set fractions in duplicate. Assuming 50% recovery after digestion, 4 µL 0.75 ug µL $^{-1}$ aliquots were injected to give 3 ug of protein on the column (30 cm x 0.075 mm ID, Proteo C18, 4 µm, 90 Å column, self-packed in a Picofrit fused silica nanospray emitter (New Objective, Woburn, MA)). Flow rate was 0.3 µL/minute during loading and equilibration and 0.25 µL/min during sample elution. 2 hour runs with a gradient of 5% to 25% acetonitrile (0.1% formic acid) over 46 minutes and then 25% to 55% acetonitrile over 25 minutes followed by 7 minutes at 95% acetonitrile were conducted. A lock mass of 445.12003 m/z was used for internal mass calibration. The ion spray voltage was set to 1.6 kV and capillary temperature was 275 °C. Advanced gain control targets were 1e6, 5e4, and 1e4 for Orbitrap full MS, MSn scans and ion trap MSn scans, respectively. For each MS event with injection time of up to 250 and 150 ms for Oribitrap and ion trap MSn respectively, a single microscan was performed. MS1 scan range was 300-2000 m/z at a resolution of 30,000. From this selection, the 10 precursors with the highest intensity were selected for MS2 scans via collision induced dissociation with 35% normalized collision energy and a precursor isolation window of 2 m/z. Only peptides with charge states of 2+ to 5+ and at least a 3e4 MS1 intensity were eligible for MS2. The highest-intensity ion from MS2 was selected for high-energy collision dissociation at 65% normalized collision energy and resolution of 15,000.

2.3.5 TMT Data Analysis – Mass spectrometry data was processed with Proteome Discoverer v2.1 to conduct a database search for all samples. The database was comprised

of a protein coding model generated from a *F. cylindrus* genome assembly downloaded from NCBI and supplemented with chloroplast sequences (also from NCBI) along with a database of common protein contaminants (cRAP) downloaded on June 11, 2021. Precursor and fragment ion mass tolerances were set to 15 ppm and 0.8 Da, respectively. Full trypsin enzyme specificity allowed for two missed cleavages. Both fixed and variable modifications were accounted for. Fixed modifications included peptide N-terminus and Lys TMT10plex (+229.163 Da) and carbamidomethyl cysteine (+57.021 Da). The variable modifications were Methionine oxidation, N-Terminal Glutamine to pyro-Glutamate, and N-terminal protein Methionine-loss and Acetylation. A false discovery rate (FDR) of 1% was estimated using decoy database searches and validated using Percolator with a delta Cn of 0.05 (Käll *et al.,* 2007). Peptides with a co-isolation of more than 40% were excluded from quantification. Reporter ion integration mass tolerance was set to 0.003 Da. For protein quantification, the mean of all unique peptides matching to a given protein plus the shared peptides allocated according to Occam's Razor was calculated. Abundance values were reported as signal to noise ratios.

The data was normalized with IRS (internal reference scaling) after contaminants identified from cRAP database were removed. The IRS normalization pipeline, adapted from the methods modified from Plubell *et al.,* 2017 by Wu *et al.,* 2019 for a similar dataset, is available at https://github.com/bertrand-lab/phaeo-mn-fe. For this normalization procedure, a protein must be observed in all TMT channels. Empty channels for a protein in the dataset were imputed as half of the minimum value for the protein in question. If a protein contained missing values for more than half of the samples, it was excluded from quantification (Webb-Robertson *et al.,* 2015). Two samples were removed from the

analysis as their removal yielded a 174% increase in the number of proteins that were able to be quantified (Supporting Information, Table S2.4). Results from each step of the normalization procedure can be seen in Supporting Information Figure S2.3. A principal component analysis was used to visualize the relationships between sample treatments (Supporting Information Figure S2.4). Normalized values were then used to determine differential protein expression using empirical Bayes quasi-likelihood F-tests via the glmQLFTest function in edgeR. To determine how protein expression in different treatments varied from the control (4 °C, +B_{12}), three pairwise comparisons were made. These yielded information about (1) responses to B_{12} deprivation (control vs. 4 °C, - B_{12}) (2) elevated temperature response (control vs. 12 °C, + B_{12}), and (3) the interaction between the two stressors (control vs. 12 °C, - B_{12}). Proteins were considered differentially expressed with a p-value < 0.05. NCBI protein accession numbers for differentially proteins were matched to functional assignments from the Kyoto Encyclopedia of Genes and Genomes (KEGG) database (Kanehisa *et al.,* 2016) using the KEGGREST API. Henceforth, proteins ID's refer to JGI protein ID's.

2.4 Results

2.4.1 Growth Parameters – After approximately 3 months of semicontinuous dilutions, the *F. cylindrus* cultures were determined to be acclimated. Mean growth rate (d^{-1}) over the last 10 dilutions before the cultures were exposed to temperature treatments were not significantly different (Table 2.1; student's t-test; p = 0.20).

Table 2.1: Mean growth rates (μ; d^{-1}) of the last 10 dilutions of *F. cylindrus* cultures before temperature treatment. Growth rates were computed from RFU measured every two days (pre-and post-dilution), which serves as a proxy for cell density (Supporting Information Fig. S2.1c). $\mu = \ln(N_t/N_0)/\Delta t$

B_{12} Treatment	μ (d^{-1})	St. Dev.
$+B_{12}$	0.20	0.07
$-B_{12}$	0.20	0.06

F. cylindrus cell abundance was observed over a 72-hour period after upshift to the lethal temperature (12 °C) from the control temperature (4 °C). Cell density declined significantly after 24 hours of exposure to the 12 °C treatment (student's t-test; $p < 0.001$; Figure 2.1a). The F_v/F_m of the lethal temperature treatments decreased significantly after 24 hours (student's t-test; $p < 0.001$; Figure 2.1b).

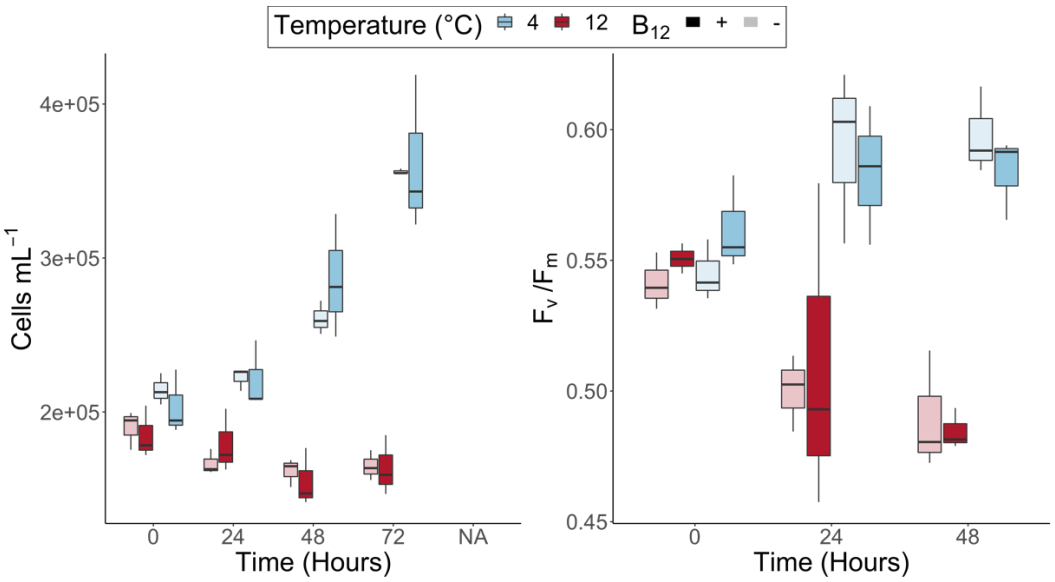

Figure 2.1: Cell densities and photosynthetic efficiency responses over time of *F. cylindrus* to change in temperature. **a)** Boxplot of *F. cylindrus* cell densities, measured with flow cytometry, over time after exposure to control (4 °C) and elevated (12 °C) temperature treatments at 0 hours, and with and without the addition of vitamin B_{12} to the culture medium (n=3 for each treatment). Boxes show IQR (interquartile range), with horizontal lines denoting the median and vertical lines showing minimum and maximum values. Blue boxes represent 4° C treatments and red boxes represent 12 °C treatments. Color saturation represents B_{12} treatment, with saturated boxes representing B_{12}-replete treatments and translucent boxes representing B_{12}-deplete treatments. Cell number at 24 hours was significantly different between temperatures. A t-test for difference of means at 24 hours was conducted, showing a significant decline in cell number between the 4 and 12 °C treatment ($p < 0.001$). **b)** Boxplots with the same scheme showing change in F_v/F_m in *F. cylindrus* after exposure to the control and elevated temperature treatments. Data from each biological replicate represents the 2 technical measurements.

2.4.2 Methionine Synthase Concentrations – 24 hours after exposure to temperature treatment, protein per cell was significantly higher in the elevated temperature treatments (Figure 2.2a; student's t-test; $p < 0.01$) and did not vary with B_{12} treatment. Peptide markers for MetH and MetE methionine synthases were quantified in *F. cylindrus* cultures (Figure 2.2b,c). MetH quotas were comparatively low and remained constant with B_{12} and temperature treatments (Figure 2.2b). In contrast, MetE peptide content increased starkly

in cultures provided deprived of exogenous B_{12} ($p < .001$; Figure 2.2c). There was no significant impact of temperature on MetE per cell (Figure 2.2c).

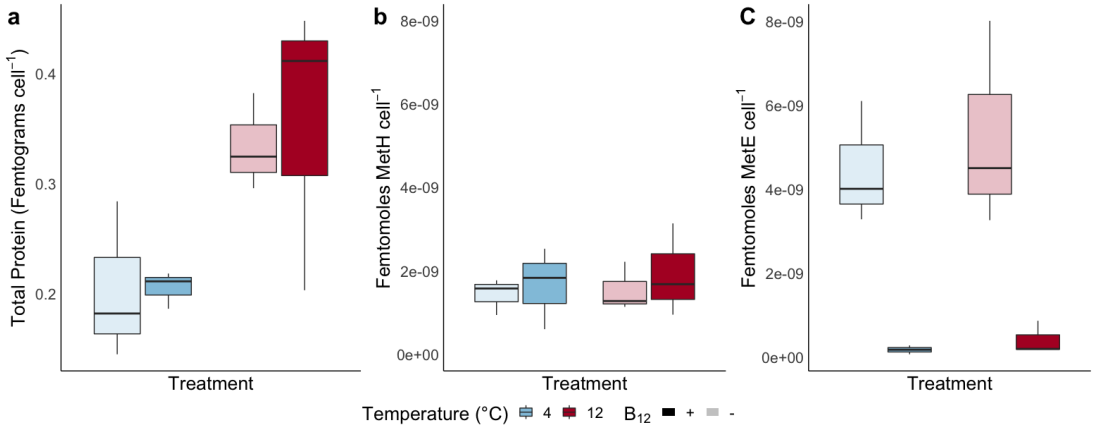

Figure 2.2: Protein measurements from *F. cylindrus* cultures 24 hours after exposure to control (4 °C) and elevated (12 C) temperature treatments, with and without the addition of exogenous B_{12}. **a)** Total protein (femtograms cell^{-1}) **b)** Femtomoles of diagnostic MetH peptide (KJ866915.1) cell^{-1} and **c)** Femtomoles of diagnostic MetE peptide (KJ866917.1) cell^{-1}. Boxes show IQR (interquartile range), with horizontal lines denoting the median and vertical lines showing minimum and maximum values of 3 biological replicates per treatment and duplicate injections. Blue boxes represent 4 °C treatments and red boxes represent 12 °C treatments. Color saturation represents B_{12} treatment, with translucent boxes representing B_{12}-deplete and saturated boxes representing B_{12}-replete treatments.

2.4.3 Proteomic Discovery Experiment – A Tandem Mass Tagging (TMT) discovery experiment was conducted with biomass from control and lethal temperatures after 24 hours of exposure. 3,004 proteins were initially detected from 18,349 predicted from the genome. After normalization and imputation steps, 1,357 protein expression profiles were quantified. A differential expression analysis was conducted by making three pairwise comparisons to determine how protein expression in different treatments varied from the control (4 °C, +B_{12}). These yielded information about (1) responses to B_{12} deprivation (control vs. 4 °C, - B_{12}) (2) elevated temperature response (control vs. 12 °C, + B_{12}), and (3) the interaction between the two stressors (control vs. 12 °C, - B_{12}). The results of this differential expression analysis showed that 96 (7%) of the proteins that were quantified

were differentially expressed in response to B_{12} deprivation and elevated temperature (including the interactive effects of the two stressors) compared to control (Figure 2.3). The highest number of proteins were differentially expressed in response to the interactive effects of B_{12} deprivation and elevated temperature (197), followed by elevated temperature (50) and B_{12} deprivation alone (25; Figure 2.3).

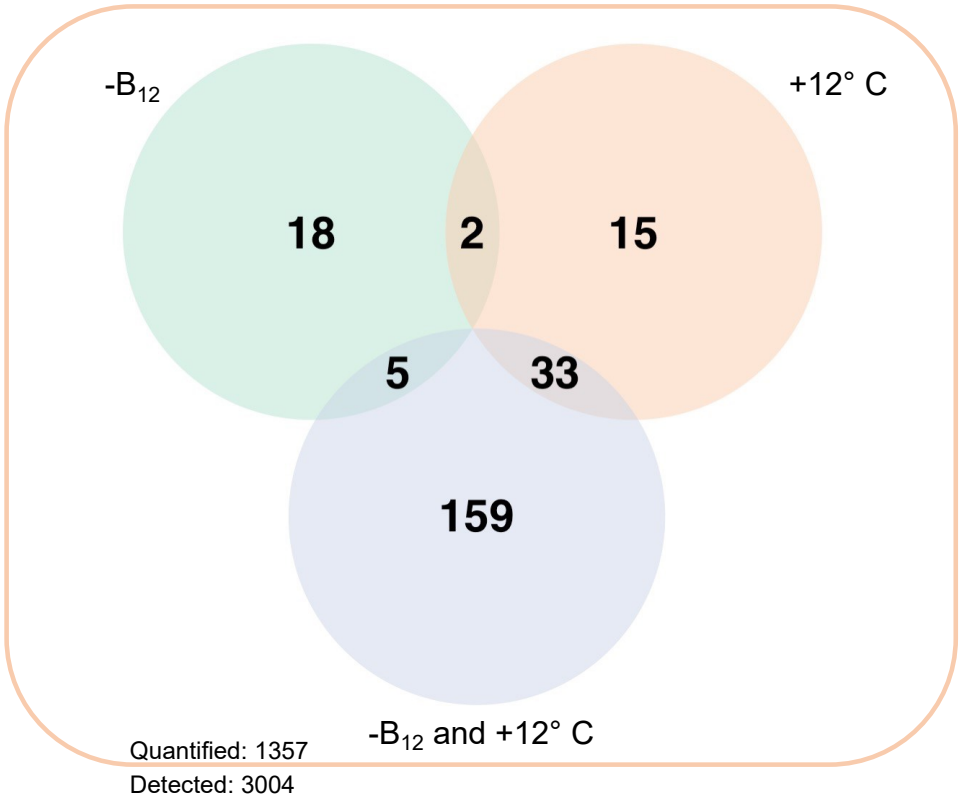

Figure 2.3: Venn Diagram of the number differentially expressed proteins in *F. cylindrus* compared to the control treatment (4 °C, + B_{12}) in samples harvested 24 hours after temperature treatment. 3004 proteins were initially detected and 1,357 were quantified. Each circle shows the number of quantified proteins found to be differentially expressed via a Bayes quasi-likelihood F-test conducted in edgeR with a corrected p-value < 0.05. Three pairwise comparisons were made: the response to B_{12} deprivation (green; control vs. 4° C, -B_{12}); the response to elevated temperature treatment (pink; control vs. 12° C, + B_{12}); and the response between the two stressors (purple; control vs. 12° C, -B_{12}).

The functional assignments of differentially expressed proteins that had annotations available in the KEGG database can be seen in Figure 2.4. The B_{12} response appears to be characterized by proteins associated with the Transport and Catabolism, Carbohydrate Metabolism, and Genetic Information processing. The elevated temperature response was associated with Transport and Catabolism and Genetic Information Processing, in addition to Cofactor and Vitamin metabolism. Many more proteins annotated as associated with Genetic Information Processing were differentially expressed in response to both B_{12} deprivation and elevated temperature, with a large portion belonging to the Translation category. There were also many more Carbohydrate and Energy Metabolism-associated proteins, as well as signal transduction proteins: nearly 4 times more than in either other comparison.

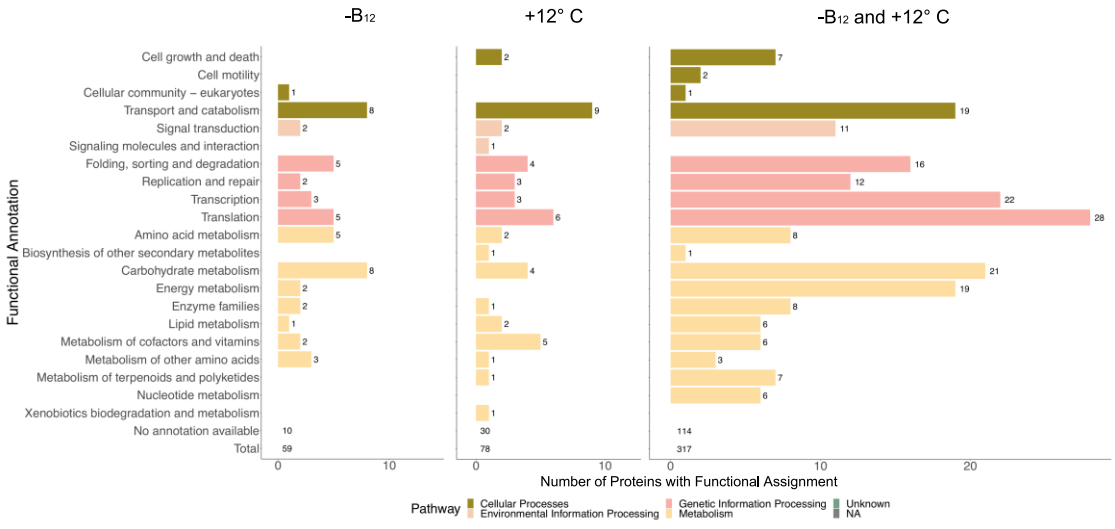

Figure 2.4: Total functional assignments for differentially expressed ($p < 0.05$) proteins that have available KEGG annotations for the 3 pairwise comparisons, representing proteins that are differentially expressed in response to B_{12} deprivation, elevated temperature, and the combined effects of B_{12} deprivation and elevated temperature. Color represents KEGG level A annotations, with KEGG level B annotations along the left side. A single protein may have multiple assignments.

Figure 2.5 shows a heatmap of significantly differentially expressed proteins with a $\log_2$ mean abundance greater than 10.5 from all three pairwise comparisons. Hierarchical clustering was used to group proteins by expression pattern. 53% of proteins had no annotation available. Most of the visualized proteins can be attributed to the interaction between B_{12} deprivation and elevated temperature (Fig. 2.5).

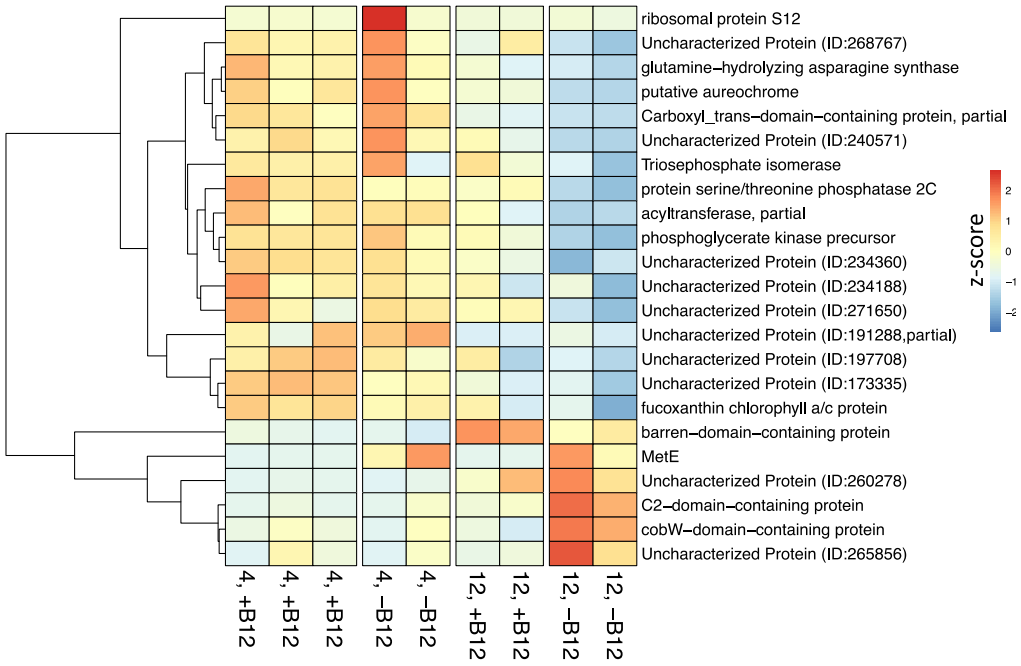

Figure 2.5: Heatmap of differentially expressed proteins from TMT experiment in *F. cylindrus* with a $\log_2$ mean abundance more than 10.5 and $p < 0.01$ from any pairwise comparisons between the control (4° C, $+B_{12}$) representing the response to B_{12} deprivation (control vs. 4° C, $-B_{12}$); the response to elevated temperature treatment (control vs. 12° C, $+ B_{12}$); and the response between the two stressors (control vs. 12° C, $-B_{12}$). Each row is one protein, and each column is one biological replicate. Dendrograms represent hierarchical clustering by protein from Pearson's correlation with average linkage. Columns are ordered by treatment. The cell colors are based on mean-scaled z-score, with blue representing a protein with decreased expression and red an increased expression compared to the mean. n = 2 for three treatments the due to removal after normalization (12° C, $+ B_{12}$, 12° C, $- B_{12}$; Supporting Information, Table S2.3) and failure to process due to a labeling error (4° C, $-B_{12}$).

2.4.4 Proteomic Responses to B_{12} Deprivation – A heatmap of the seven proteins differentially expressed at $p < .01$ in response to B_{12} deprivation can be seen in Figure 2.6. A full list of proteins differentially expressed in response to B_{12} deprivation can be seen in

Supporting Information, Table S2.5, along associated with p-values and fold changes. All proteins differentially expressed with a significance threshold of $p < 0.01$ were enriched in the B_{12}-depleted cultures. This prominently included B_{12}-independent methionine synthase (MetE; ID: 228154), a cobalamin acquisition protein (CBA1; ID: 246327), and a P-ATPase (ID: 168079) associated with transmembrane activity. A cytosolic chaperone, T-complex protein 1 subunit gamma (195967) was also found to be upregulated. Additionally, a P-loop containing nucleoside triphosphate hydrolase protein (ID: 274747), and ribosomal protein S12 (ID: 271288) were upregulated, but this trend was not consistent between replicates.

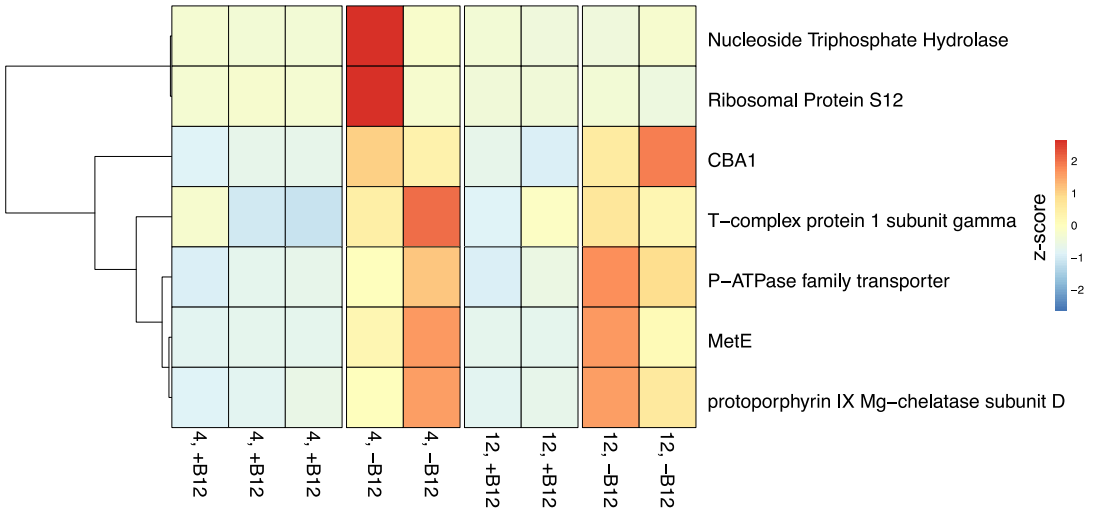

Figure 2.6: Heatmap of differentially expressed proteins from TMT experiment in *F. cylindrus* representing the response to B_{12} deprivation (control vs. 4° C, -B_{12}). Each row shows a proteins found to be differentially expressed via a Bayes quasi-likelihood F-test conducted in edgeR with a corrected p-value < 0.01. Each column represents the protein expression of one biological replicate. Dendrograms represent hierarchical clustering by protein from Pearson's correlation with average linkage. Columns are ordered by treatment. The cell colors are based on mean-scaled z-score, with blue representing a protein with decreased expression and red an increased expression compared to the mean.

Other proteins of interest differentially expressed with a significance threshold of $p < 0.05$ included two additional proteins associated with the methionine cycle: cytosolic serine

hydroxymethyltransferase (cSHMT; ID: 277738), which was found to be upregulated and methionine gamma lyase (ID: 259901), which was downregulated in response to B_{12} deprivation. A suite of proteins annotated as participating in heme biosynthesis were also among the differentially expressed proteins. Protein 247844, which is annotated as protoporphyrin IX Mg-chelatase subunit D (ChlD2-H) in NCBI was upregulated in the absence of B_{12}, whilst porphobilinogen synthase (ID: 218256) was downregulated. Furthermore, phosphofructokinase (ID: 263182), belonging to the glycolytic pathway, was upregulated as well, in addition to a putative blue light sensing auerochrome (ID: 260397). Additionally, acetate CoA ligase (ID: 239808), which is known to be involved in fatty acid biosynthesis was downregulated.

2.4.5 Proteomic Responses to Elevated Temperatures – A heatmap of the twenty proteins differentially expressed in response to the 12° C treatment with $p < 0.01$ is shown in Figure 2.7. A full list of proteins differentially expressed in response to the elevated temperature treatment can be seen in Supporting Information, Table S2.6, along associated with p-values and fold changes. Many of the proteins involved in responses to temperature were identified as putatively related to protein synthesis and included ribosomal biosynthesis proteins in addition to ribosomes themselves. For example, 60S ribosomal protein L24 (ID: 268718), the GTP-binding protein EngA (ID: 196010), a DEAD-domain containing protein (ID: 183391), and an unidentified protein which has similarities to RNA polymerase II (ID: 275154) were all downregulated.

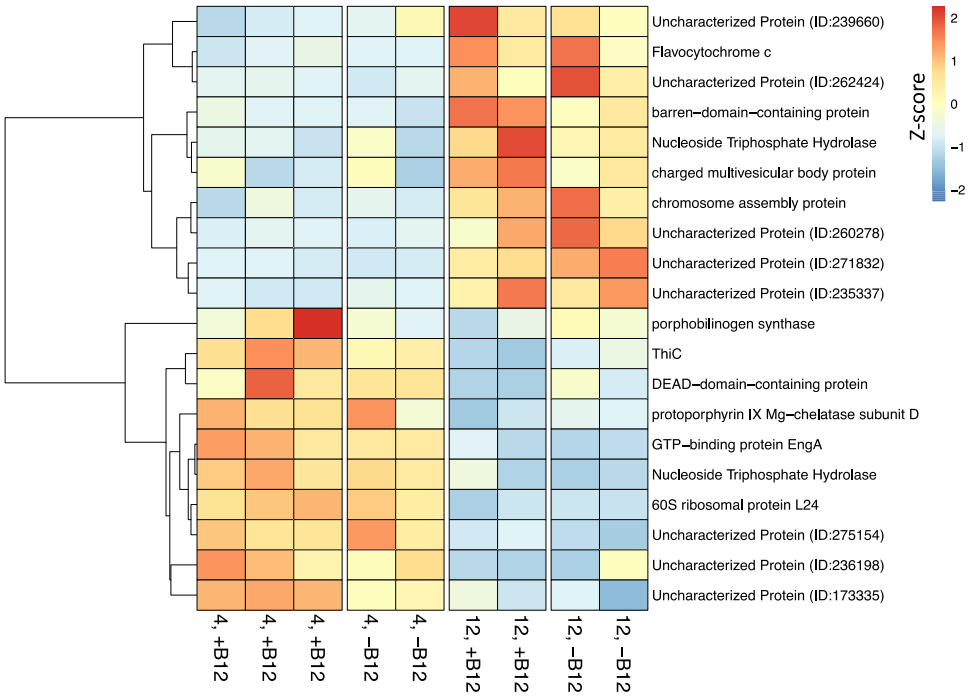

Figure 2.7: Heatmap of differentially expressed proteins from TMT experiment in *F. cylindrus* representing the response to elevated temperature (control vs. 12° C, $+B_{12}$). Each row shows a protein found to be differentially expressed via a Bayes quasi-likelihood F-test conducted in edgeR with a corrected p-value < 0.01. Each column represents the protein expression of one biological replicate. Dendrograms represent hierarchical clustering by protein from Pearson's correlation with average linkage. Columns are ordered by treatment. The cell colors are based on mean-scaled z-score, with blue representing a protein with decreased expression and red an increased expression compared to the mean.

Proteins related to genetic information processing were broadly affected by temperature. 3 P-loop containing nucleoside triphosphate hydrolase proteins (ID's: 208780, 205573, 182871), which are known to export peptides across membranes but also can be involved in translation and DNA repair, were found to be both up and downregulated. Furthermore, proteins associated with the condensin complex, which is involved in chromosome assembly, were also observed to be upregulated (ID's: 233571 and 210755). Additionally, the alpha subunit of ribonucleotide reductase (RNR; ID: 205957) was downregulated with high temperatures. The thiamine biosynthesis protein ThiC was also downregulated under

high temperatures, in addition to Methionine sulfoxide reductase B (ID: 274188), which is known to be a cold response protein in Arabidopsis (Dos Santos *et al.,* 2005).

As in the B_{12} treatment, proteins related to tetrapyrrole biosynthesis were also differentially expressed. However, all tetrapyrrole synthesis proteins differentially expressed in the temperature treatment were downregulated in response to the elevated temperature treatment. A protoporphyrin IX Mg-chelatase subunit D (ID: 170289), different from the sequence which was upregulated in response to the B_{12} deprivation treatment, was downregulated in response to the 12° C treatment, in addition to porphobilinogen synthase (ID: 218256), and uroporphyrinogen III decarboxylase (ID: 268500). The most significantly differentially expressed protein was an unknown possibly cytoskeletal protein (ID: 271832) labeled as "projectin/twitchin-related" that was upregulated at high temperatures. A BLAST search of this protein yields no similar sequences in other organisms. There were 3 other proteins differentially expressed at $p < 0.01$ (ID's: 262424, 236198, 173335) that yielded a similar lack of information.

2.4.6 Interactive Proteomic Responses to Elevated Temperatures and B_{12} Deprivation – A heatmap of proteins differentially expressed in response to the combined elevated temperature and B_{12} deprivation treatments can be seen in Figure 2.8. A full list of proteins differentially expressed in response to the combined stressors can be seen in Supporting Information Table S2.7, along with associated with p-values and fold changes. The interaction response shares several proteins with the canonical B_{12} (ex: cSHMT, MetE, CBA1, P-ATPase, casein kinase delta, Mg-chelatase subunit D (ID: 247844)) and temperature (including several ribosomal and genetic information processing proteins, a Mg-chelatase subunit D (ID:170289), ThiC, and others) responses,

leaving 69 proteins unique to the treatment. The unique proteins made up 71% of all differentially expressed proteins from all treatments at $p < 0.01$. Among these unique proteins, there were additional tetrapyrrole synthesis proteins such as a partial uroporphyrinogen III decarboxylase (ID: 216482) and a chloroplastic protoporphyrin IX Mg-chelatase (ID: 1773362895). A CobW-domain containing protein (ID: 274493) was upregulated as well.

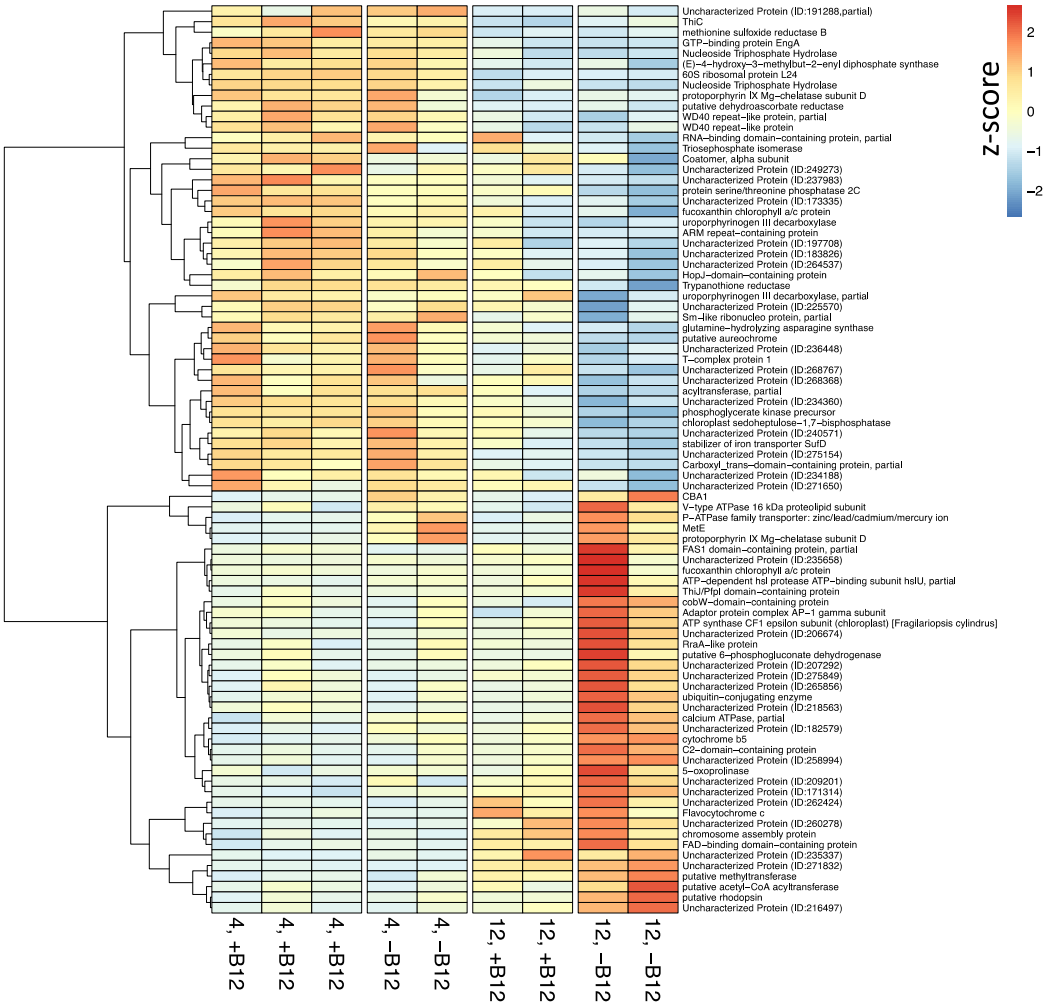

Figure 2.8: Heatmap of differentially expressed proteins from TMT experiment in *F. cylindrus* representing the interactive response to B_{12} deprivation and elevated temperature (control vs. 12° C, -B_{12}). Each row shows a protein found to be differentially expressed via a Bayes quasi-likelihood F-test conducted in edgeR with a corrected p-value < 0.01. Each column represents the protein expression of one biological replicate. Dendrograms represent hierarchical clustering by protein from Pearson's correlation with average linkage. Columns are ordered by treatment. The cell colors are based on mean-scaled z-score, with blue representing a protein with decreased expression and red an increased expression compared to the mean.

Plots of the relationship between mean abundance and fold change of the differentially expressed proteins in the three comparisons can be seen in Figure 2.9. The individual responses to B_{12} deprivation and elevated temperature are small (Figure 2.9a,b) compared to the response to the combined stressors, in which an increased number of proteins show high abundance and significant fold changes. It appeared that many proteins differentially

expressed in response to the combination of these external stressors displayed an apparent relationship between fold change and abundance, with larger fold changes corresponding to decreased abundance (Figure 2.9c). A few proteins do not adhere to this relationship, including MetE, an uncharacterized protein (ID: 271832), CBA1, EngA, and a nucleoside triphosphate hydrolase. An additional protein (ID: 182880) is also an outlier, but this trend is not reproduced amongst replicates (Figure 2.9c).

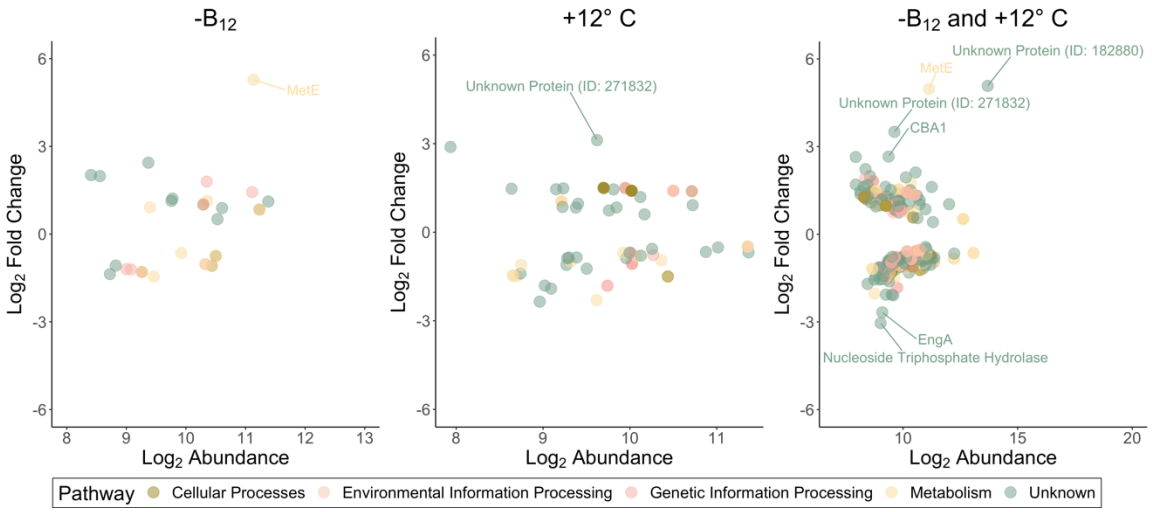

Figure 2.9: Log_2 mean abundance and log_2 fold change of proteins differentially expressed in response to **a)** B_{12} deprivation **b)** elevated temperature **c)** combined B_{12} deprivation and elevated temperature ($p < 0.05$) in *F. cylindrus.* Colors represent KEGG functional assignment. Proteins with an absolute log_2 fold change and log_2 mean abundance more than 2.5 and 8, respectively, are labelled.

2.5 Discussion

This study suggests that the combined effects of B_{12} deprivation and temperature on the proteome of *F. cylindrus* are synergistic rather than additive, leading to differences in protein expression in cultures exposed to both stressors not seen in cells treated with each stressor individually. While we found that growth decreased at supra-optimal temperatures, regardless of B_{12} availability, complex proteomic rearrangements were observed in response to the combined stressors. Amongst these rearrangements, we identify a host of interactively enriched uncharacterized proteins, including proteins that may be used to remodel B_{12}.

2.5.1 B_{12}-Mediated Heat Resistance – We expected that the presence of exogenous B_{12} would rescue *F. cylindrus* from heat stress. After exposure to the lethal temperature treatment, cells experienced markers of heat stress, such as cell number decline and decreased photosynthetic capacity (Figure 2.1a,b), regardless of the addition of exogenous B_{12} to the culture medium, in contrast to results from Xie *et al.,* 2013 in *C. reinhardtii*. Therefore, our results provide evidence against the existence of B_{12}-mediated heat resistance in *F. cylindrus.* In the absence of B_{12}, Xie *et al.,* 2013 found that *metE t*ranscripts decreased in *C. reinhardtii* in response to increased temperatures, likely leading to decreased methylation capacity and declines in cell density. In contrast, we found no significant impact on MetE due to temperature, suggesting that the enzyme persists even at lethal temperatures, in *F. cylindrus* (Fig. 2.2b & c).

Diatoms are known to dominate in dynamic, post succession environments, demonstrating high phenotypic plasticity (Cox 2014; Sackett *et al.,* 2013). Evidence suggests that SO diatoms like *F. cylindrus* depend heavily on the use of MetE, as cobalamin is often in short

supply (Ellis *et al.,* 2017; Bertrand *et al.,* 2015). Notably, a higher proportion of SO diatoms possess the ability to utilize the B_{12}-independent methionine synthase pathway via MetE than others globally (Ellis *et al.,* 2017). Although the reasons behind why *F. cylindrus* is able to maintain the production of MetE at supra-optimal temperatures whilst *C. reinhardtii* is not remain unclear, this may be further evidence of these diatom's resilience to the SO's harsh conditions, including periodic B_{12} limitation and heat stress.

2.5.2 Proteomic Responses to B_{12} Deprivation – Bertrand *et al.* 2012 describes three strategies taken by diatoms to manage the effects of vitamin B_{12} deprivation. They include efforts to (1) increase cobalamin acquisition capacity (2) decrease cobalamin demand and (3) manage their decreased methionine synthesis ability. The proteomic responses to B_{12} deprivation observed in *F. cylindrus* by this study include these strategies, in addition to additional changes not previously identified in diatoms.

Cobalamin Acquisition: Uptake and Remodelling – Proteins which may be used to increase cobalamin acquisition, included increased expression of a cobalamin acquisition protein, in addition to possible remodelling activity. The cobalamin acquisition protein CBA1 was upregulated in response to B_{12} deprivation (Figure 2.10). Transcripts encoding CBA1 (cobalamin acquisition protein 1), were first identified in Bertrand *et al.* 2012 in diatoms from a variety of marine environments. Although the exact mechanism of CBA1 function remains unclear, its differential expression in this study provides additional evidence of its role in cobalamin uptake in diatoms.

We hypothesize that a protein detected here may be acting as a previously undescribed part of a B_{12} remodelling or scavenging response by activating the lower ligand of partial

cobalamin molecules, as described below (Fig. 2.10). Some B_{12} remodellers, including some diatoms, can transform cobalamin-related compounds into cobalamin by altering the lower ligand. Helliwell and colleagues found that 2 of 8 tested alga were able to produce cobalamin when provided with pseudocobalamin and cobalamin's lower ligand, DMB (5, 6-di-methylbenzimidazole) and that this ability was removed in CobT mutants (Helliwell *et al.,* 2016). The remodeling capabilities of *F. cylindrus* have, to date, not been examined. In this study, Protein 247844, which is annotated in the JGI database as Chl-D (Mg-chelatase subunit D), was upregulated in response to B_{12} deprivation. We will henceforth refer to this protein as a B_{12}-dependent Chl-D. The small, large, and small subunits of Mg-chelatase are hypothesized to have common evolutionary origins with corresponding subunits of the Co-chelatase enzyme (Fodje *et al.,* 2001). In particular, both Mg-chelatase and Co-chelatase share an integrin I domain and an acidic and proline-rich region (Fodje *et al.,* 2001). The Co-chelatase subunits CobT, CobS, and CobN are associated with cobalamin remodeling and are thought to be involved in DMB synthesis and activation in bacteria (Yi et al. 2012). There is evidence that some organisms may utilize a chimeric Co-Chelatase, using Chl-D in the place of CobT (Rodionov *et al.,* 2003). The length of the B_{12}-dependent Chl-D in *F. cylindrus* is very similar to other Mg-Chelatase subunits in bacteria and archaea (Antonov 2021) and conducting a BLAST search shows that it's closest annotated match is a *Blastochloris* sp. Chld-D (Mg-chelatase subunit D). Other close matches are a number of putative cobalt chelatses in a varity of other organsisms. It is possible that *F. cylindrus* is using the B_{12}-dependent Chl-D as part of a chimeric Co-chelatase protein to activate DMB for use in remodeling cobalamin-related molecules in response to B_{12} deprivation. We have yet to examine whether *F. cylindrus* is able to

scavenge degraded B_{12} molecules or pseudocobalamin for use as cobalamin when provided with DMB. However, the expression patterns of this protein warrant further investigation into *F. cylindrus'* possible role as an algal cobalamin remodeller. While the original work examining cobalamin-related compound remodeling focused on pseudcobalamin, pseudocobalamin is not expected to be as common in the SO as in other ocean regions due small cyanobacterial populations (Bertrand *et al.,* 2011). The majority of B_{12} producers in the SO, for example Thaumarchaeota and gamma proteobacteria, produce cobalamin rather than pseudocobalamin (Doxey *et al.,* 2015). However, degraded tetrapyrrole rings could be outfitted with DMB via this putative pathway in B_{12}-scarce conditions to alleviate the effects of B_{12} deprivation. As a potential remodeller, *F. cylindrus* may increase the pool of biologically labile B_{12} for other consumers, contributing to their ability to survive in B_{12} scarce environments like the SO. This result illustrates that the relationship between producers and consumers of B_{12} has become increasingly blurred as we improve our understanding of cycling dynamics and microbial function (Helliwell *et al.,* 2016).

Moreover, an additional protein belonging to the tetrapyrrole synthesis pathway (Figure 2.10), which produces precursors to heme, chlorophyll, and vitamin B_{12} (Oborník *et al.,* 2005) was downregulated. Porphobilinogen Synthase (PBGS; ID: 218256) is involved in the early stage of tetrapyrrole ring formation, and has been identified as a B_{12} biosynthesis protein (Raux *et al.,* 2000). In contrast, Rao 2020 found members of the tetrapyrrole synthesis pathway to be upregulated in *P. antarctica,* a psychrophilic haptophyte, in response to B_{12} deprivation. Like *F. cylindrus*, *P. antarctica* is incapable of producing cobalamin *de novo*, but both organisms appear to differentially express portions of the cobalamin biosynthetic pathway in response to cobalamin deprivation.

Cobalamin Demand – In addition to investing in strategies for obtaining more cobalamin, organisms can also attempt to decrease cobalamin demand to alleviate the effects of B_{12} deprivation. This study highlighted the methionine synthase, MetE as a key protein for this task, consistent with previous work (Helliwell *et al.,* 2011; Bertrand *et al.,* 2012; Ellis *et al.,* 2017). In *F. cylindrus*, MetE was upregulated in B_{12}-deplete treatments in order to utilize the B_{12}-independent methionine synthase pathway (Figure 2.10). This trend was demonstrated in the global proteomic data as well (Figure 2.6). A P-ATPase (ID: 168079) was identified is being upregulated in the absence of B_{12} (Figure 2.6). These types of ATP-ases are known to be involved in metal transport activity. MetE is known to utilize zinc as a cofactor (Zhou *et al.,* 1999) and Bertrand *et al.,* 2013 suggests that B_{12} deprivation can lead to up to a 40-fold increase in zinc requirements in *P. tricornutum*. Therefore, it may be possible that this protein is involved in facilitating zinc uptake to meet this demand. Interestingly, neither Methylmalonyl CoA Mutase (MCM) nor any ATP:corrinoid adenosyltransferases, which is required to produce its cofactor adenosylcobalamin from cyanocobalamin (Suh *et al.,* 1993), were detected in the proteome despite their sequences' presence in the genome.

Methionine Synthase Capacity – Managing decreased methionine synthase capacity is the final described strategy for coping with B_{12} deprivation (Bertrand *et al.,* 2012). The effects of decreased methionine synthase capacity are disruptions to folate cycling and methionine scarcity, leading to methyl folate trapping and DNA synthesis (Scott & Weir 1981; Roje 2006). Two proteins falling under this category of response were differentially expressed – cSHMT and Methionine gamma lyase. cSHMT (cytosolic serine hydroxymethyltransferase), which interconverts THF (tetrahydrofolate) and 5,10-MTHF

(5,10-methylene tetrahydrofolate), was found to be upregulated in response to B_{12} deprivation. 5,10-MTHF is known to disrupt folate cycling in low cobalamin conditions in (Scott & Weir 1981). It has been hypothesized that cSHMT upregulation can help to prevent these disruptions (Bertrand *et al.,* 2012).

Furthermore, METase (ID: 25990; methionine gamma lyase) was downregulated in response to B_{12} deprivation (Fig. 2.10). Decreases to SAM (S-Adenosyl Methionine; of which methionine is a precursor) are prevalent in B_{12}-deprived diatom cultures (Bertrand and Allen 2012; Bertrand *et al.* 2012; Heal *et al.* 2019. METase converts L-methionine into methanethiol to balance homocysteine levels (Sato & Nozaki 2009) and therefore, it is possible that this enzyme was no longer needed in the event of an absence of available surplus of methionine for conversion.

Other Impacts of B_{12} Deprivation – A putative blue-light sensing auerochrome (ID: 260397) was found to upregulated in the absence of B_{12}. The light regime in the SO is one characterized by prolonged periods of darkness, requiring extensive adaptations to preserve function without light for up to four months per year (Kennedy *et al.,* 2019). Light dependent gene regulation mediated by vitamin B_{12} has been observed in the bacterium, *Myxococcus xanthus*. In this pathway, adenosylcobalamin is involved in the transcriptional response that deals with the production of carotenoids for avoidance of light stress (Ortiz-Guerrero *et al.,* 2011). In the dark, adenosylcobalamin can bind to the CarH transcriptional factor and block a promoter region that synthesizes carotenoids. When the cell is exposed to light, adenosylcobalamin is rapidly photolyzed and the synthesis of carotenoids can begin. It is possible a similar B_{12} response can activate the expression of this blue light

sensing aureochrome as a secondary block to unnecessary carotenoid production, warranting further investigation.

2.5.3 Proteomic Responses to Elevated Temperature – A total of 50 proteins were identified as differentially expressed in response to elevated temperature (4% of the quantified proteome). Although few studies have examined the effect of elevated temperature on the proteome in diatoms, this value is aligned with others from the literature, which ranged from 0.6 to 17% in supra-optimal temperature treatments, and lower than one study with a lethal temperature treatment in which 22% of proteins were differentially expressed (**Table 2.2**).

Table 2.2: Literature comparisons of the proteome fraction of differentially expressed proteins after exposure to elevated temperature. Included are organism type, temperature treatment (including whether the temperature treatment was an upshift or comparison between previously acclimated treatments and effect to the organism), the total number of identified proteins, the number of differentially expressed proteins, and the percentage of differentially expressed proteins out of the total number of identified proteins.

Source	Organism	Organism Type	Temperature Treatment	Number identified proteins	Number DE'd proteins
This study	*F. cylindrus*	Diatom (psychrophile)	4° → 12° C (upshift; lethal)	1357	50 (4%; $p < .05$)
Boyd. *et al.,* 2016	*P. multiseries*	Diatom (subantarctic)	11° → 14° C (acclimated; supra-optimal)	1640	11 (0.6%;)
Mühlhaus *et al.,* 2011	*C. reinhardtii*	Green microalga	25 → 42 ° C (upshift, lethal)	1116	244 (22%; $p < .01$)
Xing *et al.*, 2018	*A. protothecoides*	Green microalga	28° → 32° C (acclimated; supra-optimal)	4181	728 (17%; $p < .05$)
Xu et al. 2012	*P. haitanensis*	Red macroalga	21° → 29°C (upshift; supra-optimal)	1263	59 (5%; $p<.05$)

Cold adapted organisms require substantial changes to their protein expression and function to maintain growth at low temperatures, which reduce protein turnover and membrane fluidity (Feller *et al.,* 2013). To address reduced turnover, psychrophiles can overexpress photosynthetic proteins, cold shock proteins, including chaperones for increasing folding, and proteins involved in protein transcription and translation (Collins & Margesin 2019; Toseland *et al.,* 2013). The responses to the elevated temperature treatment in *F. cylindrus* included changes to the expression of critical enzymes like those involved in protein production, photosynthetic proteins, and cold shock responses. Surprisingly, no heat shock proteins were included in the list of proteins differentially expressed in response to temperature. It may be that the temperature response was dominated by changes to baseline expression normally associated with cold adapted

organisms. A few proteins related to genetic processing, particularly translation, could be considered responses to protein degradation and misfolding due to elevated temperatures. Cold-adapted enzymes are known to be more heat-labile than others, especially within the active site (Feller 2013). A variety of ribosomal proteins were also down regulated with elevated temperature (Figure 2.8). This may have been due to a reduced demand for protein production under conditions which increase protein turnover. Additionally, two proteins associated with tetrapyrrole synthesis were downregulated in the high temperature treatment - PBGS (porphobilinogen synthase; ID: 218256) and UROD (uroporphyrinogen III decarboxylase; ID: 216482) (Figure 2.10). Liang *et al.,* 2019 observed the downregulation of tetrapyrrole synthesis transcripts in an experiment in which a cold-adapted *Chaetoceros* species was exposed to supra-optimal temperatures. Perhaps this change is associated with the upregulation of photosynthesis-related proteins at low temperatures. If this was the case, in response to high temperatures, *F. cylindrus* would no longer need to overexpress proteins upstream from chlorophyll synthesis.

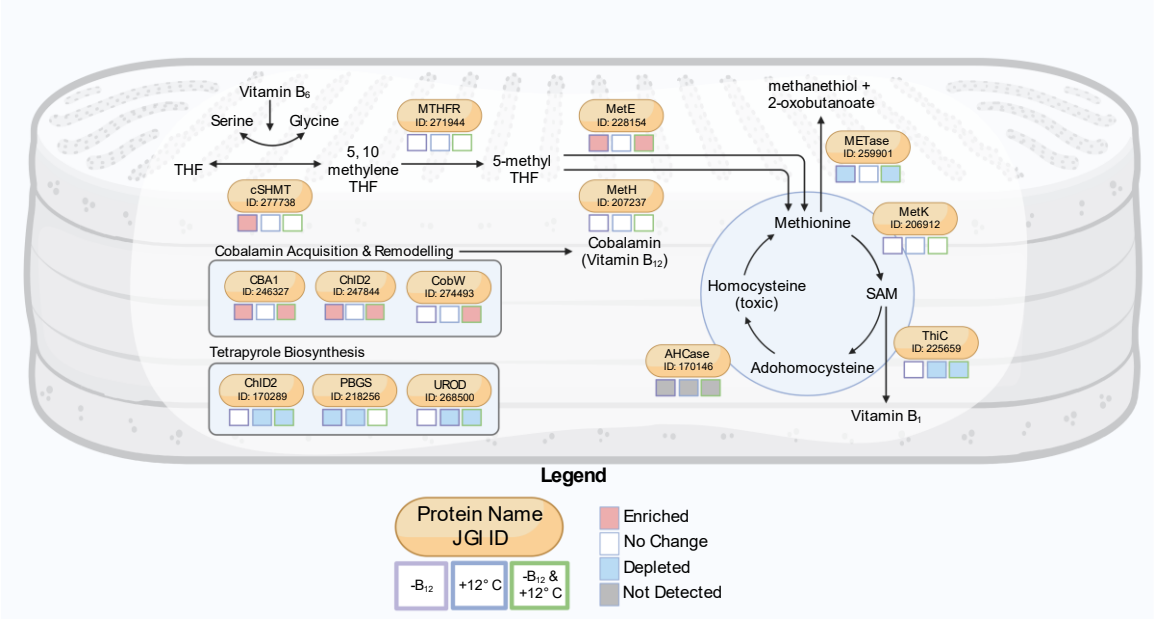

Figure 2.10: Illustration demonstrating the differential expression of proteins in the methionine cycle and related processes. Enzymes/proteins are represented as orange ovals, with JGI protein ID's below their name. Metabolites are written in black text. Each of the three boxes below a protein represent their differential expression in response to B_{12}-stavation (purple outline) elevated temperature (blue outline) the interaction between the two stressors (green outline). The box fill color represents protein expression: enriched (red), no change (white), depleted (blue) or not detected (grey). Adapted from Bertrand *et al.,* 2012 and created with BioRender.com.

2.5.4 Interactive Proteomic Responses to Elevated Temperature and B_{12} Deprivation – These results demonstrate that the interactive responses to elevated temperature and B_{12} deprivation in *F. cylindrus* involve complex proteomic rearrangements. The most statistically significant responses were shared with the individual temperature and B_{12} responses, demonstrating that biomarkers historically used to survey diatoms for B_{12} deprivation are reliable, even at lethal temperatures. Additionally, the majority of proteins differentially expressed in response to the combined stressors were unique to this treatment. From this group, a number of highly abundant proteins with exceptional fold changes were identified in response to the interactive treatment. The presence of these unique proteins is

evidence of synergistic responses to multiple stressors, as the combined response was found to be different than the sum of the responses to each stressor individually.

2.5.5 Conclusions – Mounting evidence places B_{12} among important drivers of microbial ecology and biogeochemistry in the SO, making it worthy of expanded exploration in the context of increasing sea surface temperatures. This study is the first to observe the molecular effects of vitamin B_{12} deprivation and elevated temperature in a psychrophilic diatom. Our results provide baseline information about the molecular effects of B_{12} deprivation, providing a framework for understanding the vitamin's role in the growth and physiology of other cold-adapted diatoms and their broader communities. Clarifying how the effects of B_{12} deprivation are affected by temperature is a crucial secondary step, as exposure to elevated temperature has become increasingly relevant as the potential for extreme microclimates and heat waves increase as ocean temperatures rise due to anthropogenic inputs of carbon dioxide. B_{12} deprivation and elevated temperature responses were found to persist at the intersection of the two stressors, suggesting that proteomic biomarkers used to survey B_{12} limitation in diatoms *in-situ* are reliable, even at lethal temperatures.

Clarifying controls on the growth of primary producers has proved important for making climatic predictions but making distinctions between auxotrophy and non-auxotrophy by growth rate only addresses a single facet of the physiological effects of vitamin deprivation and their broader biogeochemical consequences. We found that growth was unaffected by B_{12} availability but observed that *F. cylindrus* employed various proteomic strategies for managing the combined stressors via an increased number of differentially expressed proteins, including possible enrichment of B_{12} remodelling pathways. Considering *F.*

cylindrus' potential as a putative remodeller, it is possible that it can contribute to the biologically labile B_{12} pool, allowing it and other consumers to persist in B_{12} scarce conditions like those in the SO, affecting community composition. The results of this study highlight the important role of vitamin B_{12} availability on the SO's biogeochemistry in the face of a warming ocean.

Chapter III: The Effects of Vitamin B_{12} Deprivation on Physiology and Metabolite Production of the Polar Diatom, *Fragilariopsis cylindrus*

3.1 Abstract

Vitamin B_{12}, also known as cobalamin, is a cobalt-containing micronutrient estimated to be required for growth by half of all eukaryotic phytoplankton. Despite its importance, our knowledge of vitamin B_{12} requirements and utilization remains limited in diatoms. In this study, we examine the effects of vitamin B_{12} deprivation on diatom physiology and metabolite production and present the first direct measurements of cellular B_{12} quotas in an ecologically significant polar diatom, *Fragilariopsis cylindrus.* We grew *F. cylindrus* cultures at 6 °C, with and without the addition of exogenous B_{12} and, using targeted metabolite quantification approaches, we monitored the abundance of four cobalamin factors, in addition to a suite of metabolites previously shown to be affected by B_{12} deprivation. We also measured the expression of the B_{12}-requiring methionine synthase enzyme, MetH and its B_{12}-independent alternative, MetE. *F. cylindrus* cells contained an average of 0.30 attomoles of B_{12} per cell in B_{12}-replete conditions and B_{12} quotas far exceeded the MetH content of the cell, suggesting luxury uptake of the vitamin. Additionally, the abundance of DMSP and the vitamin B_1 precursor cHET increased significantly in response to B_{12} deprivation. Our results suggest that the effects of B_{12} scarcity may result in impacts to *F. cylindrus'* role in microbial assemblages via the potential differential production of growth stimulating compounds.

3.2 Introduction

Vitamin B_{12}, also known as cobalamin, is a cobalt-containing micronutrient found in picomolar to sub-picomolar concentrations in the ocean (Sañudo-Wilhelmy *et al.,* 2006). Over half of surveyed algal species in culture collections are B_{12} auxotrophs, meaning that they require the vitamin for growth (Croft *et al.,* 2005). Given its combined scarcity and requirement by many microbes, it is likely that vitamin B_{12}'s availability may act as an important control of microbial community structure and bloom dynamics. The link between B_{12} availability and community-level effects on oceanic microbes has been explored by several studies, which have demonstrated that B_{12} availability can alter community composition, net productivity, and growth in a variety of marine environments (Sañudo-Wilhelmy *et al.,* 2006; Gobler *et al.,* 2017; Koch *et al.,* 2011; Bertrand *et al.,* 2007; Browning *et al.,* 2017). As with other trace nutrients, low concentrations of vitamin B_{12} may significantly affect individual and community microbial dynamics in the ocean, putatively influencing processes such as nutrient cycling, carbon export, and the production of important allelopathic and climatically relevant compounds (Moore *et al.,* 2013). However, despite its importance, our knowledge of B_{12} utilization, uptake, and cycling in ecologically significant phytoplankton species remains scarce. To date, only a single study has explored the metabolic impacts of vitamin B_{12} deprivation in diatoms (Heal *et al.,* 2019) and no direct measurements of B_{12} cellular quotas have been made for a cultured psychrophilic (cold-adapted) diatom.

In addition to being difficult to detect in the ocean due to low concentration and high photolability, the production and utilization of cobalamin varies significantly between microbial clades, making it challenging to study comprehensively (Helliwell *et al.,* 2016).

Cobalamin-related compounds have an upper and lower ligand, leading to various combinations that are produced and utilized by different clades and can play different biological roles. Either DMB (5, 6-di-methylbenzimidazole) or adenine can act as the lower ligand in B_{12}. The four cobalamin compounds all possess DMB as a ligand (Figure 3.1). If the lower ligand is adenine, the resulting cobamide is a pseudocobalamin variant (Tanioka *et al.,* 2009; Helliwell *et al.,* 2016). Certain groups of the prokaryotes, including some cyanobacteria, can synthesize B_{12}, in the form of pseudocobalamin (Raux *et al.,* 2000) and evidence provided by Helliwell *et al.,* 2016 suggests that pseudocobalamin is on the order of 100 times less available for use by eukaryotic algae. The four variants of cobalamins which possess DMB as the lower ligand, are adenosyl-, cyano-, methyl- and hydroxocobalamin (Figure 3.1). Adenosyl- and methylcobalamin are used in the cell as cofactors in the highly conserved enzymes, MetH (B_{12}-dependent methionine synthase) and MCM (methylmalonyl-CoA mutase), which participate in methylation and radical rearrangements, respectively, in eukaryotic algae (Croft *et al.,* 2006). Adenosyl- and methylcobalamin are both extremely photolabile, quickly degrading to hydroxocobalamin, which is considered an intermediate product, upon exposure to light (Juzeniene & Nizauskaite 2013). Hydroxo- and cyanocobalamin are not biologically active and must be converted to a biologically active form before use in the cell (Banjaree & Ragsdale 2003).

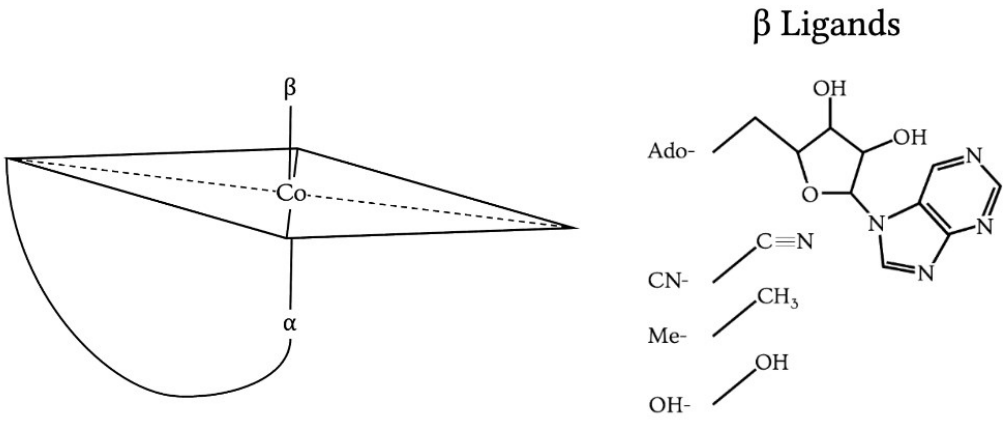

Figure 3.1: Four possible structural variants of vitamin B_{12} based on the nature of the upper ligand. On the left, the corrin ring structure of cobalamin with a cobalt ion in the centre can be seen. Variations of the cobalamin molecule may be produced by different lower (α) or upper (β) ligand. On the right, four possible β ligands are presented: an Ado-, CN-, Me-, and OH-, which produce adenosyl-, cyano-, methyl-, and hydroxocobalamin respectively. In cobalamin, the alpha ligand is DMB. Adapted from Heal *et al.,* 2016.

Vitamin B_{12} is used as a cofactor in the enzyme MetH, which catalyses the production of the essential amino acid methionine from methyltetra-hydrofolate using methylcobalamin as a cofactor (Banjaree & Matthews 1990). Some organisms can use a B_{12}-independent alternative, MetE, to meet their methionine synthesis needs in the absence of B_{12} (Banjaree & Matthews 1990). Evidence suggests that MetH is the primary sink for vitamin B_{12} in eukaryotic microalgae, as organisms with the presence of genes encoding MetH but not MetE are most often B_{12} auxotrophs (Helliwell *et al.,* 2011). Compared to MetH, MetE has a 60-100 times slower rate of catalysis (Taylor & Weissbach 1973), which may be why it has been observed to be expressed at much higher abundance under B_{12} deprivation than MetH. For example, Bertrand *et al.,* 2013 found that B_{12}-depleted cultures of *P. tricornutum*, a temperate diatom, expressed MetE at values proportional to the differences

in the enzymes' turnover rates, with an approximately 60-fold greater abundance of MetE compared to MetH levels in replete conditions. Bertrand and others have suggested that trade-offs between the benefits of the enzyme efficiency and resource costs of the B_{12} dependent and independent methionine synthase pathways based on B_{12} availability may drive the retention of MetE as a methionine synthesis strategy in eukaryotic algae (Bertrand *et al.,* 2013; Bertrand & Allen 2012; Helliwell *et al.,* 2011; Ellis *et al.,* 2017).

B_{12} deprivation appears to have widespread effects on physiology and metabolite production in B_{12} auxotrophs and non-auxotrophs alike, as shown by measurements made from cultures of the diatoms *Phaeodactylum tricornutum* (non-auxotrophic for B_{12}) and *Thalassiosira pseudonana* (a B_{12} auxotroph) (Bertrand *et al.,* 2012; Heal *et al.,* 2017; Heal *et al.,* 2019). These studies suggest that there are specific cellular processes which appear to be disrupted by B_{12} deprivation in diatoms: (1) the production of methionine and its precursors and products, (2) vitamin B_1 biosynthesis, and (3) the abundance of cellular osmolyte pools.

Previous works imply that methionine synthesis capacity is reduced in both B_{12} auxotrophs and non-auxotrophs in B_{12}-deplete conditions. Methionine is a precursor to SAM (S-adenosyl methionine), which has been demonstrated to be depleted in cobalamin-deprived cells (Bertrand & Allen 2012; Bertrand *et al.,* 2012; Heal *et al.,* 2017; Heal *et al.,* 2019). After use in methylation reactions, SAM is degraded to SAH (S-adenosyl homocysteine), which, in high concentrations, can inhibit additional methylation reactions. Bertrand *et al.,* 2012 found that the abundances of a SAM-producing protein (SAM synthetase) and a SAH-degrading protein (SAH hydrolase) in *P. tricornutum* increased with B_{12} deprivation, likely in efforts to balance SAM starvation and SAH buildup.

SAM plays a variety of roles in the cell, including as a precursor to vitamin B_1 (thiamin) biosynthesis and the production of osmolytes like DMSP (Stefels 2000; Chatterjee *et al.,* 2008). Indeed, Bertrand and colleagues have observed that the B_1 biosynthesis protein, ThiC and its transcripts increased in response to vitamin B_{12} deprivation in diatoms with and without MetE (Bertrand *et al.,* 2012; Bertrand & Allen 2012). ThiC catalyses the production of the B_1-precursor HMP (4-amino-5-hydroxymethyl-2-methylpyrimidine) using SAM. Bertrand and colleagues have hypothesized that it is possible that ThiC is upregulated in response to SAM deprivation, perhaps to maintain B_1 biosynthesis despite the low abundance of SAM, a required precursor.

Heal *et al.,* 2019 also noted changes to osmoregulatory and acylcarnitine pools due to B_{12} deprivation-driven SAM starvation, including a decrease in intracellular DMSP concentrations. DMSP is an osmolyte and precursor to DMS, which is a critical component of the sulfur cycle and acts as a cloud condensation nucleus, classically thought to contribute to global albedo when released by phytoplankton exposed to supra-optimal temperature or light conditions (Charlson *et al.,* 1987), though more recent work suggests that DMSP release by phytoplankton is primarily driven by senesce cause by viral lysis or bloom termination (Ayers & Cainey 2007). Furthermore, dissolved DSMP may make up to 13% of carbon pool available for uptake by heterotrophic bacteria (Kiene *et al.,* 2000) and dissolved DMSP abundance may lead to increased DMS production after bacterial assimilatory sulfur requirements have been met (Kiene *et al.,* 2000). Heal *et al.,* were not able to determine that the aforementioned decrease in particulate DMSP in diatoms due to the absence of vitamin B_{12} was not growth rate driven, as DMSP production appeared to mirror growth rate. Exploring the link between vitamin B_{12} and metabolite abundance is

important to improve our understanding of the vitamin's impact on the production of compounds that stimulate microbial growth and play key roles in sulfur and carbon cycles such as vitamin B_1 and DMSP.

The consequences of vitamin B_{12} deprivation on physiology and metabolite production have yet to be explored in a psychrophilic diatom species. *F. cylindrus*, an ecologically significant Southern Ocean diatom and emerging model organism (Kang & Fryxell 1992; Faktorová *et al.,* 2020). *F. cylindrus* is non-auxotrophic, possesses the genes for production of MetE (Helliwell *et al.,* 2011) and, as established in Chapter II and previous studies (Ellis *et al.,* 2017), demonstrates no difference in growth rate due to the deprivation of vitamin B_{12}.

In this study, we aim to determine how the absence of B_{12} affects this organisms' basic physiological properties and metabolite abundance, in addition to how those metabolites relate to the abundance of the methionine synthase enzymes, MetE and MetH. There are currently few datasets that quantitatively examine protein and metabolites together in organisms like *F. cylindrus*. Here we present a unique opportunity to examine the relationship between how much B_{12} is taken up by *F. cylindrus*, and the resulting changes to its cellular physiology and abundance of select metabolites.

To determine how vitamin B_{12} deprivation affects *F. cylindrus*, we grew axenic semicontinuous cultures with and without the addition of exogenous vitamin B_{12}. After acclimation, we measured particulate carbon and nitrogen, cell size, and methionine synthase expression. We also analyzed the biomass for cobalamin-related compounds and a select number of metabolites previously identified as being impacted by B_{12} deprivation by Heal *et al.,* 2019 (Table S3.1). Our findings provide baseline information about an

ecologically significant polar diatom's responses to B_{12} deprivation, laying the framework for future study of other microbes in the SO and how they interact with vitamin B_{12}, and the possible implications for microbial growth and nutrient cycling.

3.3 Methods

3.3.1 Semicontinous Culturing – Axenic cultures of *Fragilariopsis cylindrus (strain* CCMP 1102) were obtained from Provasoli-Guillard National Center for Marine Algae and Microbiota. After inoculation into 250 mL vent-capped flasks, the cultures were maintained with sterile techniques at 6 °C. 6 °C was chosen as the optimal growth temperature for *F. cylindrus* based on previous measurements (Jabre & Bertrand 2020; Mock & Hoch 2005; Supporting Information, Figure S3.1). Cells were grown in f/2 medium (Guillard and Ryther 1962; Guillard 1975) made from sterilized synthetic seawater (Sunda *et al.,* 2005, Price *et al.,* 1988/89), with and without the addition of 369 pM cyanocobalamin. Irradiance in the incubators was set to approximately 100 μE m^{-2} s^{-1} in a 12:12 hour light-dark cycle. Cultures were diluted every three days, keeping them in a range of cell densities corresponding with exponential growth phase at this temperature, as established by previous cultures (Supporting information, Figure S3.2). Culture fluorescence was used to monitor cell number, as established with cell counts via flow cytometry (Supporting information, Figure S3.2). Cell counts were taken at the time of harvest with a BD Accuri™ C6 flow cytometer (BD Biosciences). These measurements were also used to estimate cell size.

3.3.2 Cell Size Estimation – Three different sizes (0.75, 3, and 10 μm) of size calibration beads were suspended in Milli-Q water on a BD Accuri™ C6 flow cytometer (BD

Biosciences). Forward scatter was calibrated to bead size, allowing us to estimate *F. cylindrus* cell sizes (Figure S3.3). After plotting red fluorescence by forward scatter, a gate was manually tuned to select the cell populations. A calibration was conducted for every batch of flow cytometry runs to account for interreference caused by instrument drift. Cells were assumed to be cuboid.

3.3.3 Quantification of Particulate Carbon and Nitrogen – 30 mL of each culture was filtered onto on 25 mm pre-combusted GF/F filters and stored at -80 °C. The samples were acidified for 6 hours in a glass desiccator with an open bottle of concentrated hydrochloric acid and later dried overnight in an oven at 45 °C. Then, filters were then packed in tin capsules and analyzed for particulate carbon and nitrogen on an elemental analyzer (Elementar Vario microcube) coupled to an IRMS (Isoprime 100). The samples were flash combusted at 1150 °C to convert particulate nitrogen and carbon into N_2 and CO_2 gas. These gaseous components were then analyzed by the Isoprime 100. The values were blank-corrected and divided by cell number to give per cell quota.

3.3.4 Sample Preparation for Targeted Protein Analyses – Protein extractions for methionine synthase measurements were as described in Chapter II. A Micro BCA Protein Assay Kit (Thermo Scientific) was used to determine protein concentration in the supernatant. Proteins were digested with an S-Trap procedure modified from Profiti 2022. 5 mM DTT (1,4-Dithiothreitol) was used to reduce the proteins. The samples were cooled and alkylated with 15 mM IAM (Iodoacetamide). The reaction was quenched with another addition of 5 mM DTT. Samples were acidified with 12% phosphoric acid to a final

concentration of 1.2%. S-Trap buffer (90% aqueous methanol in 100 mM Triethylamonium bicarbonate, pH 7.1) was added in a 1:7 vol:sample vol ratio and loaded onto an S-Trap mini columns (Protifi) attached to a vacuum manifold. After 10 washes with 600 µL of S-Trap buffer, 125 µL of digestion buffer (50 mM ammonium bicarbonate containing 25:1 wt:wt protein:trypsin) was used to saturate the column and moved to a 37 °C for 16 hours. 80 µL of 50 mM Ammonium bicarbonate was added and the columns were centrifuged at 4,000 XG for 1 min at room temperature. 80 µL 0.2% aqueous formic acid was added and the columns were centrifuge again as previously. Lastly, 80 µL of 50% acetonitrile containing 0.2% formic acid was added and the columns were centrifuged again. The peptide solutions were pooled and brought to dryness with a centrifuge concentrator. The dried peptide sample was resuspended in a 1% formic acid, 3% Acetonitrile solution to aim for 0.16 µg protein μL^{-1}. A peptide BCA (Thermo Scientific) was conducted to confirm protein concentration of each sample before injection.

3.3.5 Targeted Proteomic Analysis – As in Chapter II, a Dionex Ult 3000 UPLC integrated to a TSQ Quantiva mass spectrometer with the run same settings was used for targeted proteomic analysis. Heavy isotope labelled standards for MetE and MetH peptides were also added to the samples, as in Chapter II. For this experiment, 1 µg of protein was injected, with triplicate injections per biological replicate. The monitored peptides can be are the same from those in Chapter II (Supporting Information, Table S2.2).

3.3.6 Metabolite Sample Preparation – Our metabolite extraction is modified from Heal *et al.,* 2014 and 2017. The entirety of the sample procedure was conducted in a dark room

with a red light source and samples were kept on ice whenever possible. Sample filters were placed in bead beater tubes and an internal standard mixture with heavy C13- labelled standards sourced from Cambridge Isotope Labs was added to each filter to achieve 1 picomole of heavy labelled cyanocobalamin, 10 picomoles of thiamine (vitamin B_1) and riboflavin (vitamin B_2), and 20 picomoles of biotin (vitamin B_7) per 1000 µLs of extract. 0.2 mLs of each 100 and 400 µm silica beads were added to the tubes, along with 1000 µLs of ice-cold solvent mixture (40:40:20 acetonitrile:methanol:water) per 1.21 x 10^7 cells. A bead beater (MP Biomedicals) was used to agitate the cells in 3 x 40 second pulses at 1800 rotations per minute (RPM) over a 20-minute period. The tubes were briefly centrifuged, and the supernatant was removed to a clean tube. The centrifugation step was repeated once more and then the filter was rinsed with 30 µL of solvent mixture and centrifuged again. Two more similar washes were repeated with 300 µL of ice-cold methanol. At this point, the sample volume was aliquoted for metabolite analysis. The samples were then dried down with a Vacufuge and stored at -80 °C until analysis.

3.3.7 Sample Preparation for Targeted Metabolite Analyses – Samples were resuspended in varying amounts of buffer A (0.1% formic acid, 2% Acetonitrile) to correct for differences in transferred sample volume and diluted 2-fold in conical polypropylene HPLC vials (Phenomenex, Torrance, CA). A QC (Quality Control) sample was prepared by mixing 10 µL of each sample. Samples and QC's were loaded onto a Dionex Ultimate-3000 LC system coupled to the electrospray ionization source of a TSQ Quantiva triple quadrupole mass spectrometer (Thermo Scientific, Waltham, MA) in selected reaction monitoring (SRM) mode, operating under the following conditions: Q1 and Q3 resolution

0.7 (FWHM), 50 msec dwell time, spray voltage 3500 (positive ion mode), sheath gas 6, aux gas 2, ion transfer tube 325ºC, vaporizer temp 100ºC. A 150 x 0.3 mm ID column (Acclaim PepMap RSLC, C-18, 2 µm, 100 Å) with a 5 x 0.3 mm ID guard column in front, held at 50 ºC was used and subject to an HPLC gradient of 2 – 32% B over 6 min, then 32 - 60% B over 0.5 min (A, 20 mM ammonium formate, 0.1% formic acid; B, 0.1% formic acid in acetonitrile) at 10 µl per min. The total run time including washing and equilibration was 12 minutes. 5 µL of each diluted sample was injected, with QC injections throughout the run to monitor instrument response and compound degradation. Authentic standards were spiked at increasing relevant concentrations (ranging from 0.5-100 femtomoles for the B_{12} analogs (Ado-, CN-, OH-, and Me-B_{12}) and DMB and 2.5-500 femtomoles for all other compounds) in the QC and injected to create a calibration curve (Figure S3.6). Sample injection order for this experiment was randomized and interspersed between additional *F. cylindrus* extracts not included in this analysis. A list of monitored compounds and transitions can be found in Supporting Information, Table S3.1.

3.3.8 Metabolite Data Analysis – Metabolite data was processes with methods adapted from Boysen *et al.,* 2018 and modified by the Bertrand Lab. Metabolites were normalized to their corresponding heavy internal standards. The B_{12} analogs were normalized to heavy cyanocobalamin. Thiamin (vitamin B_1) was normalized to heavy thiamin. Riboflavin (Vitamin B_2) was normalized to heavy riboflavin. Although we also added a heavy biotin (Vitamin B_7), it was not used for normalization to biotin as it led to a decrease in QC variation (Supporting Information, Figure S2). For metabolites without a corresponding internal standard, a best matched internal standard (BMIS) was chosen by selecting

normalizations that reduced QC coefficient of variation by more than 30% (Supporting Information, Figure S3.). The effect of the final chosen BMIS on QC variation in each metabolite can be seen in Supporting Information, Figure S3.5. Calibration curves were used to quantify metabolite concentration after correcting for the amount of metabolite already in each QC sample before standard addition (Figure S3.).

3.4 Results

3.4.1 Physiological Measurements – Estimated cell density for the cultures' dilution series can be seen in Figure 3.2Growth rate during the final ten dilutions before harvest was not found to be significantly different due to B_{12} treatment ($p = 0.63$; Table 3.1).

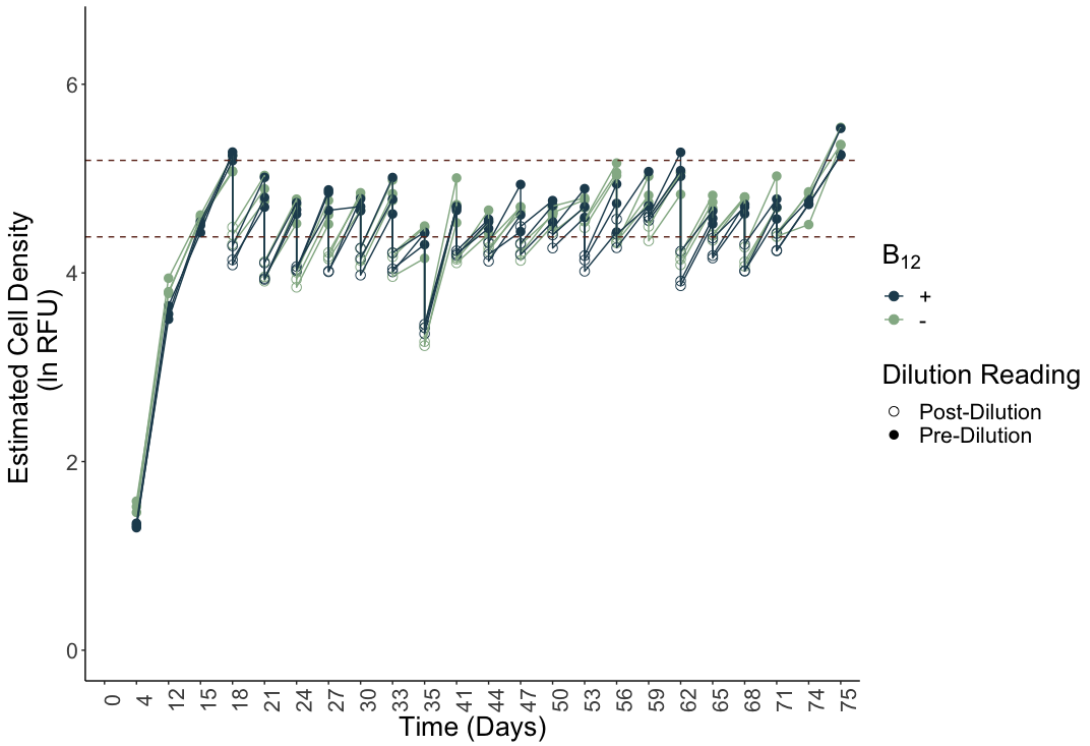

Figure 3.2: Semicontinuous dilutions of axenic *F. cylindrus* cultures with and without the addition of exogenous B_{12}. Fluorescence (RFU; relative fluorescence units) of each culture was measured before (filled in circles) and after (open circles) each dilution. Dotted lines represent an estimation of cell densities corresponding to exponential growth phase as established by previous cultures. Color represents B_{12} treatment, with B_{12}-replete (+) in navy and B_{12}-deplete (-) in green. Cultures were harvested shortly after the final timepoint (day 75).

Table 3.1: Physiological parameters of *F. cylindrus* cells grown at 6 °C. Growth rates were calculated from RFU's measured during the last 10 dilutions before harvest and other parameters were measured from samples taken on day 75 (Figure 3.2). Mean and standard deviation of 3 biological replicates per treatment are presented, except for cellular carbon and nitrogen quotas, for which one $+B_{12}$ treatment which was unable to be quantified due to sample loss. Cellular B_{12} quota estimates include summed adenosyl-, methyl-, and hydroxocobalamin quantifications. Any cyanocobalamin in the cultures was below the limit of detection (Supporting Information Figure S3.7). Specific uptake rate (u) was estimated using $u = \mu Q$, where Q represents intracellular quota (Droop 1973). Significance was tested with a Welsh's t-test. p-values are represented in the Significance column, with $p < 0.05$ = *; $p < 0.01$ = **; and ns = no significance.

Parameter	$+B_{12}$ Mean	$+B_{12}$ St. Dev.	$-B_{12}$ Mean	$-B_{12}$ St. Dev.	Significance
μ (d^{-1})	0.16	1.47×10^{-3}	0.16	1.02×10^{-2}	ns
Pg C $cell^{-1}$	11.30	0.64	11.40	1.86	ns
Pg N $cell^{-1}$	2.72	0.16	2.76	0.16	ns
Estimated Diameter (μm)	6.09	0.04	6.18	0.03	*
Femtograms protein $cell^{-1}$	0.27	4.73×10^{-3}	0.32	4.31×10^{-2}	ns
Attomoles B_{12} $cell^{-1}$	0.30	0.16	-	-	-
C:N:B_{12}	106 : 26 : 0.00356	-	-	-	-
Moles total B_{12}:MetH	1.047×10^{5}	1.11×10^{5}	-	-	-
Moles Me-B_{12}:MetH	4.48×10^{4}	5.93×10^{4}	-	-	-
Specific Uptake Rate (attomoles d^{-1} $cell^{-1}$)	0.05	0.03	-	-	-

Mean carbon and nitrogen quotas were found to be 11.3 and 2.74 pg $cell^{-1}$, respectively, and did not vary due to B_{12} treatment (Figure 3.3; $p = 0.92$; 0.78). Molar C:N ratios were found to be below Redfield (6.625; Redfield *et al.,* 1963), with a mean of 4.077. An extended Redfield ratio, including vitamin B_{12} was calculated (Table 3.1).

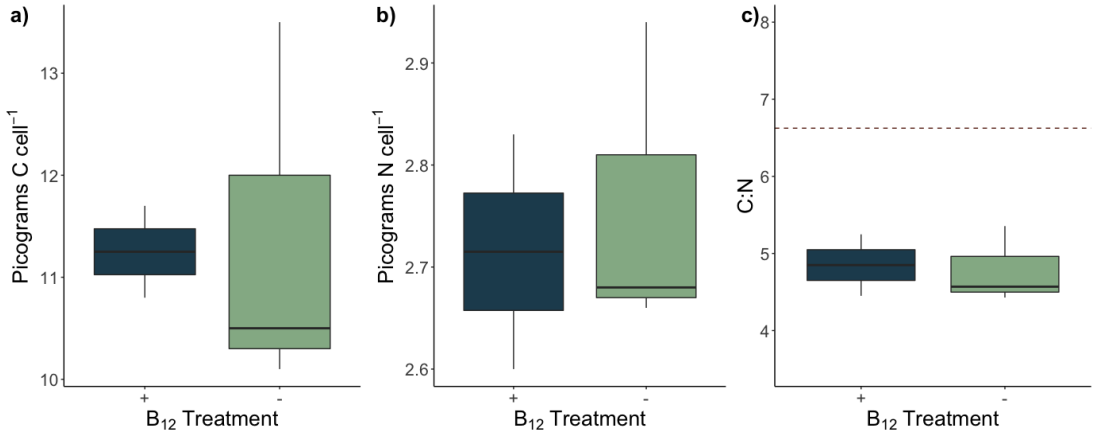

Figure 3.3: Particulate carbon and nitrogen measurements from *F. cylindrus* cultures grown at 6 °C with and without the addition of exogenous B_{12}. a) Picograms of carbon per cell b) Picograms of nitrogen per cell c) and molar C:N ratios (dotted line = Redfield; 106 C: 16 N; Redfield 1963) Boxes show IQR (interquartile range), with horizontal lines denoting the median and vertical lines showing minimum and maximum values of 3 biological replicates per treatment and triplicate injections. Color represents B_{12} treatment, with B_{12}-replete (+) in navy and B_{12}-deplete (-) in green.

Cell size was estimated to be 6.14 µm on average, and B_{12} deprivation appeared to result in larger cells (Table 1; Figure 3.4a; $p < 0.05$). By assuming cuboidal cells, we were able to calculate an estimated biovolume for *F. cylindrus* cells as well (Figure 3.4b).

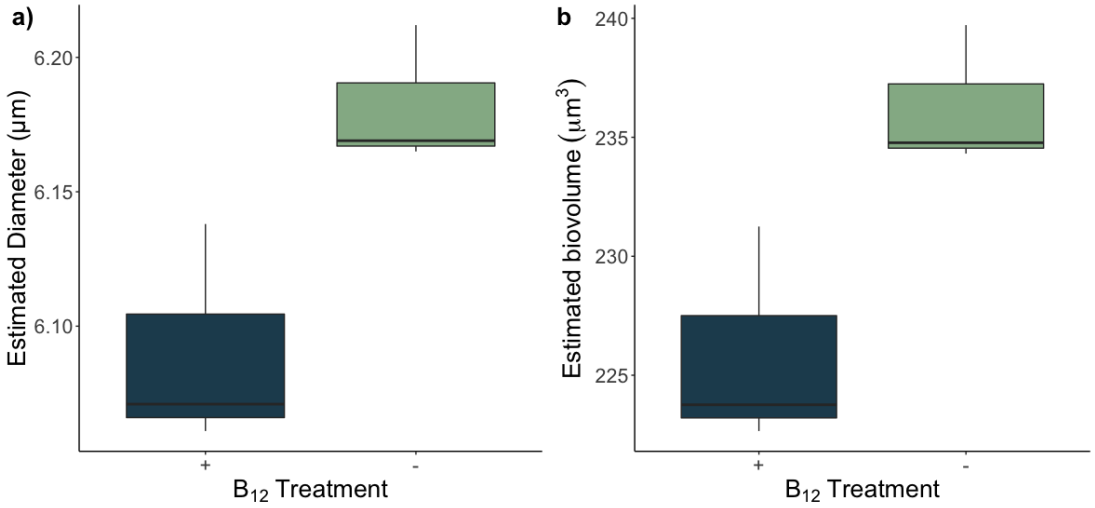

Figure 3.4: a) Estimated cell diameter and **b)** estimated cell volume of *F. cylindrus* cultures grown at 6 °C, with and without the addition of exogenous B_{12}. Boxes show IQR (interquartile range), with horizontal lines denoting the median and vertical lines showing minimum and maximum values of 3 biological replicates per treatment. Color represents B_{12} treatment, with B_{12}-replete (+) in navy and B_{12}-deplete (-) in green.

3.4.2 Methionine Synthase Concentrations – Total protein per cell increased from 0.27 to 0.32 femtograms cell^{-1} in the B_{12} deprived treatment, but this change was not statistically significant (Table 3.1, Figure 3.5a; $p = 0.19$). MetE abundance in the B_{12}-deprived cultures was 4.5-fold that of the MetH expression in B_{12} replete cultures. Cellular MetH quotas were, on average, 4.37 x 10^{-9} femtomoles per cell under B_{12} replete conditions and decreased in B_{12}-deprived cultures, but not significantly ($p = 0.40$; Figure 3.5b). However, MetE abundance did vary significantly, and was starkly reduced in the presence of B_{12} to an average abundance of 1.95 x 10^{-8} femtomoles per cell ($p < 0.01$; Figure 3.5c).

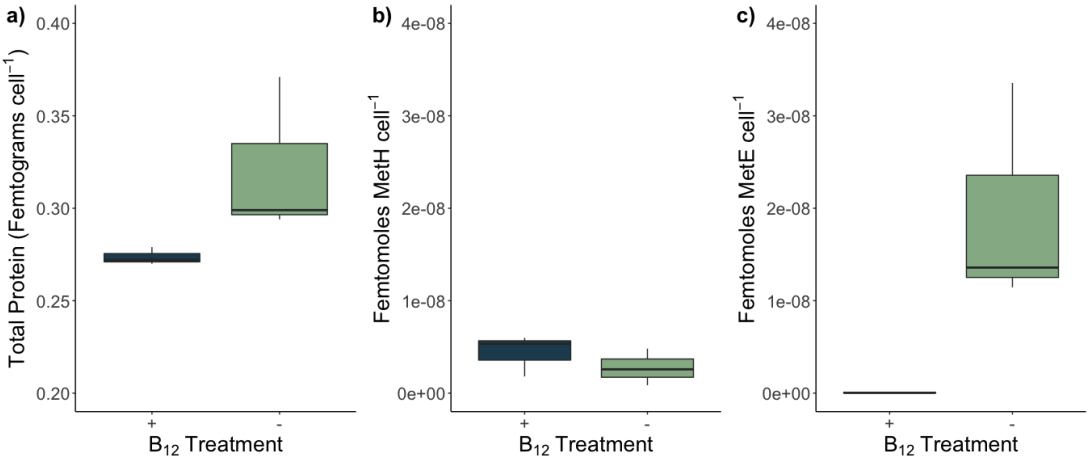

Figure 3.5: Protein measurements from *F. cylindrus* cultures grown at 6 °C, with and without the addition of exogenous B_{12}. **a)** Total cellular protein content (µg cell^{-1}) **b)** Femtomoles of diagnostic MetH (KJ866915.1) peptide cell^{-1} and **b)** Femtomoles of diagnostic MetE (KJ866917.1). Boxes show IQR (interquartile range), with horizontal lines denoting the median and vertical lines showing minimum and maximum values of 3 biological replicates per treatment and triplicate injections. Color represents B_{12} treatment, with B_{12}-replete (+) in navy and B_{12}-deplete (-) in green.

3.4.3 Metabolite Measurements – Out of the 25 compounds we sought to monitor, we were able to provide relative quantification for 8 compounds and absolute quantification for an additional 8 (Supporting Information, Table S3.2). The amino acids methionine and homocysteine were below the limit of detection in most of our samples. We found that *F.*

cylindrus took up a mean of 0.30 ± 0.16 attomoles of B_{12} per cell, with the majority of the cellular B_{12} quota being attributed to hydroxocobalamin (Figure 3.6; Table 3.1). All B_{12} replete samples contained trace or quantifiable amounts of adenosyl- and methylcobalamin. Trace amounts of adenosylcobalamin were also identified in one B_{12} deplete replicate (Supporting Information, Figure S3.7). All cyanocobalamin measurements in the samples were below our calculated limit of detection (Supporting Information, Figure S3.7).

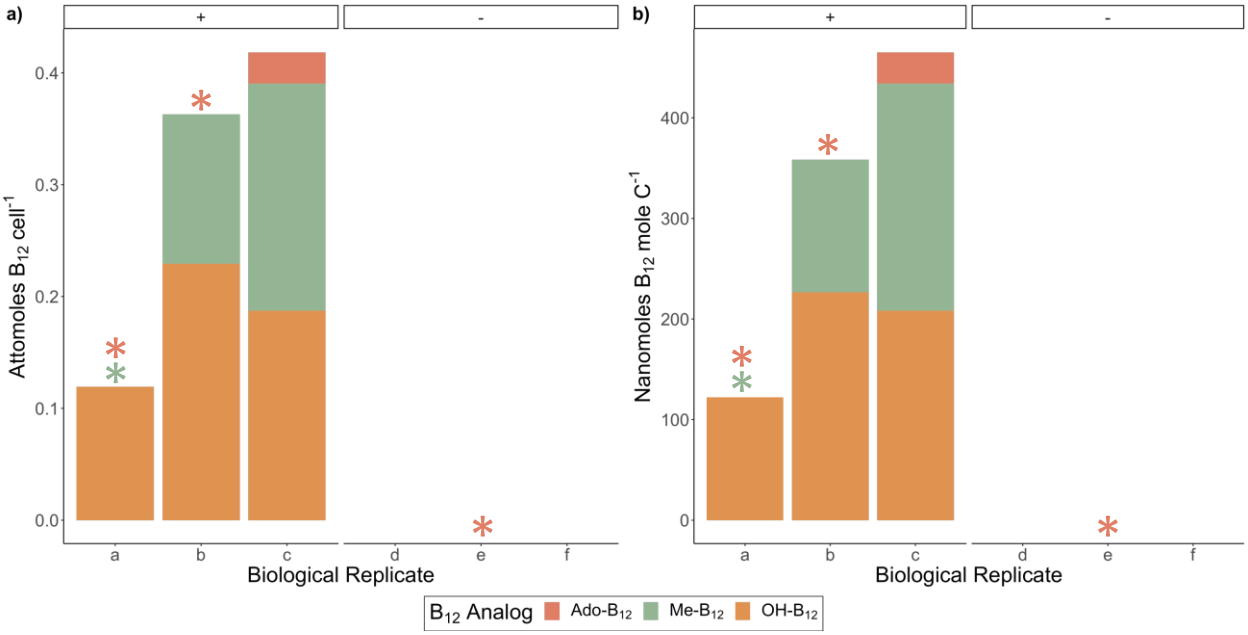

Figure 3.6: B_{12} quotas from *F. cylindrus* cultures grown at 6 °C, with and without the addition of exogenous B_{12} shown in **a)** attomoles cell^{-1} b) Nanomoles mole C^{-1}. Color represents B_{12} analog, which include adenosylcobalamin (Ado-B_{12}, pink), methylcobalamin (Me-B_{12}, green), and hydroxocobalamin (OH-B_{12}, orange). The mean of triplicate injections for three biological replicates per B_{12} treatment (+ and -) are shown. A star indicates that trace quantities of an analog were detected in a sample but was below the LOQ. Cyanocobalamin was not detected in any sample.

Measurements of the osmolytes GBT and DMSP yielded relative quantification. GBT levels remained constant with B_{12} treatment (Figure 3.7a; $p = 0.22$). In contrast, DMSP

concentration significantly increased with B_{12} deprivation (Figure 3.7b; $p < 0.05$). Another major osmolyte in *F. cylindrus,* proline, was also monitored and did not change significantly (Supporting Information Table S3.2).

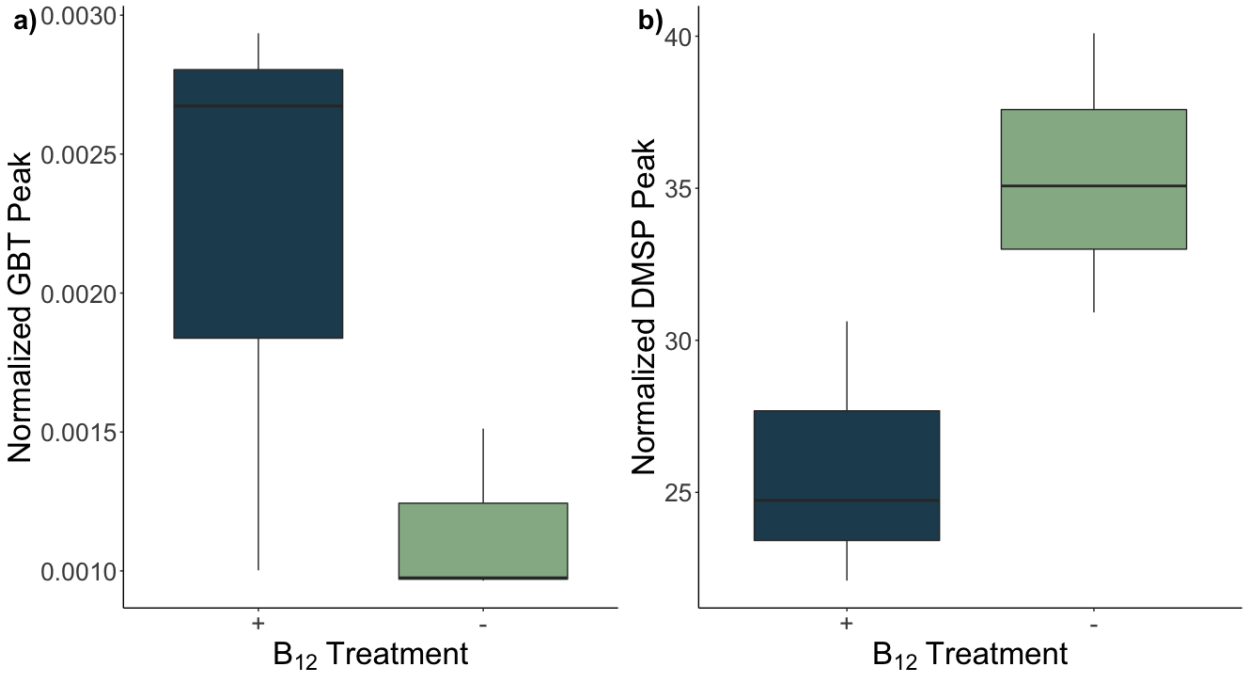

Figure 3.7: Metabolite measurements from *F. cylindrus* cultures grown at 6 °C, with and without the addition of exogenous B_{12}. **a)** Normalized GBT (Glycine betaine) peak area $cell^{-1}$ and **b)** Normalized DMSP peak area $cell^{-1}$. Boxes show IQR (interquartile range), with horizontal lines denoting the median and vertical lines showing minimum and maximum values of 3 biological replicates per treatment and triplicate injections. Color represents B_{12} treatment, with navy boxes representing B_{12}-replete treatments and green boxes representing B_{12}-deplete treatments.

SAH levels increased with B_{12} deprivation, but this change was not found to be statistically significant (Figure 3.8a; $p = 0.23$). SAM levels appeared to be approximately the same between B_{12} treatments and did not change significantly (Figure 3.8b; $p = 0.22$). The ratio of SAH:SAM was also found to increase with B_{12} deprivation (Figure 3.8c).

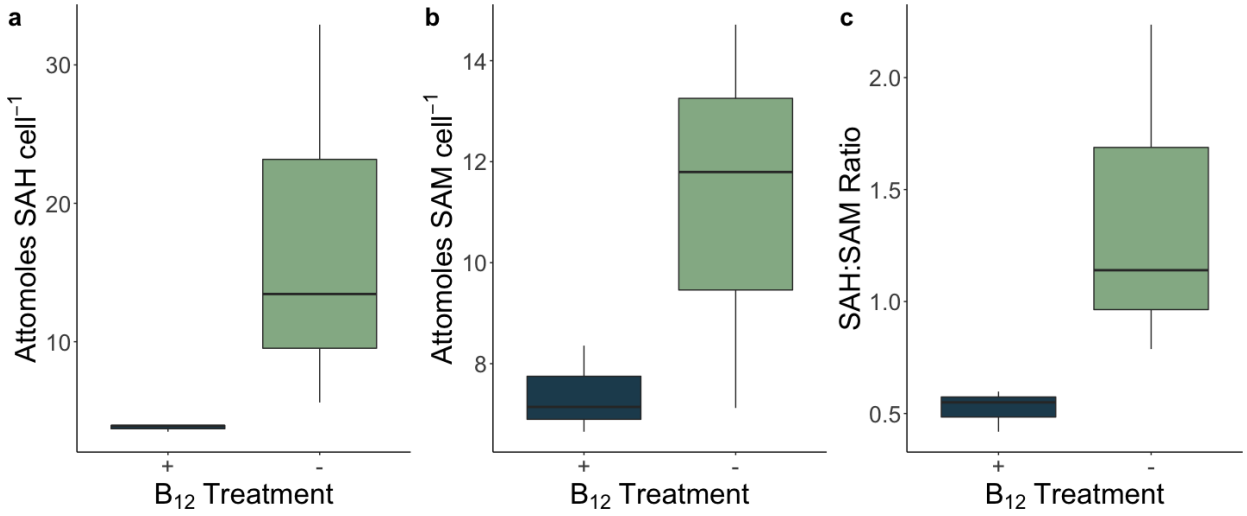

Figure 3.8: Metabolite measurements from *F. cylindrus* cultures grown at 6 °C, with and without the addition of exogenous B_{12}. **a)** Attomoles of SAH (S-Adenosyl Homocysteine) cell^{-1} and **b)** Attomoles of SAM (S-Adenosyl Methionine) cell^{-1} **c)** Ratio of cellular SAH:SAM content. Boxes show IQR (interquartile range), with horizontal lines denoting the median and vertical lines showing minimum and maximum values of 3 biological replicates per treatment and triplicate injections. Color represents B_{12} treatment, with navy boxes representing B_{12}-replete treatments and green boxes representing B_{12}-deplete treatments.

Vitamin B_1 quotas did not change significantly with vitamin B_{12} treatment and were 4.40 ± 1.98 attomoles cell^{-1} on average (Figure 3.9a; $p = 0.376$). The vitamin B_1 biosynthesis precursors, cHET and HMP, were also monitored. Cellular cHET content increased significantly with B_{12} deprivation (Figure 3.9b; $p < 0.05$). There were also trace amounts of HMP detected, but only in B_{12} -replete samples. All HMP measurements were below the detection limit in B_{12} deprived samples.

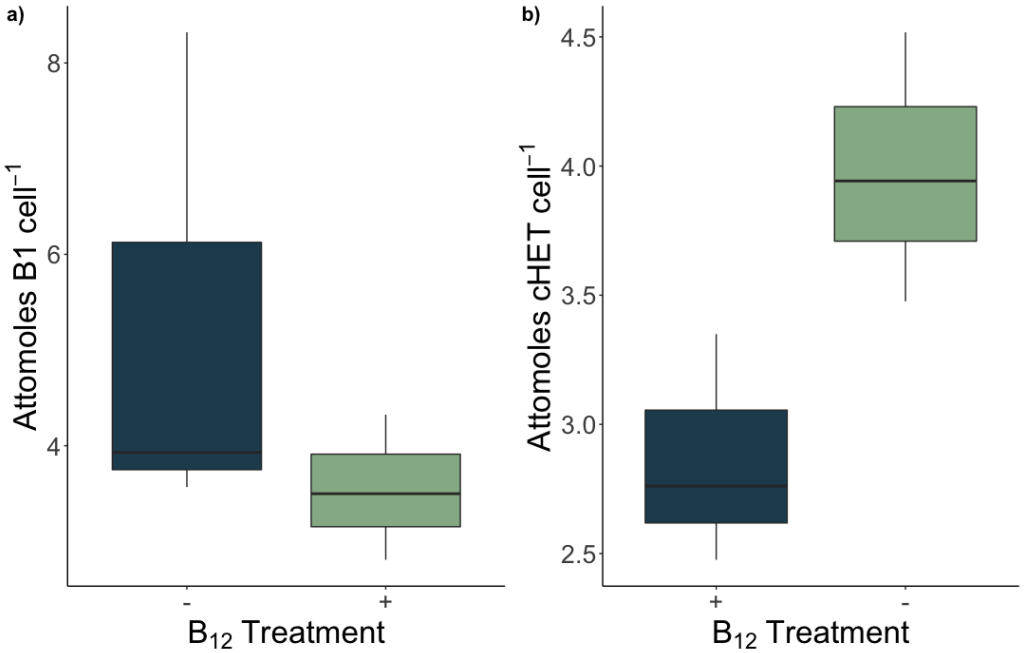

Figure 3.9: Metabolite measurements from *F. cylindrus* cultures grown at 6 °C, with and without the addition of exogenous B_{12} **a)** Normalized peak area of Vitamin B_1 (thiamine) cell^{-1} **b)** Attomoles of cHET (5-(2-hydroxyethyl)-4-methyl-1,3-thiazole-2-carboxylic acid) cell^{-1}. Boxes show IQR (interquartile range), with horizontal lines denoting the median and vertical lines showing minimum and maximum values of 3 biological replicates per treatment triplicate injections. Color represents B_{12} treatment, with navy boxes representing B_{12}-replete treatments and green boxes representing B_{12}-deplete treatments.

3.5 Discussion

3.5.1 Physiological parameters – Broadly, physiological parameters in *F. cylindrus* were not affected by vitamin B_{12} deprivation, with the exception of size (Table 3.1). Cellular C:N ratios content was found to be lower than Redfield, but comparable to previous measurements made in *F. cylindrus* cultures (Mills *et al.,* 2010; Alderkamp *et al.,* 2012) and the range of variation observed for a single species under identical culture and analysis conditions in other microalgae (Geider & LaRoche 2002). Cell size increased with B_{12} deprivation, which could have been fueled by swelling driven by increases in osmolyte content, notably DMSP (Figure 3.7; Stefels 2000).

3.5.2 Methionine Synthase Measurements – Observations of the two methionine synthase enzymes, MetH and MetE, were comparable to those in Chapter II from *F. cylindrus* cultures grown at 4 °C and previous studies (Figure 3.10; Bertrand *et al.,* 2013). Comparisons between methionine synthase expressions in *F. cylindrus* and *P. tricornutum* suggest that *F. cylindrus* may maintain a higher baseline expression of MetH to cope with reduced catalysis rates of the enzyme at colder temperatures. At maximal expression, *F. cylindrus* cultures grown at 6 °C produce 298 times more MetH than *P. tricornutum* (Fig. 3.10). In contrast, they only produce 18 times more MetE (Figure 3.10). It is possible that MetH works less efficiently at low temperatures, resulting in overexpression of the enzyme in psychrophilic species and leading to reduced disparity between the effects of utilization of the B_{12}-dependent methionine pathway via MetH compared to the B_{12}-independent pathway via MetE. Further supporting this hypothesis, environmental samples collected in strongly diatom dominated communities in Antarctic waters (McMurdo Sound) showed

less of a disparity compared to our measurements, with MetH expression being about 26 times higher in *F. cylindrus* (Figure 3.10; Bertrand *et al.,* 2013). The MetE signal is more difficult to compare as B_{12} concentrations were not measured at the time of sampling in Bertrand *et al.,* 2013. The MetE peptide which was used was also less specific to diatoms, so there may be an additional signal from bacterial and fungal MetE (Bertrand *et al.,* 2013). The catalysis rate of MetH and MetE at temperatures of 37 °C and higher has been measured in *E. coli* (Grabowski *et al.,* 2012), but not at lower temperatures to our knowledge. Notably, increased baseline expression of critical enzymes has been proposed as an adaptation to address reduced reaction rates at cold temperatures in psychrophiles (Collins & Margesin 2019). The high MetH abundance in *F. cylindrus* and polar diatom dominated communities (Bertrand *et al.,* 2013; Figure 3.10) compared to the mesophile *P. tricornutum* illustrates the selective pressure to maintain methionine synthesis in Southern Ocean diatoms. The Southern ocean's environment, including low populations of producers and high levels of UV radiation leading to degradation, make vitamin B_{12} scarce (Bertrand *et al.,* 2011; Cruzen 1992 as cited in Bertrand *et al.,* 2007). Overexpression of MetH may mean that the enzyme has an increased chance of encountering a co-factor in the cell at low intracellular B_{12} concentrations. The selective pressure for methionine production despite B_{12} deprivation the Southern Ocean is also illustrated by findings in Ellis *et al.,* 2017, which demonstrated that a higher proportion of Southern Ocean diatom have genes for the biosynthesis of MetE than diatoms from other regions.

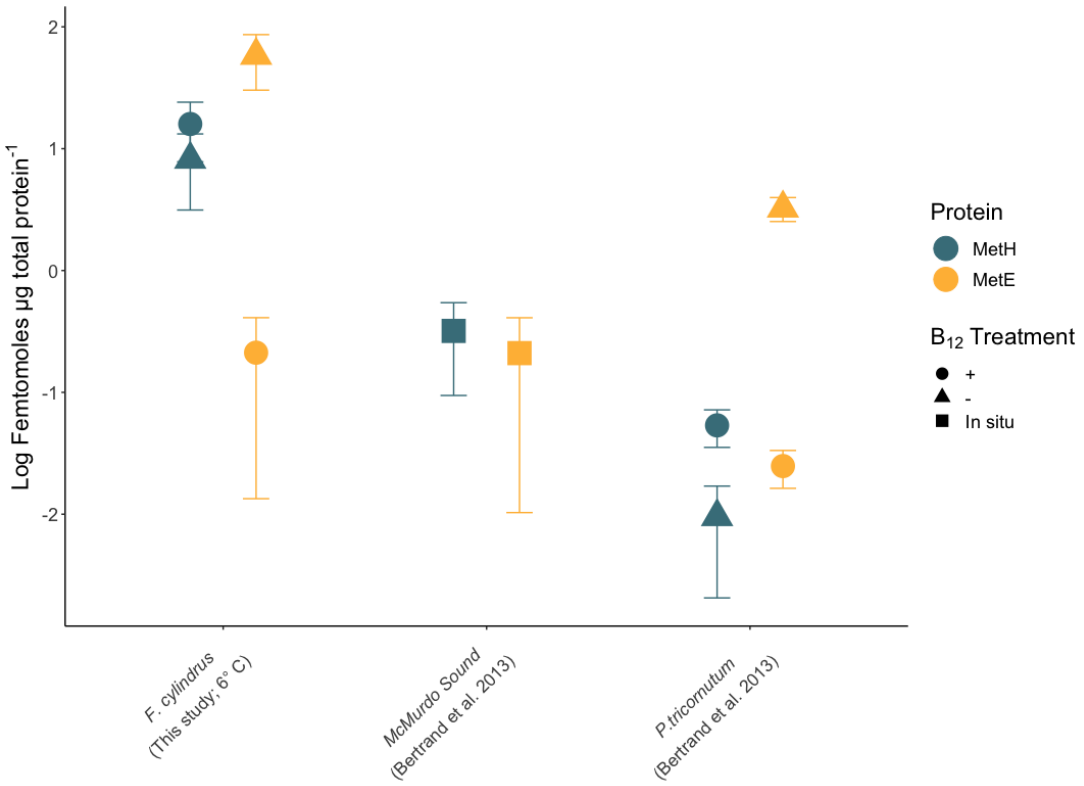

Figure 3.10: Measurements (femtomoles µg total protein^{-1}) of diagnostic MetH (blue) and MetE (yellow) peptide in F. *cylindrus* in this study, compared to measurements from *P. tricornutum* and environmental samples collected in McMurdo Sound, Antarctica in Bertrand *et al.,* 2013. B_{12} treatment is represented by shape, with circles denoting B_{12}-replete cultures and triangles B_{12}-deplete cultures. Environmental measurements taken *in situ* are shown as squares.

3.5.3 Cobalamin quotas – Mean B_{12} quotas in *F. cylindrus* (315.27 nmol mol C^{-1}) were comparable to measurements of cobalamin in *T. pseudonana* (800 ± 85 nmol mol C^{-1}) presented in Heal *et al.,* 2019. Additionally, experiments which measured B_{12} quotas in sea ice algae with a >90% diatom makeup, also demonstrated comparable values, with a mean of 550 nmol mol C^{-1} of cobalamin (Taylor & Sullivan 2008). Trace amounts of adenosylcobalamin were detected in B_{12}-deplete sample "e" (Supporting Information, Figure S3.7). However, this trend was not consistent throughout replicate injections (Supporting Information, Figure S3.7). It is possible that this compound was still present in samples without the addition of exogenous B_{12} due to carryover from when the culture

was initially inoculated. Another explanation is that there is analytical carryover between injections due to analytes remaining on the column. In the future, an increased number of blank injections should be run between samples to further explore this. Molar B_{12} to MetH ratios were much higher in *F. cylindrus* than expected (Table 3.1). There were six orders of magnitude more total available molecules of B_{12} and five more of solely methylcobalamin than could be used in MetH (Table 3.1). Mechanisms of B_{12} storage in diatoms have not been explored, but this result suggests luxury uptake and storage in the cell, and/or cryptic uses for B_{12} which have yet to be identified.

A rough estimation of uptake rate by *F. cylindrus* was calculated using the formula for specific uptake rate (0.048 attomoles d^{-1} $cell^{-1}$; Droop 1973). Considering published *F. cylindrus* cell densities in the Wendell Sea ice edge zone during late austral summer/early austral autumn, which were found to be 5.28×10^9 cells m^{-2}, integrated over the first 150 meters of water (Kang & Fryxell 1993), 1.7×10^6 attomoles L^{-1} d^{-1} would be taken up by *F. cylindrus* cells. Although B_{12} production rates in the SO remain largely unexplored, we can provide context for this rate by comparing it the few measurements of ambient dissolved B_{12}. Heal and colleagues' work suggests that the upper estimates of total dissolved B_{12} was 7 pM in Puget Sound, Washington (mostly composed of hydroxo- and adocobalamin; 5.8 and 1.2 pM, respectively; Heal *et al.,* 2014). In the case of a pulse of B_{12} at this concentration, an *F. cylindrus* community of the aforementioned size could take up all of the available B_{12} within 5.76 hours. This small timescale suggests that dense blooms of *F. cylindrus* may be capable of quickly taking up the majority of available B_{12} in the Southern Ocean, illustrating the disparity between B_{12} availability and B_{12} demands in the Southern Ocean. However, this value may be an underestimation as SO B_{12}

availability is expected to be less than values in Heal *et al.,* 2014 due absence of cyanobacteria and otherwise small populations of heterotrophic bacterial producers (Bertrand *et al.,* 2007).

3.5.4 Other Metabolic Effects – We were unable to detect the amino acids methionine and homocysteine in our samples. Targeted MS metabolite methods like ours tend to be biased against small polar molecules such as amino acids (Johnson *et al.,* 2017). The abundance of most metabolites examined here (SAM, SAH, B1, GBT, Proline) did not change with B_{12} deprivation. However, contrary to original hypotheses, DMSP content increased in B_{12}-deprived cultures rather than decreased, as was observed by Heal *et al.,* 2019. Heal and colleagues hypothesized that the decrease in DMSP production in *T. pseudonana* in B_{12}-deplete condition was driven by methionine deprivation. DMSP production in many eukaryotes is known to be catalyzed by DYSB enzymes which facilitate SAM-dependent MMT (methylthiohydroxybutryate methyltransferases) reactions (Curson et al., 2018). In *F. cylindrus*, we did not observe significant changes to SAM content, which may explain the absence of a decrease in DMSP production. DMSP is a precursor to DMS, which is a key player in the sulfur cycle, in addition to its climactic importance as a cloud forming nucleus (Charlson *et al.,* 1987). Additionally, DMSP is hypothesized to be a significant carbon and sulfur source for bacteria in some environments (Kiene *et al.,* 2000). Studies place pennate diatoms such as *Fragilariopsis spp.* among significant DMSP producers in the SO (Sheehan *et al.,* 2020). Increases in DMSP production in *F. cylindrus* due to B_{12} deprivation could potentially increase dissolved DMSP concentrations in the Southern Ocean via senescence-driven release during bloom termination. This increase in DMSP could fuel bacterial growth, accelerating the microbial loop and decreasing carbon export.

Furthermore, there is potential for a negative feedback loop between B_{12} deprivation and production via DMSP exchange, as heterotrophic bacteria and chemoautotrophic archaea are known to be the main cobalamin producers in the absence of cyanobacteria in the Antarctic waters (Doxey *et al.,* 2015). This increase in DMSP production should be further explored, with emphasis on improving our method for quantification of this compound in order to present absolute DMSP quotas in the presence and absence of vitamin B_{12}.

The abundance of cHET, which is a precursor for *de novo* synthesis of vitamin B1, also increased with B_{12} deprivation. It has been postulated that vitamin B_1 biosynthesis and B_{12} availability may be linked due to connections related to sulfur metabolism. cHET has been observed to be used in place of vitamin B_1 by microalgal eukaryotes when provided with HMP, another precursor to vitamin B_1 biosynthesis (Paerl *et al.,* 2018). HMP was found in trace concentration in B_{12}-replete samples and not detected in B_{12}-deprived samples. Bertrand *et al.,* 2012 found that the thiamine biosynthesis protein ThiC was more abundant in response to B_{12} deprivation and postulated whether it might be activated in response to SAM starvation. The changing balance in the abundance of these two vitamin B_1 precursors, despite absence of SAM starvation, implies that there may be an upstream control to their dynamics that may not regulated be directly regulated by SAM, but rather B_{12} availability, warranting further investigation.

3.5.5 Conclusions – Our results provide baseline physiological information about cold-adapted diatom's responses to vitamin B_{12} deprivation. We postulate that *F. cylindrus'* physiological parameters are not as firmly regulated by the availability of the vitamin as organisms that display decreases to growth rate under B_{12} scarcity such as *T. pseudonana*

(without MetE) and *P. tricornutum* (with MetE) (Heal *et al.,* 2019; Bertrand *et al.,* 2012). The disparity between the effects of utilizing B_{12}-dependent methionine synthesis as compared to the B_{12}-independent pathway may be smaller in *F. cylindrus* due to a decreased functionality of the MetH enzyme at low temperatures, as evidenced by increased MetH quotas compared to *P. tricornutum* and the difference in the magnitude of MetE and MetH responses (Figure 3.10). The maximal difference in MetE abundance changes in F. cylindrus was much less than that of MetH, emphasizing the difference in cost of use between the two enzymes. Furthermore, *F. cylindrus* B_{12} quotas were also much higher than could be used in MetH at a time suggesting luxury uptake and storage and/or use in unidentified B_{12}-requiring enzymes. Lastly, the change in abundance of metabolites, including DMSP and cHET, highlight that growth rate should not be considered the sole method for assessing the impact of nutrient deprivation in marine phytoplankton. In this study, the effects of B_{12} scarcity catalyzed changes that may have putative impacts to *F. cylindrus'* role in its wider community via the potential synthesis and differential production of growth stimulating and climatically significant compounds.

Chapter IV: Conclusions

Overview – This dissertation aimed to characterize the molecular consequences of B_{12} deprivation in an ecologically significant polar diatom. Chapter II investigated the interactive proteomic responses of B_{12} and elevated temperature. In this chapter, I found that proteomic biomarkers typically used to survey vitamin B_{12} limitation *in situ* are reliable for *F. cylindrus*, even at lethal temperatures. Furthermore, I identified a host of proteins differentially expressed in response to the combined stressors. Lastly, there were hints of a putative B_{12} remodelling pathway in this diatom, which warrants additional investigation. Chapter III examined the effects of vitamin B_{12} deprivation on diatom physiology and metabolite production, in addition to presenting the first direct measurements of cellular B_{12} quotas in *Fragilariopsis cylindrus.* We observed that *F. cylindrus* took up more B_{12} than could be used in MetH, which appears to be the main B_{12}-requiring enzymes in eukaryotes, suggesting luxury uptake, and raising questions regarding the existence of additional cryptic B_{12}-utilizing enzymes. We also noted the increased production of DMSP and thiamine related compounds in B_{12} deprived cultures. Changes to DMSP production are particularly intriguing and suggest that *F. cylindrus* may stimulate bacterial growth in the absence of B_{12}.

Recommended Future Works – There are a few experiments which could be conducted in order to expand on the research presented here. In Chapter II, we tested to see if *F. cylindrus* experiences B_{12}-mediated heat resistance, as was presented in *C. reinhardtii* by Xie et al., 2013. We determined that B_{12} did not confer heat stress tolerance in *F. cylindrus*, but were not able to propose a mechanism for the difference in responses. MetE transcripts declined in *C. reinhardtii* at lethal temperatures. In contrast, we were able to detect the protein in *F.*

cylindrus after exposure to lethal temperatures. However, it is possible we detected MetE peptides after transcripts had already decreased *in F. cylindrus.* In order to elucidate the reason for the difference in responses between *F. cylindrus* and *C. reinhardtii,* a time series experiment should be conducted with protein and transcript measurements in both organisms. The difference in activity of *F. cylindrus* and *C. reinhardtii* MetH and MetE should also be compared at a range of temperatures. Chapter II also presented possible evidence that *F. cylindrus* may be able to remodel degraded cobalamin molecules with a chimeric Co-chelatase. *F. cylindrus'* ability to utilize portions of degraded cobalamin molecules and DMB should be explored using multifactorial experiments in a -MetE mutant.

In Chapter III, it was postulated that *F. cylindrus* maintains a high baseline MetH expression compared to *P. tricornutum* due to decreased methionine synthesis capacity at low temperatures. The catalysis rate of MetH and MetE at temperatures of 37 °C and higher has been measured in *E. coli* (Grabowski *et al.,* 2012), but not at lower temperatures to our knowledge. The activity of these enzymes at temperatures between -2 °C and 37 °C should be quantified in order to continue to examine this hypothesis in the context of psychrophiles. Lastly, the quotas of major osmolytes in *F. cylindrus* (DMSP, proline, and GBT, and homarine; Boroujerdi *et al.,* 2012) under vitamin B_{12} deprivation should be quantified. We were able to provide relative quantification of DMSP between treatments for our samples, but absolute quantification would allow for calculations of carbon and sulfur availability to heterotrophic bacteria from lysed *F. cylindrus* cells. For these measurements, our MS method can be altered to facilitate better quantification of these metabolites.

Implications & Significance – As researchers studying microbial ecophysiology, we attempt to make assertations about the nature of organism function under varying environmental conditions. This is conducted in careful, controlled environments, and in the case of these experiments and many others, with a single organism in isolation. Additionally, changes to growth rate have been historically considered the prominent method for assessing nutrient limitation. However, these idealized conditions and narrow scope fail to capture the notion that microbial eukaryotes like *F. cylindrus* inhabit complex and diverse assemblages that freely exchange compounds for energy, signalling, and a variety of other purposes. Thereby, any response to an environmental variable has the possibility to impact others in the community, leading to cascading consequences. We still possess only a shallow understanding of the granularity required to address the consequences of micronutrient limitation on microbial interactions (Worden *et al.,* 2015). This research, along with other proteomic and metabolomic studies both in culture and *in situ*, contributes information that begins to allow us to unravel the mystery of microbial function and interactions in the face of stressors like vitamin B_{12} deprivation.

Sources Cited

Alderkamp AC, Kulk G, Buma AGJ, Visser RJW, Van Dijken GL, Mills MM, Arrigo KR. **2012**. The effect of iron limitation on the photophysiology of *Phaeocystis antarctica* (prymnesiophyceae) and *Fragilariopsis cylindrus* (bacillariophyceae) under dynamic irradiance. *Journal of Phycology* **48**: 45–59.

Antonov I V. 2021. Two cobalt chelatase subunits can be generated from a single chld gene via programed frameshifting. *Molecular Biology and Evolution* **37**: 2268–2278.

Arrigo KR, van Dijken GL, Bushinsky S. **2008**. Primary production in the Southern Ocean, 1997-2006. *Journal of Geophysical Research: Oceans* **113**: 1997–2006.

Ayers GP, Cainey JM. **2007**. The CLAW hypothesis: A review of the major developments. *Environmental Chemistry* **4**: 366–374.

Ballantyne AP, Alden CB, Miller JB, Trans PP, White JWC. **2012**. Increase in observed net carbon dioxide uptake by land and oceans during the past 50 years. *Nature* **488**: 70–73.

Banerjee R V., Matthews RG. **1990**. Cobalamin-dependent methionine synthase. *The FASEB Journal* **4**: 1450–1459.

Banerjee R V., Ragsdale SW. **2003**. The many faces of vitamin B_{12}: Catalysis by cobalamin-dependent enzymes. *Annual Review of Biochemistry* **72**: 209–247.

Barker JD, Sharp MJ, Fitzsimons SJ, Turner RJ. **2006**. Abundance and dynamics of dissolved organic carbon in glacier systems. *Arctic, Antarctic, and Alpine Research* **38**: 163–172.

Bender DA. 2003. Nutritional biochemistry of the vitamins. Cambridge university press.

Bertrand EM, Allen AE, Dupont CL, Norden-Krichmar TM, Bai J, Valas RE, Saito MA. **2012**. Influence of cobalamin scarcity on diatom molecular physiology and identification of a cobalamin acquisition protein. *Proceedings of the National Academy of Sciences of the United States of America* **109**: E1762–E1771.

Bertrand EM, Allen AE. **2012**. Influence of vitamin B auxotrophy on nitrogen metabolism in eukaryotic phytoplankton. *Frontiers in Microbiology* **3**: 1–16.

Bertrand EM, McCrow JP, Moustafa A, Zheng H, McQuaid JB, Delmont TO, Post AF, Sipler RE, Spackeen JL, Xu K, *et al.* 2015. Phytoplankton–bacterial interactions mediate micronutrient colimitation at the coastal Antarctic sea ice edge. *Proceedings of the National Academy of Sciences* **112**: 9938–9943.

Bertrand EM, Moran DM, McIlvin MR, Hoffman JM, Allen AE, Saito MA. **2013**. Methionine synthase interreplacement in diatom cultures and communities: Implications for the persistence of B_{12} use by eukaryotic phytoplankton. *Limnology and Oceanography* **58**: 1431–1450.

Bertrand EM, Saito MA, Lee PA, Dunbar RB, Sedwick PN, Ditullio GR. **2011**. Iron limitation of a springtime bacterial and phytoplankton community in the Ross Sea: Implications for vitamin B_{12} nutrition. *Frontiers in Microbiology* **2**: 932–941.

Bertrand EM, Saito MA, Rose JM, Riesselman CR, Lohan MC, Noble AE, Lee PA, DiTullio GR. **2007**. Vitamin B_{12} and iron colimitation of phytoplankton growth in the Ross Sea. *Limnology and Oceanography* **52**: 1079–1093.

Boroujerdi AFB, Lee PA, DiTullio GR, Janech MG, Vied SB, Bearden DW. 2012. Identification of isethionic acid and other small molecule metabolites of *Fragilariopsis*

cylindrus with nuclear magnetic resonance. Analytical and Bioanalytical Chemistry 404: 777–784.

Boyd PW. **2002**. Environmental factors controlling phytoplankton processes in the Southern Ocean. *Journal of Phycology* **38**: 844–861.

Boysen AK, Heal KR, Carlson LT, Ingalls AE. **2018**. Best-Matched Internal Standard Normalization in Liquid Chromatography-Mass Spectrometry Metabolomics Applied to Environmental Samples. *Analytical Chemistry* **90**: 1363–1369.

Browning TJ, Achterberg EP, Rapp I, Engel A, Bertrand EM, Tagliabue A, Moore CM. **2017**. Nutrient co-limitation at the boundary of an oceanic gyre. *Nature* **551**: 242–246.

Carlucci AF, Silbernagel SB, McNally PM. **1969**. Influence of Temperature and Solar Radiation on Persistence of Vitamin B_{12}, Thiamine, and Biotin in Seawater. *Journal of Phycology* **5**: 302–305.

Charlson RJ, Lovelock JE, Andreaei MO, Warren SG. **1987**. Oceanic phytoplankton, atmospheric sulphur, cloud. *Nature* **330**: 1987.

Chatterjee A, Li Y, Zhang Y, Grove TL, Lee M, Krebs C, Booker SJ, Begley TP,Ealik SE. **2008**. Reconstitution of ThiC in thiamine pyrimidine biosynthesis expands the radical SAM superfamily. *Nature Chemical Biology* **4**: 758–765.

Collins T, Margesin R. **2019**. Psychrophilic lifestyles: mechanisms of adaptation and biotechnological tools. *Applied Microbiology and Biotechnology* **103**: 2857–2871.

Cooper MB, Kazamia E, Helliwell KE, Kudahl UJ, Sayer A, Wheeler GL, Smith AG. **2019**. Cross-exchange of B-vitamins underpins a mutualistic interaction between Ostreococcus tauri and Dinoroseobacter shibae. *ISME Journal* **13**: 334–345.

Cox EJ. **2014**. Diatom identification in the face of changing species concepts and evidence of phenotypic plasticity. *Journal of Micropalaeontology* **33**: 111–120.

Croft MT, Lawrence AD, Raux-Deery E, Warren MJ, Smith AG. **2005**. Algae acquire vitamin B_{12} through a symbiotic relationship with bacteria. *Nature* **438**: 90–93.

Croft MT, Warren MJ, Smith AG. **2006**. Algae need their vitamins. *Eukaryotic Cell* **5**: 1175–1183.

Curson ARJ, Williams BT, Pinchbeck BJ, Sims LP, Martínez AB, Rivera PPL, Kumaresan D, Mercadé E, Spurgin LG, Carrión O, *et al.* 2018. DSYB catalyses the key step of dimethylsulfoniopropionate biosynthesis in many phytoplankton. *Nature Microbiology* **3**: 430–439.

de Baar HJW. **1994**. von Liebig's law of the minimum and plankton ecology (1899-1991). *Progress in Oceanography* **33**: 347–386.

Depauw FA, Rogato A, D'Alcalá MR, Falciatore A. **2012**. Exploring the molecular basis of responses to light in marine diatoms. *Journal of Experimental Botany* **63**: 1575–1591.

Dos Santos CV, Cuiné S, Rouhier N, Rey P. **2005**. The *Arabidopsis* plastidic methionine sulfoxide reductase B proteins. Sequence and activity characteristics, comparison of the expression with plastidic methionine sulfoxide reductase A, and induction by photooxidative stress. *Plant Physiology* **138**: 909–922.

Doxey AC, Kurtz DA, Lynch MDJ, Sauder LA, Neufeld JD. **2015**. Aquatic metagenomes implicate Thaumarchaeota in global cobalamin production. *ISME Journal* **9**: 461–471.

Droop MR. **1968**. Vitamin B_{12} and Marine Ecology. IV. The Kinetics of Uptake, Growth and Inhibition in Monochrysis Lutheri. *Journal of the Marine Biological Association of the United Kingdom* **48**: 689–733.

Droop MR. **1973**. Some Thoughts on Nutrient Limitation in Algae. *Journal of Phycology* **9**: 264–272.

Ducklow HW, Steinberg DK, Buesseler KO. **2001**. Upper ocean carbon export and the biological pump. *Oceanography* **14**: 50–58.

Ellis KA, Cohen NR, Moreno C, Marchetti A. **2017**. Cobalamin-independent Methionine Synthase Distribution and Influence on Vitamin B_{12} Growth Requirements in Marine Diatoms. *Protist* **168**: 32–47.

Eppley R W. **1972**. Temperature and Phytoplankton Growth in the Sea. *Fishery Bulletin* **70**: 1063–1085.

Faktorová D, Nisbet E, Fernández Robledo J, Casacuberta E, Sudek L, Allen A, Ares Jr. M, Aresté C, Balestreri C, Barbrook A, *et al.* 2019. Genetic tool development in marine protists: Emerging model organisms for experimental cell biology. *Nature Methods*.

Falciatore A, Jaubert M, Bouly JP, Bailleul B, Mock T. **2020**. Diatom molecular research comes of age: Model species for studying phytoplankton biology and diversity[open]. *Plant Cell* **32**: 547–572.

Feller G. **2013**. Psychrophilic Enzymes: From Folding to Function and Biotechnology. *Scientifica* **2013**: 1–28.

Ferreira F, Straus NA. **1994**. Iron deprivation in cyanobacteria. *Journal of Applied Phycology* **6**: 199–210.

Field CB. **1998**. Primary Production of the Biosphere: Integrating Terrestrial and Oceanic Components. *Science* **281**: 237–240.

Fodje MN, Hansson A, Hansson M, Olsen JG, Gough S, Willows RD, Al-Karadaghi S. **2001**. Interplay between an AAA module and an integrin I domain may regulate the function of magnesium chelatase. *Journal of Molecular Biology* **311**: 111–122.

Folt CL, Chen CY, Moore M V., Burnaford J. **1999**. Synergism and antagonism among multiple stressors. *Limnology and Oceanography* **44**: 864–877.

Geider RJ, La Roche J. **2002**. Redfield revisited: Variability of C:N:P in marine microalgae and its biochemical basis. *European Journal of Phycology* **37**: 1–17.

Gobler CJ, Norman C, Panzeca C, Taylor GT, Sañudo-Wilhelmy SA. **2007**. Effect of B-vitamins (B_1, B_{12}) and inorganic nutrients on algal bloom dynamics in a coastal ecosystem. *Aquatic Microbial Ecology* **49**: 181–194.

Grabowski M, Banasiuk R, Wegrzyn A, Kedzierska B, Lica J, Banecka-Majkutewicz Z, Banecki B. **2012**. Role of heat-shock proteins and cobalamine in maintaining methionine synthase activity. *Acta Biochimica Polonica* **59**: 489–493.

Gross EM. **2003**. Allelopathy of aquatic autotrophs. *Critical Reviews in Plant Sciences* **22**: 313–339.

Guillard RRL, Ryther JH. **1962**. Studies of marine planktonic diatoms. I. *Cyclotella nana* Hustedt, and *Detonula confervacea* (cleve) Gran. *Canadian journal of microbiology* **8**: 229–239.

Guillard RRL. 1975. Culture of Phytoplankton for Feeding Marine Invertebrates. In: Smith WL, Chanley MH, eds. *Culture of Marine Invertebrate Animals*. Boston, MA: Springer, 29-60

Harding K, Turk-Kubo KA, Sipler RE, Mills MM, Bronk DA, Zehr JP. **2018**. Symbiotic unicellular cyanobacteria fix nitrogen in the Arctic Ocean. *Proceedings of the National Academy of Sciences of the United States of America* **115**: 13371–13375.

Heal KR, Carlson LT ruxa., Devol AH, Armbrust EV, Moffett JW, Stahl DA, Ingalls AE. **2014**. Determination of four forms of vitamin B_{12} and other B vitamins in seawater by liquid chromatography/tandem mass spectrometry. *Rapid communications in mass spectrometry : RCM* **28**: 2398–2404.

Heal KR, Kellogg NA, Carlson LT, Lionheart RM, Ingalls AE. **2019**. Metabolic Consequences of Cobalamin Scarcity in the Diatom Thalassiosira pseudonana as Revealed Through Metabolomics. *Protist* **170**: 328–348.

Heal KR, Qin W, Ribalet F, Bertagnolli AD, Coyote-Maestas W, Hmelo LR, Moffett JW, Devol AH, Armbrust EV, Stahl DA, *et al.* 2017. Two distinct pools of B_{12} analogs reveal community interdependencies in the ocean. *Proceedings of the National Academy of Sciences of the United States of America* **114**: 364–369.

Helliwell KE, Lawrence AD, Holzer A, Kudahl UJ, Sasso S, Kräutler B, Scanlan DJ, Warren MJ, Smith AG. **2016**. Cyanobacteria and Eukaryotic Algae Use Different Chemical Variants of Vitamin B_{12}. *Current Biology* **26**: 999–1008.

Helliwell KE, Wheeler GL, Leptos KC, Goldstein RE, Smith AG. **2011**. Insights into the evolution of vitamin B 12 auxotrophy from sequenced algal genomes. *Molecular Biology and Evolution* **28**: 2921–2933.

Helliwell KE. **2017**. The roles of B vitamins in phytoplankton nutrition: New perspectives and prospects. *New Phytologist*.

Hutner SH, Provasoli L, Stockstad ELR, Hoffmann CE, Belt M, Franklin AL, Jukesm TH. 1949. Assay of antipernicious anemia factor with Euglena. Proc Soc Exp Biol Med 70: 118—120

Jabre L, Bertrand EM. **2020**. Interactive effects of iron and temperature on the growth of *Fragilariopsis* cylindrus. *Limnology and Oceanography Letters*.

Johnson WM, Kido Soule MC, Kujawinski EB. **2017**. Extraction efficiency and quantification of dissolved metabolites in targeted marine metabolomics. *Limnology and Oceanography: Methods* **15**: 417–428.

Juzeniene A, Nizauskaite Z. **2013**. Photodegradation of cobalamins in aqueous solutions and in human blood. *Journal of Photochemistry and Photobiology B: Biology* **122**: 7–14.

Käll L, Canterbury JD, Weston J, Noble WS, MacCoss MJ. **2007**. Semi-supervised learning for peptide identification from shotgun proteomics datasets. *Nature Methods* **4**: 923–925.

Kanehisa M, Sato Y, Kawashima M, Furumichi M, Tanabe M. **2016**. KEGG as a reference resource for gene and protein annotation. *Nucleic Acids Research* **44**: D457–D462.

Kang SH, Fryxell GA. **1992**. *Fragilariopsis cylindrus* (Grunow) Krieger: The most abundant diatom in water column assemblages of Antarctic marginal ice-edge zones. *Polar Biology* **12**: 609–627.

Kang SH, Fryxell GA. **1993**. Phytoplankton in the Weddell Sea, Antarctica: composition, abundance and distribution in water-column assemblages of the marginal ice-edge zone during austral autumn. *Marine Biology: International Journal on Life in Oceans and Coastal Waters* **116**: 335–348.

Kennedy F, Martin A, Bowman JP, Wilson R, McMinn A. **2019**. Dark metabolism: a molecular insight into how the Antarctic sea-ice diatom *Fragilariopsis cylindrus* survives long-term darkness. *New Phytologist* **223**: 675–691.

Kiene RP, Linn LJ, Bruton JA. **2000**. New and important roles for DMSP in marine microbial communities. *Journal of Sea Research* **43**: 209–224.

Kiene RP, Linn LJ. **2000**. Distribution and turnover of dissolved DMSP and its relationship with bacterial production and dimethylsulfide in the Gulf of Mexico. *Limnology and Oceanography* **45**: 849–861.

Koch F, Hattenrath-Lehmann TK, Goleski JA, Sañudo-Wilhelmy S, Fisher NS, Gobler CJ. **2012**. Vitamin B_1 and B_{12} uptake and cycling by plankton communities in coastal ecosystems. *Frontiers in Microbiology* **3**: 1–11.

Liang Y, Koester JA, Liefer JD, Irwin AJ, Finkel Z V. 2019. Molecular mechanisms of temperature acclimation and adaptation in marine diatoms. *ISME Journal* **13**: 2415–2425.

Martin JH, Coale KH, Johnson KS, Fitzwater SE, Gordon RM, Tanner SJ, Hunter CN, Elrod VA, Nowicki JL, Coley TL, *et al.* 1994. Testing the iron hypothesis in ecosystems of the equatorial Pacific Ocean. *Nature* **371**: 123–129.

Martin JH. **1990**. Glacial-interglacial CO2 change: The Iron Hypothesis. *Paleoceanography* **5**: 1–13.

Michaels AF, Silver MW. 1988. Primary production, sinking fluxes and the microbial food web. *Deep Sea Research Part A, Oceanographic Research Papers*, **35**:473–490.

Mills MM, Kropuenske LR, Van Dijken GL, Alderkamp AC, Berg GM, Robinson DH, Welschmeyer NA, Arrigo KR. **2010**. Photophysiology in two southern ocean phytoplankton taxa: Photosynthesis of *Phaeocystis antarctica* (prymnesiophyceae) and

Fragilariopsis cylindrus (bacillariophyceae) under simulated mixed-layer irradiance. *Journal of Phycology* **46**: 1114–1127.

Minot GR, Murphy WP. **1926**. Treatment of pernicious anemia by a special diet. *Journal of the American Medical Association* **87**: 470–476.

Mock T, Hoch N. **2005**. Long-term temperature acclimation of photosynthesis in steady-state cultures of the polar diatom *Fragilariopsis cylindrus*. *Photosynthesis Research* **85**: 307–317.

Mock T, Robert P, Strauss J, Mcmullan M, Paajanen P, Schmutz J, Salamov A, Sanges R, Toseland A, Ward BJ, *et al.* 2017. Evolutionary genomics of the cold-adapted diatom *Fragilariopsis cylindrus*. *Nature Publishing Group* **541**: 536–540.

Moore CM, Mills MM, Arrigo KR, Berman-Frank I, Bopp L, Boyd PW, Galbraith ED, Geider RJ, Guieu C, Jaccard SL, *et al.* 2013. Processes and patterns of oceanic nutrient limitation. *Nature Geoscience* **6**: 701–710.

Mühlhaus T, Weiss J, Hemme D, Sommer F, Schroda M. **2011**. Quantitative shotgun proteomics using a uniform 15N-labeled standard to monitor proteome dynamics in time course experiments reveals new insights into the heat stress response of *Chlamydomonas reinhardtii*. *Molecular and Cellular Proteomics* **10**: 1–27.

Obeid R, Fedosov SN, Nexo E. 2015. Cobalamin coenzyme forms are not likely to be superior to cyano- and hydroxyl-cobalamin in prevention or treatment of cobalamin deficiency. *Molecular Nutrition and Food Research* **59**: 1364–1372.

Oborník M, Green BR. **2005**. Mosaic origin of the heme biosynthesis pathway in photosynthetic eukaryotes. *Molecular Biology and Evolution* **22**: 2343–2353.

Ortiz-Guerrero JM, Polanco MC, Murillo FJ, Padmanabhan S, Elías-Arnanz M. **2011**. Light-dependent gene regulation by a coenzyme B_{12}-based photoreceptor. *Proceedings of the National Academy of Sciences of the United States of America* **108**: 7565–7570.

Paerl RW, Bertrand EM, Rowland E, Schatt P, Mehiri M, Niehaus TD, Hanson AD, Riemann L, Yves-Bouget F. **2018**. Carboxythiazole is a key microbial nutrient currency and critical component of thiamin biosynthesis. *Scientific Reports* **8**: 1–8.

Panzeca C, Beck AJ, Leblanc K, Taylor GT, Hutchins DA, Sañudo-Wilhelmy SA. **2008**. Potential cobalt limitation of vitamin B_{12} synthesis in the North Atlantic Ocean. *Global Biogeochemical Cycles* **22**: 1–7.

Petrou K, Kranz SA, Doblin MA, Ralph PJ. **2012**. Photophysiological responses of *Fragilariopsis cylindrus* (bacillariophyceae) to nitrogen depletion at two temperatures. *Journal of Phycology* **48**: 127–136.

Pilson MEQ. **2012**. *An Introduction to the Chemistry of the Sea*.

Plubell DL, Wilmarth PA, Zhao Y, Fenton AM, Minnier J, Reddy AP, Klimek J, Yang X, David LL, Pamir N. **2017**. Extended multiplexing of tandem mass tags (TMT) labeling reveals age and high fat diet specific proteome changes in mouse epididymal adipose tissue. *Molecular and Cellular Proteomics* **16**: 873–890.

Price NM, Harrison GI, Hering JG, Hudson RJ, Nirel PM V., Palenik B, Morel FMM. **1989**. Preparation and Chemistry of the Artificial Algal Culture Medium Aquil. *Biological Oceanography* **6**: 443–461.

Protifi. 2022. S-trap mini spin column digestion:Protocol. Retrieved from **https://files.protifi.com/protocols/s-trap-mini-long-4-1.pdf**.

Provasoli L, Carlucci AF. 1974. Vitamins and growth regulators, p. 741–787. In W. D. P. Stewart (ed.), Algal physiology and biochemistry. Blackwell Scientific Publications, Oxford, United Kingdom

Rao D. **2020**. *Characterizing cobalamin cycling by Antarctic marine microbes across multiple scales*. PhD thesis, Massachusetts Institute of Technology, Cambridge, MA, USA

Raux E, Schubert HL, Warren MJ. **2000**. Biosynthesis of cobalamin (vitamin B_{12}): A bacterial conundrum. *Cellular and Molecular Life Sciences* **57**: 1880–1893.

Redfield AC, Ketchum BH, Richards F a. **1963**. The influence of organisms on the composition of sea water. *The sea* **2**: 26–77.

Redfield AC. **1958**. The Biological Control of Chemical Factors in the Environment. **46**: 205–221.

Rodionov DA, Vitreschak AG, Mironov AA, Gelfand MS. **2003**. Comparative Genomics of the Vitamin B_{12} Metabolism and Regulation in Prokaryotes. *Journal of Biological Chemistry* **278**: 41148–41159.

Roje S. **2006**. S-Adenosyl-l-methionine: Beyond the universal methyl group donor. *Phytochemistry* **67**: 1686–1698.

Sackett O, Petrou K, Reedy B, Grazia A De, Hill R, Doblin M, Ralph P, Heraud P. **2013**. Phenotypic Plasticity of Southern Ocean Diatoms : Key to Success in the Sea Ice Habitat? **8**: 1–12.

Sallée J-B, Llort J, Tagliabue A, Lévy M. **2015**. Characterization of distinct bloom phenology regimes in the Southern Ocean. *ICES Journal of Marine Science* **72**: 1985–1998.

Sando GN, Blakley RL, Hogenkamp HPC, Hoffmann PJ. **1975**. Studies on the mechanism of adenosylcobalamin dependent ribonucleotide reduction by the use of analogs of the coenzyme. *Journal of Biological Chemistry* **250**: 8774–8779.

Sañudo-Wilhelmy SA, Gobler CJ, Okbamichael M, Taylor GT. **2006**. Regulation of phytoplankton dynamics by vitamin B_{12}. *Geophysical Research Letters* **33**: 10–13.

Sañudo-Wilhelmy SA, Gómez-Consarnau L, Suffridge C, Webb EA. **2014**. The role of B vitamins in marine biogeochemistry. *Annual Review of Marine Science* **6**: 339–367.

Sarmiento JL, Gruber N, Brzezinski MA, Dunne JP. **2004**. High-latitude controls of thermocline nutrients and low latitude biological productivity. *Nature* **427**: 56–60.

Sato D, Nozaki T. **2009**. Methionine gamma-lyase: The unique reaction mechanism, physiological roles, and therapeutic applications against infectious diseases and cancers. *IUBMB Life* **61**: 1019–1028

Scott JM, Weir DG. **1981**. The methyl folate trap. *The Lancet* **318**: 337–340.

Shane B, Stokstad EL. **1985**. Vitamin B_{12} -folate interrelationships. *Annual review of nutrition* **5**: 115–141.

Sheehan CE, Petrou K. **2020**. Dimethylated sulfur production in batch cultures of Southern Ocean phytoplankton. *Biogeochemistry* **147**: 53–69.

Stefels J. **2000**. Physiological aspects of the production and conversion of DMSP in marine algae and higher plants. *Journal of Sea Research* **43**: 183–197.

Suffridge C, Cutter L, Sañudo-Wilhelmy SA. **2017**. A new analytical method for direct measurement of particulate and dissolved B-vitamins and their congeners in seawater. *Frontiers in Marine Science* **4**: 1–11.

Suh SJ, Escalante-Semerena JC. **1993**. Cloning, sequencing and overexpression of cob A which encodes ATP:corrinoid adenosyltranferase in Salmonella typhimurium. *Gene* **129**: 93–97.

Sunda WG, Price NM, Morel FM. 2005. Trace Metal Ion Buffers And Their Use In Culture Studies. In: Andersen RA, eds. *Algal Culturing Techniques*. Burlington, MA: Academic Press, 35-63

Taylor GT, Sullivan CW. **2008**. Vitamin B_{12} and cobalt cycling among diatoms and bacteria in Antarctic sea ice microbial communities. *Limnology and Oceanography* **53**: 1862–1877.

Webb-Robertson BJM, Wiberg HK, Matzke MM, Brown JN, Wang J, McDermott

JE, Smith RD, Rodland KD, Metz TO, Pounds JG, *et al.* 2015. Review, evaluation, and discussion of the challenges of missing value imputation for mass spectrometry-based label-free global proteomics. *Journal of Proteome Research* **14**: 1993–2001.

Sunda WG, Huntsman SA. **1998**. Interactive effects of external manganese , the toxic metals copper and zinc , and light in controlling cellular manganese and growth in a coastal diatom. **43**: 1467–1475.

Tanioka Y, Yabuta Y, Yamaji R, Shigeoka S, Nakano Y, Watanabe F, Inui H. **2009**. Occurrence of pseudovitamin B_{12} and its possible function as the cofactor of cobalamin-dependent methionine synthase in a cyanobacterium Synechocystis sp. PCC6803. *Journal of Nutritional Science and Vitaminology* **55**: 518–521.

Taylor GT, Sullivan CW. **2008**. Vitamin B_{12} and cobalt cycling among diatoms and bacteria in Antarctic sea ice microbial communities. *Limnology and Oceanography* **53**: 1862–1877.

Taylor RT, Weissbach H. **1973**. N5-Methyltetrahydrofolate-Homocysteine Meihyltransferases. *Enzymes* **9**: 121–165.

Toseland A, Daines SJ, Clark JR, Kirkham A, Strauss J, Uhlig C, Lenton TM, Valentin K, Pearson GA, Moulton V, *et al.* 2013. The impact of temperature on marine phytoplankton resource allocation and metabolism. *Nature Climate Change* **3**: 979–984.

Vancaester E, Depuydt T, Osuna-Cruz CM, Vandepoele K. **2020**. Comprehensive and functional analysis of horizontal gene transfer events in diatoms. *Molecular Biology and Evolution* **37**: 3243–3257.

Worden AZ, Follows MJ, Giovannoni SJ, Wilken S, Zimmerman AE, Keeling PJ. **2015**. Rethinking the marine carbon cycle: Factoring in the multifarious lifestyles of microbes. *Science* **347**.

Wu M, McCain JSP, Rowland E, Middag R, Sandgren M, Allen AE, Bertrand EM. **2019**. Manganese and iron deficiency in Southern Ocean *Phaeocystis antarctica* populations revealed through taxon-specific protein indicators. *Nature Communications* **10**: 1–10.

Xie B, Bishop S, Stessman D, Wright D, Spalding MH, Halverson LJ. **2013**. *Chlamydomonas reinhardtii* thermal tolerance enhancement mediated by a mutualistic interaction with vitamin B_{12}-producing bacteria. *ISME Journal* **7**: 1544–1555.

Xing GL, Yuan HL, Yang JS, Li JY, Gao QX, Li WL, Wang ET. **2018**. Integrated analyses of transcriptome, proteome and fatty acid profilings of the oleaginous microalga Auxenochlorella protothecoides UTEX 2341 reveal differential reprogramming of fatty acid metabolism in response to low and high temperatures. *Algal Research* **33**: 16–27.

Xu Y, Chen C, Ji D, Hang N, Xie C. **2014**. Proteomic profile analysis of Pyropia haitanensis in response to high-temperature stress. *Journal of Applied Phycology* **26**: 607–618.

Yachandra VK, Sauer K, Klein MP. **1996**. Manganese cluster in photosynthesis: Where plants oxidize water to dioxygen. *Chemical Reviews* **96**: 2927–2950.

Yi S, Seth EC, Men YJ, Stabler SP, Allen RH, Alvarez-Cohen L, Taga ME. **2012**. Versatility in corrinoid salvaging and remodeling pathways supports corrinoid-dependent metabolism in Dehalococcoides mccartyi. *Applied and Environmental Microbiology* **78**: 7745–7752.

Young JN, Schmidt K. **2020**. It's what's inside that matters: physiological adaptations of high-latitude marine microalgae to environmental change. *New Phytologist* **227**: 1307–1318.

Zhou ZS, Pearlso K, Penner-Hahn JE, Matthews RG. **1999**. Identification of the zinc ligands in cobalamin-independent methionine synthase (MetE) from Escherichia coli. *Biochemistry* **38**: 15915–15926.

Appendix A: Supporting Information

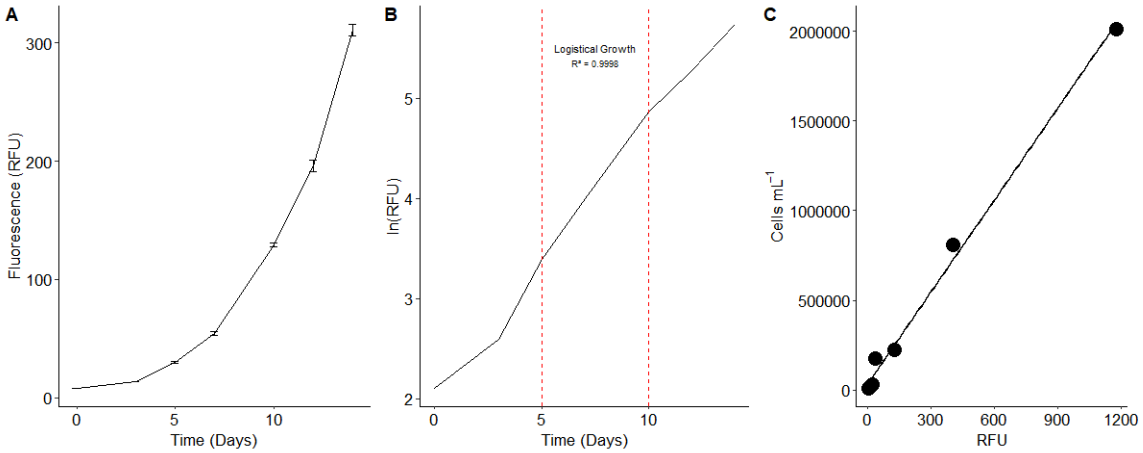

Figure S2.1: a) Fluorescence measurements in RFU (Relative Fluorescence Units) of a single culture of *F. cylindrus* with each symbol representing the mean of 3 technical replicates taken by a Turner hand-held fluorometer. Error bars represent standard deviation. Fluorescence is expected to increase proportionally with cell density due to the presence of chlorophyll-a. **b)** ln(RFU) of the same culture's growth. Exponential growth phase marked by the time points at which the lope of ln(RFU) is linear (between 29 and 129 RFU) . R= .9998**. c)** Regression demonstrating a linear relationship between cell counts and RFU measure on a Turner handheld fluorometer from *F. cylindrus* cells in the logistical stage of growth. R^2= .9941; y= 5.827e-04x - 1.866e+01.

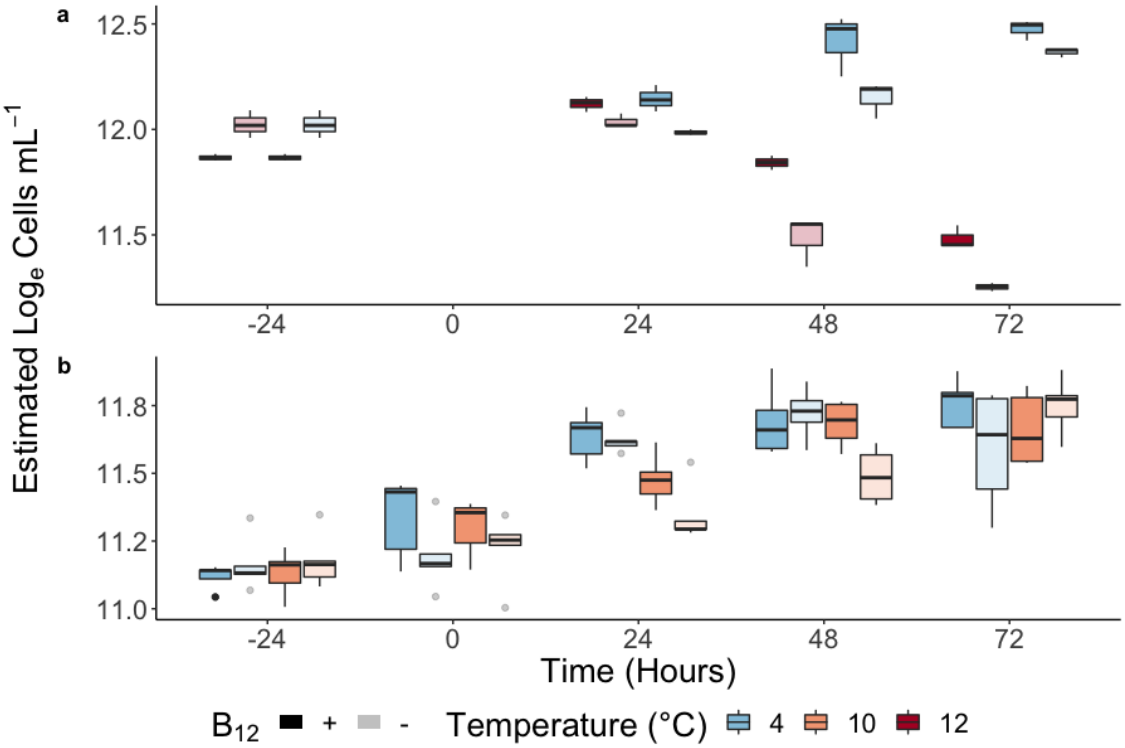

Figure S2.2: Boxplot of *F. cylindrus* cell densities over time after exposure to temperature treatments, estimated from chl-a fluorescence measured with a handheld fluorometer. **a)** Biomass was split and exposed to control (4 °C; blue), and lethal (12 °C; red) temperature treatments at 0 hours, and with and without the addition of vitamin B_{12} to the culture medium. Cell density declines over time after exposure to 12° C compared to control. **b)** Biomass was split and exposed to control (4 °C; blue), and sub-lethal (10 °C; orange) temperature treatments at 0 hours, and with and without the addition of vitamin B_{12} to the culture medium. Cell density in the 10 °C treatment remains similar to that of the control. In both plots, boxes show IQR (interquartile range), with horizontal lines denoting the median and vertical lines showing minimum and maximum values of 3 biological replicates per treatment. Color saturation represents B_{12} treatment, with translucent boxes representing B_{12}-deplete and saturated boxes representing B_{12} replete treatments.

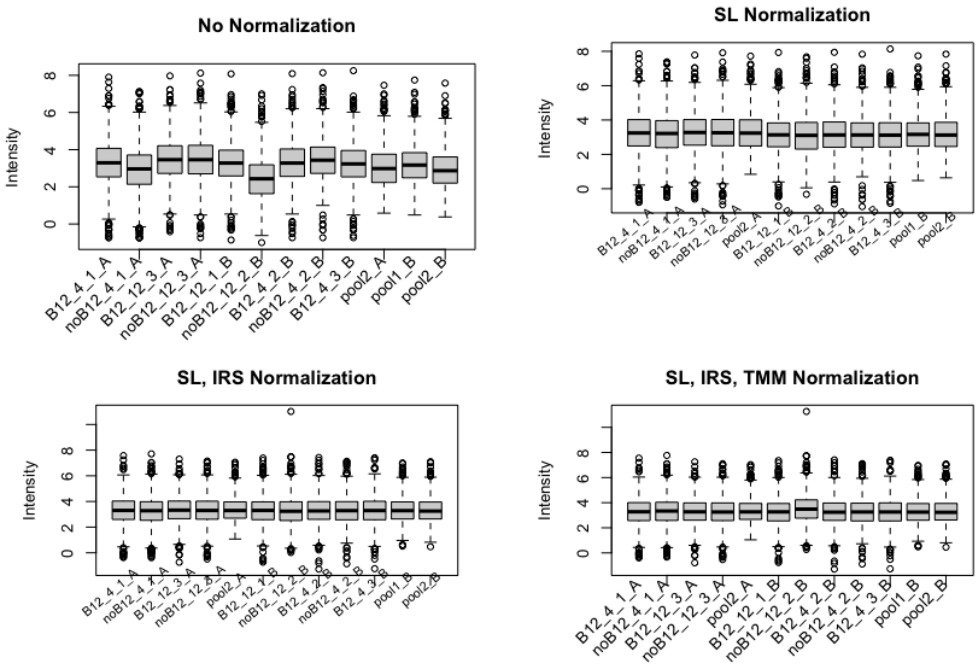

Figure S2.3: Plots showing the effects of each normalization step for protein data collected from the TMT discovery experiment. Protein intensity distributions are shown for each treatment or pool. Panel A shows protein intensities before normalization, panel B shows them after sample loading normalization, panel C shows them after internal reference scaling (IRS) normalization, and panel D shows them after trimmed mean of M-values (TMM) normalization. Sample names on the x-axis are denote treatment details as follows: B_{12} treatment (B_{12} or noB_{12}) temperature treatment (4 or 12 °C), replicate number (1, 2, or 3) and TMT pool (A or B).

Table S2.1: Wash steps for in-gel protein digestion procedure

Volume (µl)	Solvent	time (min.)	Temp (°C)	Note
1000	50% Acetonitrile 50% 100 mM Ammonium Bicarbonate	60	20	350 rpm shaking
1000	Acetonitrile	5	20	350 rpm shaking
300	10 mM Dithiothreitol, 100 mM Ammonium Bicarbonate	30	56	350 rpm shaking
1000	Acetonitrile	5	20	350 rpm shaking
1000	Acetonitrile	5	20	350 rpm shaking
300	55 mM IAM, 100 mM Ammonium Bicarbonate	30	20	incubate in the dark, no shaking
1000	Acetonitrile	5	20	350 rpm shaking
	Acetonitrile	5	20	350 rpm shaking
1000	100 mM Ambic	30	20	350 rpm shaking
1000	Acetonitrile	5	20	350 rpm shaking
	Acetonitrile	5	20	350 rpm shaking
1000	100 mM Ammonium Bicarbonate	30	20	350 rpm shaking
1000	50% Acetonitrile 50% 100 mM Ammonium Bicarbonate	30	20	350 rpm shaking
600	Acetonitrile	5	20	350 rpm shaking
600	Acetonitrile	5	20	350 rpm shaking
	Dry in vacufuge	15	-	Proceed to digestion or store at -80 °C

Table S2.2: Details of peptides analyzed for targeted proteomic analysis, including peptide sequence and charge, precusor and product m/z, fragment ions, collision enegry, and SRM rank (with 1 having greatest signal), retention time (RT), limit of detection (LOD), and limit of quantification (LOQ). Peptide details for MetE and MetH are from Bertrand *et al.,* 2012 and 2013, respectively.

Peptide name	Peptide (charge state)	Precursor (m/z)	Product (m/z)	Fragment ion	Collision Energy (V)	SRM rank	RT (min)	LOD	LOQ	Internal standard
F. cylindrus MetE	VIQVDEPALR(+2)	570.32	456.29	y4	26.8	1	20	0.2	0.6	
			700.36	y6	19.7	3				
			799.43	y7	19.1	2				
			927.49	y8	19.2	4				
	VIQVDEPAL(*13C15N*)R(+2)	573.83	463.31	y3	26.8	1				98% pure
			707.38	y4	19.7	3				
			806.45	y5	19.1	2				
			934.51	y6	19.2	4				
			588.31	y5	28	3				
			800.46	y7	32.7	4				
			1296.69	y12	26.8	2				
F. cylindrus MetH	ISGGISNLSFGFR(+2)	677.86	613.31	y5	23.9	2	27	0.2	1.3	
			840.44	y7	24.2	3				
			927.47	y8	24	1				
			1154.60	y11	24.6	4				
	ISGGISNL(*13C15N*)SFGFR(+2)	681.37	613.31	y5	23.9	2				99.8% pure
			847.45	y7	24.2	3				
			934.49	y8	24	1				
			1161.61	y11	24.6	4				

Table S2.3: Matrix of sample and pool labeling for tandem mass tagging (TMT) workflow. Each channel represents one of the ten TMT10plex isotopic labels. Each pool is one set of the two TMT10plexes used. Pools were made by mixing 10 µL of each sample. 44 µL of each sample and pool was labeled with 16 µL of corresponding TMT reagent. Samples are denoted by B_{12} (+/-B_{12}) and temperature (4 or 12) treatment. Some channels contained samples from a separate experiment not described in this manuscript.

	Channel									
Pool	**1**	**2**	**3**	**4**	**5**	**6**	**7**	**8**	**9**	**10**
A	+B_{12}/4	-B_{12}/4	+B_{12}/10	-B_{12}/10	+B_{12}/12	-B_{12}/12	+B_{12}/10	EMPTY	EMPTY	POOL
B	+B_{12}/12	-B_{12}/12	-B_{12}/12	+B_{12}/12	-B_{12}/10	+B_{12}/4	-B_{12}/4	+B_{12}/4	POOL	POOL

Table S2.4: Table demonstrating how the removal of treatments affects protein quantification yield after IRS normalization in the TMT experiment on *F. cylindrus* biomass 24 hours after exposure to high temperature treatment. We chose to exclude both B12_12_2_B and noB12_12_1_B from the analysis to increase the number of proteins which could be quantified2. Sample names indicate B_{12} treatment (B_{12} or noB_{12}), temperature treatment (4 or 12), biological replicate number (1, 2, or 3), and TMT experiment (either A or B, as we used two TMT 10plex sets) separated by underscores.

	Including all Samples	Removal of Sample B12_12_2_B	Removal of Samples B12_12_2_B and noB12_12_1_B
Number of Proteins for Relative Quantification	495	1344	1357

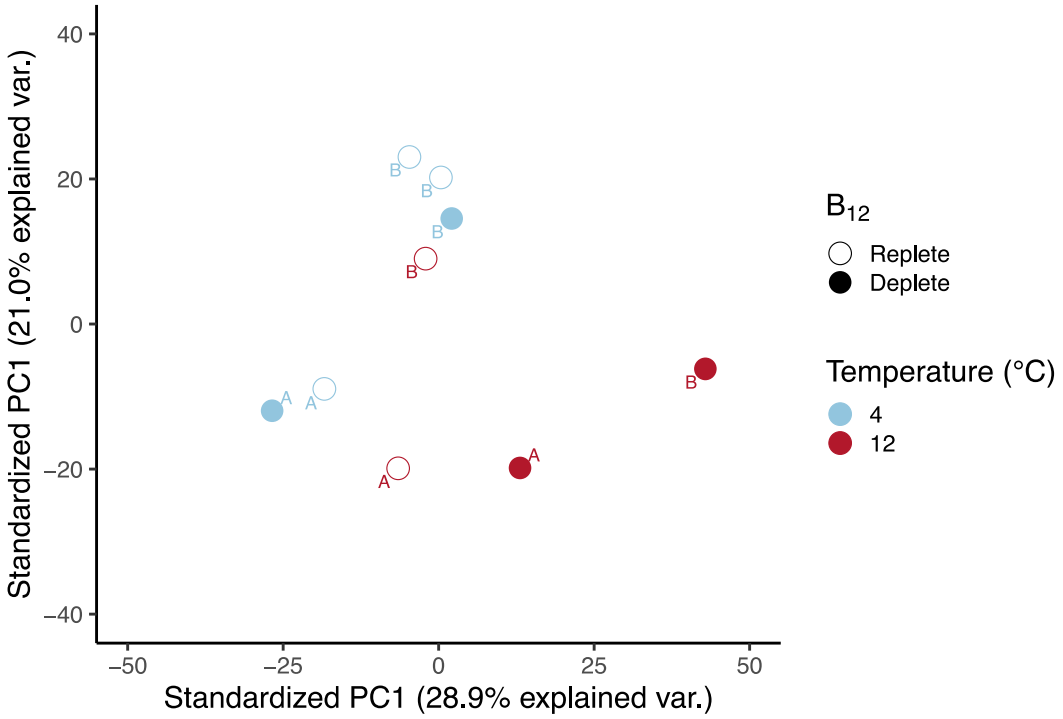

Figure S2.4: Principal component analysis of all normalized proteins observed in a TMT experiment with biomass from *F. cylindrus* cultures 24 hours after exposure to temperature treatments. Colors represent temperature treatment, with blue representing the control treatment (4 °C) and red representing the elevated temperature treatment (12 °C). Open circles represent B_{12}-replete cultures and closed circles represent B_{12}- deplete cultures. Each point is labeled by pool (either A or B, as we used two TMT 10plex sets).

Table S2.5: List of proteins differentially expressed in response to B_{12} deprivation in *F. cylindrus*. This list was generated by a pairwise comparison between control cultures (cultured at 4 °C in B_{12} replete media) and cultures grown at 4 °C with B_{12} deplete media. NCBI protein products, gene ID's and corresponding KEGG numbers (KO) are included. A negative fold change represents a protein that is downregulated in the absence of B_{12}.

Protein Product	Name	Gene ID	KO	log2 Fold Change	log2 mean spectral abundance	P-Value
OEU11144.1	MetE	228154	K00549	5.28	11.13	3.85E-06
OEU10229.1	protoporphyrin IX Mg-chelatase subunit D	247844	-	1.98	8.56	1.68E-03
OEU11214.1	CBA1	246327	-	2.44	9.37	1.84E-03
OEU18387.1	P-ATPase family transporter: zinc/lead/cadmium/mercury ion	168079	K01534	1.21	9.77	3.00E-03
OEU08987.1	T-complex protein 1 subunit gamma	195967	K09495	1.01	10.29	6.26E-03
OEU18337.1	P-loop containing nucleoside triphosphate hydrolase protein	274747	K12812	1.80	10.35	8.01E-03
OEU09871.1	ribosomal protein S12	271288	K02951	1.44	11.11	9.46E-03
OEU15295.1	hypothetical protein FRACYDRAFT_208848	208848	K14006	-1.20	9.00	1.95E-02
OEU21485.1	Cys_Met_Meta_PP-domain-containing protein	259901	-	-1.37	8.72	2.03E-02
QGA73596	photosystem I p700 chlorophyll A apoprotein B (chloroplast)	177336 2818	-	0.89	10.61	2.25E-02
OEU18451.1	hypothetical protein FRACYDRAFT_260397	260397	-	1.13	9.76	2.51E-02
OEU11984.1	casein kinase I delta	211208	K08959	-1.30	9.26	2.58E-02
OEU17392.1	Putative glucose-6-phosphate dehydrogenase	207660	K00036	0.84	11.23	2.68E-02
OEU16003.1	porphobilinogen synthase	218256	K01698	-1.09	10.44	2.76E-02
OEU09987.1	hypothetical protein FRACYDRAFT_271162	271162	-	2.02	8.41	2.82E-02
OEU17697.1	argininosuccinate synthase	207847	K01940	-0.75	10.50	3.04E-02
OEU15128.1	acetate CoA ligase	239808	K01895	-1.45	9.46	3.04E-02
OEU18543.1	TPR-like protein	183685	K09553	-1.21	9.08	3.38E-02

OEU07841.1	serine hydroxymethyltransferase	277738	K00600	1.14	10.36	3.77E-02
OEU14774.1	Chloroa_b-bind-domain-containing protein	170761	-	0.51	10.53	3.93E-02
OEU21644.1	mitochondrial 2-oxoglutarate/malate carrier protein	291486	-	1.11	11.38	4.19E-02
OEU12438.1	phosphofructokinase	263182	K00895	0.91	9.40	4.29E-02
OEU15780.1	chlorophyll a/b-binding protein	170453	-	-1.08	8.82	4.50E-02
OEU21243.1	cell division protease ftsH 4	206298	K03798	-1.03	10.33	4.72E-02
OEU15135.1	3-phosphoshikimate 1-carboxyvinyltransferase	226008	K00800	-0.65	9.92	5.00E-02

Table S2.6: List of proteins differentially expressed after 24 hours of exposure to an elevated temperature treatment (12 °C) in *F. cylindrus.* This list was generated by a pairwise comparison between control cultures (cultured at 4 °C in B_{12} replete media) and cultures grown at 12 °C with B_{12} replete media. NCBI protein products, gene ID's and corresponding KEGG numbers are included. A negative fold change represents a protein that is downregulated in response to elevated temperatures.

Protein Product	Name	Gene ID	KO	log2 Fold Change	log2 mean spectral abundance	P-Value
OEU08040.1	hypothetical protein FRACYDRAFT_271832	271832	-	3.12	9.62	1.49E-05
OEU16390.1	ThiC	225659	K03147	-2.30	9.62	6.55E-05
OEU17510.1	60S ribosomal protein L24	268718	K02896	-1.81	9.74	1.18E-04
OEU23398.1	barren-domain-containing protein	233571	K06676	1.39	10.71	2.38E-04
OEU08856.1	GTP-binding protein EngA	196010	-	-1.91	9.09	2.41E-04
OEU12584.1	chromosome assembly protein	210755	K06674	1.50	9.95	5.88E-04
OEU08435.1	Flavocytochrome c	196661	-	1.45	9.81	8.51E-04
OEU15214.1	P-loop containing nucleoside triphosphate hydrolase protein	208780	-	-1.81	9.02	1.50E-03
OEU19288.1	hypothetical protein FRACYDRAFT_235337	235337	-	2.89	7.93	1.61E-03
OEU23066.1	P-loop containing nucleoside triphosphate hydrolase protein	205573	-	1.45	9.15	1.80E-03
OEU13881.1	hypothetical protein FRACYDRAFT_262424	262424	-	1.48	9.23	2.43E-03
OEU20131.1	hypothetical protein FRACYDRAFT_236198	236198	-	-2.35	8.96	2.78E-03
OEU17620.1	hypothetical protein FRACYDRAFT_275154	275154	-	-1.24	9.50	3.01E-03
OEU18398.1	DEAD-domain-containing protein	183391	K12823	-1.07	10.02	3.92E-03
OEU20259.1	hypothetical protein FRACYDRAFT_260278	260278	-	0.92	10.72	4.43E-03
OEU15576.1	protoporphyrin IX Mg-chelatase subunit D	170289	K03404	-0.95	10.36	4.61E-03
OEU15125.1	charged multivesicular body protein	169934	K12197	1.40	10.02	4.86E-03

OEU10171.1	hypothetical protein FRACYDRAFT_173335	173335	-	-0.67	10.87	5.10E-03
OEU16003.1	porphobilinogen synthase	218256	K01698	-1.50	10.44	7.23E-03
OEU17057.1	hypothetical protein FRACYDRAFT_239660	239660	-	1.47	8.64	8.38E-03
OEU13503.1	hypothetical protein FRACYDRAFT_241836	241836	-	1.19	10.12	1.00E-02
OEU20628.1	(E)-4-hydroxy-3-methylbut-2-enyl diphosphate synthase	259614	K03526	-0.80	10.08	1.20E-02
OEU20689.1	Ribonuc_red_lgC-domain-containing protein	205957	-	-1.11	9.27	1.33E-02
OEU07775.1	putative dehydroascorbate reductase	229440	-	-0.79	10.13	1.35E-02
OEU18066.1	protoporphyrin IX Mg-chelatase subunit H	261055	K03403	-1.49	8.69	1.53E-02
OEU21646.1	methionine sulfoxide reductase B	274188	-	-1.40	8.74	1.78E-02
OEU20813.1	putative GDP-mannose 4,6-dehydratase	206067	K01711	-1.46	8.65	1.95E-02
OEU08698.1	putative glutathione S-transferase	196320	K04097	1.05	9.21	2.13E-02
OEU12494.1	hypothetical protein FRACYDRAFT_191288, partial	191288	-	-0.68	11.37	2.15E-02
OEU17774.1	FAD-binding domain-containing protein	207885	-	0.97	9.40	2.28E-02
OEU13317.1	hypothetical protein FRACYDRAFT_241655	241655	-	-0.88	9.96	2.37E-02
OEU09370.1	WD40 repeat-like protein	228652	K14830	-0.78	10.27	2.46E-02
OEU17651.1	FAD-linked oxidoreductase	268766	K00318	-1.00	9.32	2.46E-02
OEU13382.1	hypothetical protein FRACYDRAFT_170947, partial	170947	-	-0.51	11.01	2.60E-02
OEU08538.1	hypothetical protein FRACYDRAFT_174052, partial	174052	K07905	1.50	9.70	2.97E-02
OEU17546.1	proteasome subunit alpha	275128	K02729	1.40	10.50	3.11E-02
OEU20754.1	P-type ATPase	206011	K14950	0.84	9.85	3.14E-02

OEU15601.1	WD40 repeat-like protein, partial	156423	K14556	-0.70	10.01	3.21E-02
OEU21863.1	peptidyl-prolyl cis-trans isomerase B	232008	-	0.83	9.38	3.38E-02
OEU08126.1	Carboxyl_trans-domain-containing protein, partial	145710	K11262	-0.48	11.36	3.52E-02
OEU22171.1	Band_7-domain-containing protein	205091	-	0.74	9.76	3.58E-02
OEU17563.1	hypothetical protein FRACYDRAFT_237983	237983	-	-0.86	9.30	3.83E-02
OEU20373.1	hypothetical protein FRACYDRAFT_236448	236448	-	-0.85	9.39	3.90E-02
OEU18937.1	uroporphyrinogen III decarboxylase	268500	K01599	-1.11	8.75	3.94E-02
OEU15135.1	3-phosphoshikimate 1-carboxyvinyltransferase	226008	K00800	-0.70	9.92	3.95E-02
OEU22102.1	hypothetical protein FRACYDRAFT_179260	179260	-	-0.69	10.00	4.08E-02
OEU18445.1	P-loop containing nucleoside triphosphate hydrolase protein, partial	182871	-	-0.88	9.28	4.38E-02
OEU20523.1	Aldo/keto reductase	180596	-	0.60	10.17	4.39E-02
OEU07292.1	hypothetical protein FRACYDRAFT_251075	251075	-	0.86	9.22	4.90E-02
OEU17472.1	hypothetical protein FRACYDRAFT_183826	183826	-	-0.56	10.25	4.94E-02

Table S2.7: List of proteins differentially expressed after 24 hours of exposure to both the elevated temperature treatment (12 °C) and B_{12} deprivation in *F. cylindrus.* This list was generated by a pairwise comparison between control cultures (cultured at 4 °C in B_{12} replete media) and cultures grown at 12 °C with B_{12} deplete media. NCBI protein products, gene ID's and corresponding KEGG numbers (KO) are included. A negative fold change represents a protein that is downregulated in response the stressors.

Protein Product	Name	Gene ID	KO	log_2 Fold Change	log_2 mean spectral abundance	P-Value
OEU08040.1	hypothetical protein FRACYDRAFT_271832	271832	-	3.50	9.62	2.70E-06
OEU11144.1	MetE	228154	K00549	4.97	11.13	7.17E-06
OEU08856.1	GTP-binding protein EngA	196010	-	-2.67	9.09	2.81E-05
OEU17620.1	hypothetical protein FRACYDRAFT_275154	275154	-	-2.06	9.50	5.12E-05
OEU17510.1	60S ribosomal protein L24	268718	K02896	-1.83	9.74	7.77E-05
OEU15214.1	P-loop containing nucleoside triphosphate hydrolase protein	208780	-	-3.04	9.02	9.53E-05
OEU10171.1	hypothetical protein FRACYDRAFT_173335	173335	-	-1.17	10.87	1.17E-04
OEU14436.1	C2-domain-containing protein	269584	-	1.32	10.61	1.76E-04
OEU13762.1	phosphoglycerate kinase precursor	209933	K00927	-1.22	10.73	1.80E-04
OEU22265.1	hypothetical protein FRACYDRAFT_258994	258994	K01624	1.48	10.27	3.45E-04
OEU12251.1	cytochrome b5	172305	K23490	2.23	8.36	4.30E-04
OEU17472.1	hypothetical protein FRACYDRAFT_183826	183826	-	-1.31	10.25	4.30E-04
OEU16390.1	ThiC	225659	K03147	-1.51	9.62	4.81E-04
OEU19455.1	ubiquitin-conjugating enzyme	167665	K06689	1.82	8.69	5.33E-04
OEU20628.1	(E)-4-hydroxy-3-methylbut-2-enyl diphosphate synthase	259614	K03526	-1.16	10.08	5.51E-04
OEU17563.1	hypothetical protein FRACYDRAFT_237983	237983	-	-1.52	9.30	5.92E-04
OEU11214.1	CBA1	246327	-	2.66	9.37	6.78E-04
OEU18387.1	P-ATPase family transporter: zinc/lead/cadmium/mercury ion	168079	K01534	1.40	9.77	8.00E-04

OEU08126.1	Carboxyl_trans-domain-containing protein, partial	145710	K11262	-0.96	11.36	8.20E-04
OEU13881.1	hypothetical protein FRACYDRAFT_262424	262424	-	1.62	9.23	8.43E-04
OEU20381.1	5-oxoprolinase	260195	K01469	1.73	10.35	1.02E-03
OEU12584.1	chromosome assembly protein	210755	K06674	1.36	9.95	1.10E-03
OEU17661.1	hypothetical protein FRACYDRAFT_268767	268767	-	-1.05	11.19	1.14E-03
OEU10229.1	protoporphyrin IX Mg-chelatase subunit D	247844	-	1.99	8.56	1.33E-03
OEU18937.1	uroporphyrinogen III decarboxylase	268500	K01599	-2.03	8.75	1.37E-03
1773362865	ATP synthase CF1 epsilon subunit (chloroplast) [Fragilariopsis cylindrus]	-	-	1.29	9.30	1.46E-03
OEU21928.1	protein serine/threonine phosphatase 2C	204950	K14803	-0.82	11.10	1.48E-03
OEU18940.1	hypothetical protein FRACYDRAFT_207292	207292	K00326	1.06	9.86	1.61E-03
OEU20373.1	hypothetical protein FRACYDRAFT_236448	236448	-	-1.61	9.39	1.69E-03
OEU19890.1	hypothetical protein FRACYDRAFT_206674	206674	-	1.16	9.37	1.70E-03
OEU18901.1	acyltransferase, partial	158788	K00630	-1.01	10.85	1.74E-03
OEU20259.1	hypothetical protein FRACYDRAFT_260278	260278	-	1.03	10.72	1.79E-03
OEU21739.1	ATP-dependent hsl protease ATP-binding subunit hslU, partial	158033	K03667	1.90	8.34	1.96E-03
OEU14527.1	hypothetical protein FRACYDRAFT_218563	218563	K02266	0.84	10.48	2.14E-03
OEU16276.1	glutamine-hydrolyzing asparagine synthase	208140	K01953	-0.83	12.22	2.17E-03
OEU17774.1	FAD-binding domain-containing protein	207885	-	1.19	9.40	2.24E-03
OEU18445.1	P-loop containing nucleoside triphosphate	182871	-	-1.38	9.28	2.36E-03

	hydrolase protein, partial					
OEU09292.1	chloroplast sedoheptulose-1,7-bisphosphatase	195411	K01100	-1.02	10.06	2.51E-03
OEU14387.1	hypothetical protein FRACYDRAFT_275849	275849	K08994	1.04	10.24	2.57E-03
OEU15875.1	hypothetical protein FRACYDRAFT_240571	240571	-	-0.88	10.89	2.69E-03
OEU10445.1	putative rhodopsin	287459	-	1.14	9.84	2.85E-03
OEU08420.1	hypothetical protein FRACYDRAFT_264537	264537	-	-1.21	9.66	3.04E-03
OEU15601.1	WD40 repeat-like protein, partial	156423	K14556	-1.11	10.01	3.09E-03
OEU07775.1	putative dehydroascorbate reductase	229440	-	-1.02	10.13	3.13E-03
OEU22263.1	RNA-binding domain-containing protein, partial	155400	-	-2.07	9.25	3.64E-03
OEU18828.1	stabilizer of iron transporter SufD	268455	-	-1.18	9.58	3.65E-03
OEU17803.1	fucoxanthin chlorophyll a/c protein	260998	-	-0.73	10.83	3.78E-03
OEU20728.1	hypothetical protein FRACYDRAFT_234360	234360	-	-0.83	11.29	3.85E-03
OEU20070.1	putative acetyl-CoA acyltransferase	268162	K07508	1.53	9.80	3.96E-03
OEU19288.1	hypothetical protein FRACYDRAFT_235337	235337	-	2.64	7.93	4.10E-03
OEU21654.1	putative aureochrome	205854	-	-0.76	11.22	4.40E-03
OEU20818.1	HopJ-domain-containing protein	259707	-	-0.99	9.91	4.60E-03
OEU15771.1	hypothetical protein FRACYDRAFT_209201	209201	-	1.07	9.42	4.98E-03
OEU14002.1	hypothetical protein FRACYDRAFT_171314	171314	-	1.69	8.45	5.03E-03
OEU20557.1	hypothetical protein FRACYDRAFT_234188	234188	K15128	-0.85	10.56	5.06E-03
OEU18602.1	hypothetical protein FRACYDRAFT_268368	268368	-	-1.12	9.86	5.06E-03
OEU15576.1	protoporphyrin IX Mg-chelatase subunit D	170289	K03404	-0.90	10.36	5.20E-03

OEU07355.1	hypothetical protein FRACYDRAFT_197708	197708	-	-0.85	10.76	5.22E-03
OEU08435.1	Flavocytochrome c	196661	-	1.11	9.81	5.41E-03
OEU20496.1	hypothetical protein FRACYDRAFT_216497	216497	K17278	1.45	8.60	5.62E-03
OEU19598.1	hypothetical protein FRACYDRAFT_235658	235658	-	1.52	9.46	5.65E-03
OEU19234.1	cobW-domain-containing protein	274493	-	1.62	11.25	5.65E-03
OEU16551.1	fucoxanthin chlorophyll a/c protein	208340	-	1.95	10.12	5.68E-03
OEU13767.1	Coatomer, alpha subunit	226883	K05236	-0.77	10.50	5.80E-03
OEU21652.1	uroporphyrinogen III decarboxylase, partial	216482	K01599	-1.07	9.85	6.23E-03
OEU10218.1	FAS1 domain-containing protein, partial	194372	-	1.30	8.70	6.39E-03
OEU08930.1	hypothetical protein FRACYDRAFT_249273	249273	-	-1.12	9.49	6.43E-03
OEU15320.1	ThiJ/PfpI domain-containing protein	269315	-	1.62	8.29	6.54E-03
OEU22272.1	V-type ATPase 16 kDa proteolipid subunit	205176	K02155	1.41	8.76	6.55E-03
OEU16201.1	hypothetical protein FRACYDRAFT_225570	225570	K15979	-1.37	9.43	6.65E-03
OEU21646.1	methionine sulfoxide reductase B	274188	-	-1.55	8.74	6.98E-03
OEU16091.1	calcium ATPase, partial	136216	K01535	0.94	9.62	7.29E-03
OEU13387.1	ARM repeat-containing protein	170952	K20221	-0.92	9.82	7.41E-03
OEU22110.1	putative methyltransferase	178178	K07755	1.12	9.20	7.44E-03
OEU18800.1	T-complex protein 1	237081	K09496	-1.30	9.48	7.56E-03
OEU09370.1	WD40 repeat-like protein	228652	K14830	-0.97	10.27	7.89E-03
OEU20434.1	RraA-like protein	216468	-	0.85	10.02	8.02E-03
OEU09038.1	hypothetical protein FRACYDRAFT_271650	271650	-	-0.74	10.58	8.29E-03
OEU06473.1	hypothetical protein FRACYDRAFT_265856	265856	-	1.16	10.73	8.35E-03
OEU15467.1	Triosephosphate isomerase	269372	-	-0.66	12.23	8.68E-03

OEU17549.1	Adaptor protein complex AP-1 gamma subunit	225310	K12391	0.99	9.27	8.74E-03
OEU11139.1	putative 6-phosphogluconate dehydrogenase	211512	K00033	1.45	10.24	8.74E-03
OEU09673.1	Trypanothione reductase	228584	-	-1.22	9.32	8.76E-03
OEU22140.1	Sm-like ribonucleo protein, partial	215974	K11086	-1.09	10.36	8.98E-03
OEU12494.1	hypothetical protein FRACYDRAFT_191288, partial	191288	-	-0.80	11.37	9.17E-03
OEU18900.1	hypothetical protein FRACYDRAFT_182579	182579	K14617	0.96	9.52	9.35E-03
OEU20131.1	hypothetical protein FRACYDRAFT_236198	236198	-	-1.55	8.96	1.02E-02
OEU14823.1	extrinsic protein in photosystem II	269688	-	-0.91	10.85	1.08E-02
OEU19975.1	protein prenylyltransferase	260174	K14050	-1.17	9.31	1.08E-02
OEU23729.1	4-Diphosphocytidyl-2-C-methyl-D-erythritol synthase	205256	K00991	-0.77	10.13	1.09E-02
OEU18748.1	hypothetical protein FRACYDRAFT_182880	182880	-	5.08	13.69	1.15E-02
OEU11299.1	hypothetical protein FRACYDRAFT_270952	270952	-	-0.98	9.61	1.15E-02
OEU15300.1	kinase domain-containing protein	269308	K08794	0.73	10.26	1.16E-02
OEU11757.1	hypothetical protein FRACYDRAFT_263309	263309	-	1.23	8.71	1.19E-02
OEU17909.1	hypothetical protein FRACYDRAFT_238339	238339	-	1.51	10.31	1.19E-02
OEU17651.1	FAD-linked oxidoreductase	268766	K00318	-1.08	9.32	1.19E-02
OEU15623.1	Peptidase_M16-domain-containing protein	209078	K01408	-1.32	9.42	1.19E-02
OEU20689.1	Ribonuc_red_lgC-domain-containing protein	205957	-	-1.05	9.27	1.20E-02
OEU12919.1	hypothetical protein FRACYDRAFT_263086	263086	K00366	-1.04	9.41	1.20E-02
OEU10909.1	hypothetical protein FRACYDRAFT_246784	246784	-	-0.81	10.24	1.22E-02

OEU20087.1	hypothetical protein FRACYDRAFT_268171, partial	268171	-	-0.84	10.29	1.26E-02
OEU11984.1	casein kinase I delta	211208	K08959	-1.49	9.26	1.27E-02
OEU16010.1	pyruvate carboxylase	186955	K01958	-1.08	9.47	1.28E-02
OEU18398.1	DEAD-domain-containing protein	183391	K12823	-0.80	10.02	1.35E-02
OEU18742.1	hypothetical protein FRACYDRAFT_217304	217304	-	1.06	9.06	1.35E-02
OEU20457.1	NAD(P)-binding protein	267643	K00344	-2.09	9.57	1.38E-02
OEU21875.1	hypothetical protein FRACYDRAFT_232020	232020	-	1.70	7.94	1.42E-02
OEU11005.1	Band_7-domain-containing protein	270904	-	1.03	12.01	1.46E-02
OEU20597.1	eukaryotic translation initiation factor 2 subunit alpha	267694	K03237	1.32	8.97	1.47E-02
OEU16607.1	zeaxanthin epoxidase	208380	K09838	-0.74	11.00	1.52E-02
OEU16909.1	hypothetical protein FRACYDRAFT_156996, partial	156996	-	-1.17	9.33	1.53E-02
1773362895	Mg-protoporphyrin IX chelatase (chloroplast) [Fragilariopsis cylindrus]	-	-	-0.88	10.36	1.53E-02
OEU18675.1	hypothetical protein FRACYDRAFT_236954	236954	-	-0.86	10.26	1.53E-02
OEU21733.1	hypothetical protein FRACYDRAFT_231878	231878	K14721	-0.66	10.72	1.59E-02
OEU15012.1	ribulose-1,5-bisphosphate carboxylase-like protein	269187	-	-0.78	10.11	1.59E-02
OEU15501.1	ribosomal protein L13	170235	K02872	-0.79	9.98	1.60E-02
OEU18465.1	actin depolymerazing factor	206967	K05765	0.83	9.64	1.67E-02
OEU21653.1	geranylgeranyl reductase	267781	K10960	-1.03	9.66	1.68E-02
OEU15628.1	putative nucleoside-diphosphate kinase	269435	K00940	-1.02	9.42	1.70E-02
OEU07664.1	FAS1 domain-containing protein	250682	-	-0.86	9.81	1.70E-02
OEU17742.1	rieske iron-sulfur protein of cytochrome B6/F complex	268792	K02636	1.48	8.83	1.75E-02
OEU20988.1	transaldolase	216674	-	-1.70	8.45	1.76E-02

OEU18733.1	hypothetical protein FRACYDRAFT_268420	268420	K11275	1.22	8.80	1.78E-02
OEU18802.1	3HCDH_N-domain-containing protein	207194	-	-1.41	8.81	1.78E-02
OEU13018.1	GrpE nucleotide exchange factor	219337	K03687	1.06	9.70	2.03E-02
OEU10937.1	hypothetical protein FRACYDRAFT_193278	193278	-	-0.64	10.60	2.07E-02
OEU14763.1	V-ATPase subunit A4	170746	K02145	0.57	10.44	2.12E-02
OEU18180.1	putative UDP-glucose-4-epimerase	291631	K01784	-0.72	10.15	2.16E-02
OEU13634.1	cyclophilin-like protein	226832	-	0.95	9.91	2.18E-02
OEU16045.1	serine-tRNA ligase	185157	K01875	1.44	10.16	2.20E-02
OEU07882.1	putative UDP-glucose 6-dehydrogenase	271881	K00012	-0.91	9.54	2.32E-02
OEU12635.1	CKS-domain-containing protein	191189	K02219	-0.71	11.19	2.33E-02
OEU14710.1	TPT-domain-containing protein	188055	-	0.55	10.62	2.33E-02
OEU18421.1	hypothetical protein FRACYDRAFT_260383	260383	-	-1.43	9.17	2.39E-02
OEU16221.1	hydroxymethylglutaryl-CoA reductase	268919	K00021	-0.89	9.47	2.44E-02
OEU21853.1	hypothetical protein FRACYDRAFT_258825	258825	-	-0.81	9.80	2.45E-02
OEU16482.1	prohibitin 2	208283	K17081	-1.10	10.41	2.47E-02
OEU15673.1	ribosomal protein S19	261793	K02974	-1.13	9.02	2.54E-02
OEU22910.1	SpoU_methylase-domain-containing protein	178319	K15507	-0.83	10.58	2.55E-02
OEU11877.1	CONSTANS interacting protein 3	172528	-	0.74	9.81	2.58E-02
OEU23312.1	hypothetical protein FRACYDRAFT_267500, partial	267500	-	1.46	8.13	2.58E-02
OEU21268.1	hypothetical protein FRACYDRAFT_234895	234895	-	-1.17	8.95	2.59E-02
OEU22415.1	long-chain acyl-CoA synthetase	259065	-	0.80	9.70	2.60E-02
OEU13317.1	hypothetical protein FRACYDRAFT_241655	241655	-	-0.82	9.96	2.67E-02
OEU18400.1	SOUL-domain-containing protein	168094	-	-1.00	10.08	2.68E-02
OEU13347.1	HEAT repeat-containing protein	209669	K12828	0.80	9.90	2.75E-02

OEU15709.1	Ribokinase-like protein, partial	159706	K00852	-0.56	10.71	2.77E-02
OEU22459.1	chloroplast ferredoxin dependent NADH oxireductase	205285	K02641	-0.64	13.07	2.77E-02
OEU13382.1	hypothetical protein FRACYDRAFT_170947, partial	170947	-	-0.50	11.01	2.77E-02
OEU14218.1	hypothetical protein FRACYDRAFT_261913	261913	-	-0.79	9.74	2.83E-02
OEU15063.1	hypothetical protein FRACYDRAFT_275536	275536	K11275	1.20	9.15	2.86E-02
1783488216	hypothetical protein (chloroplast) [Fragilariopsis cylindrus]	-	-	0.99	9.02	2.87E-02
OEU14547.1	NAD(P)-binding protein, partial	141982	-	1.21	9.09	2.92E-02
OEU14125.1	hypothetical protein FRACYDRAFT_189149	189149	-	-0.90	9.35	2.92E-02
OEU18685.1	HAD-superfamily hydrolase	168304	-	-1.06	10.98	2.92E-02
OEU10673.1	Phosphoadenosine phosphosulfate reductase	211685	-	-0.91	9.40	2.93E-02
OEU09587.1	RecF/RecN/SMC protein	212269	K06636	-1.07	9.56	2.99E-02
OEU14009.1	hypothetical protein FRACYDRAFT_262468	262468	-	1.29	8.47	3.00E-02
OEU16586.1	protein serine/threonine phosphatase 2C	185298	K04461	1.01	8.83	3.05E-02
OEU08001.1	hypothetical protein FRACYDRAFT_250221	250221	-	-0.84	10.56	3.09E-02
OEU09192.1	pyruvate kinase	228971	-	-0.74	10.02	3.11E-02
OEU09561.1	RPB5 subunit of DNA-directed RNA polymerase	271383	K03013	-0.57	10.58	3.19E-02
OEU17018.1	valyl-tRNA synthetase	225934	K01873	-0.85	10.35	3.19E-02
OEU18358.1	hypothetical protein FRACYDRAFT_260352	260352	-	0.86	10.98	3.20E-02
OEU14082.1	hypothetical protein FRACYDRAFT_210096	210096	K09560	0.75	9.57	3.30E-02
OEU17081.1	ferredoxin NADP reductase	208164	K02641	-0.54	10.71	3.30E-02

OEU18328.1	Peptidase_M16-domain-containing protein	206890	K01408	-0.69	11.02	3.34E-02
OEU16122.1	RecF/RecN/SMC protein	208027	-	-0.93	9.75	3.36E-02
OEU16565.1	hypothetical protein FRACYDRAFT_239160	239160	-	-0.96	9.36	3.41E-02
OEU17546.1	proteasome subunit alpha	275128	K02729	1.35	10.50	3.41E-02
OEU22012.1	hypothetical protein FRACYDRAFT_258886	258886	-	-1.13	8.95	3.44E-02
OEU21377.1	hypothetical protein FRACYDRAFT_259880	259880	-	1.17	9.04	3.48E-02
OEU07692.1	hypothetical protein FRACYDRAFT_271909	271909	-	1.16	9.80	3.57E-02
OEU22606.1	S1-domain-containing protein	267338	-	-0.82	9.79	3.59E-02
OEU08045.1	hypothetical protein FRACYDRAFT_271833	271833	-	0.42	11.30	3.69E-02
OEU15101.1	phosphoglycerate kinase precursor	208673	K00927	-0.85	9.54	3.70E-02
OEU13681.1	vacuolar ATP synthase subunit D 1, partial	161225	K02149	1.20	8.39	3.76E-02
OEU19363.1	hypothetical protein FRACYDRAFT_268006	268006	-	-0.80	10.13	3.77E-02
OEU13365.1	hypothetical protein FRACYDRAFT_269789	269789	-	1.36	8.14	3.81E-02
OEU15722.1	ARM repeat-containing protein	269467	K02144	1.27	8.30	3.90E-02
OEU16192.1	hypothetical protein FRACYDRAFT_169281	169281	-	-1.09	9.44	4.03E-02
OEU19684.1	tRNA-synt_2c-domain-containing protein	206558	K01872	-0.58	10.17	4.04E-02
OEU07887.1	RecF/RecN/SMC protein	212991	-	0.96	9.79	4.05E-02
OEU13605.1	hypothetical protein FRACYDRAFT_269879	269879	-	-0.88	9.87	4.11E-02
OEU16561.1	large ribosomal subunit L27	269038	K02901	-0.77	9.65	4.15E-02
OEU09468.1	ARM repeat-containing protein	271348	-	0.95	8.81	4.18E-02
OEU21089.1	fucoxanthin chlorophyll a/c protein	206215	-	-0.84	11.09	4.21E-02

OEU13453.1	2-oxoacid_dh-domain-containing protein	170993	K00627	0.52	12.62	4.25E-02
OEU17497.1	ribosomal protein L2	268713	K02938	-0.97	9.49	4.29E-02
OEU08344.1	carbamyl phosphate synthetase	264682	-	-1.54	9.08	4.36E-02
OEU19211.1	1-deoxy-D-xylulose 5-phosphate synthase	206899	K01662	-1.18	8.65	4.67E-02
OEU11855.1	phosphoglycerate mutase	211179	K01834	0.97	9.25	4.75E-02
OEU17951.1	hypothetical protein FRACYDRAFT_238382	238382	-	1.09	8.59	4.84E-02
OEU21292.1	hypothetical protein FRACYDRAFT_259855	259855	-	2.12	10.55	4.90E-02
OEU15228.1	aminotransferase, classes I and II superfamily	226057	-	-0.78	9.52	4.91E-02
OEU10013.1	hypothetical protein FRACYDRAFT_271172, partial	271172	-	-0.44	10.98	4.97E-02
OEU17572.1	Topoisom_I_N-domain-containing protein	225326	K03163	-0.53	10.74	5.00E-02

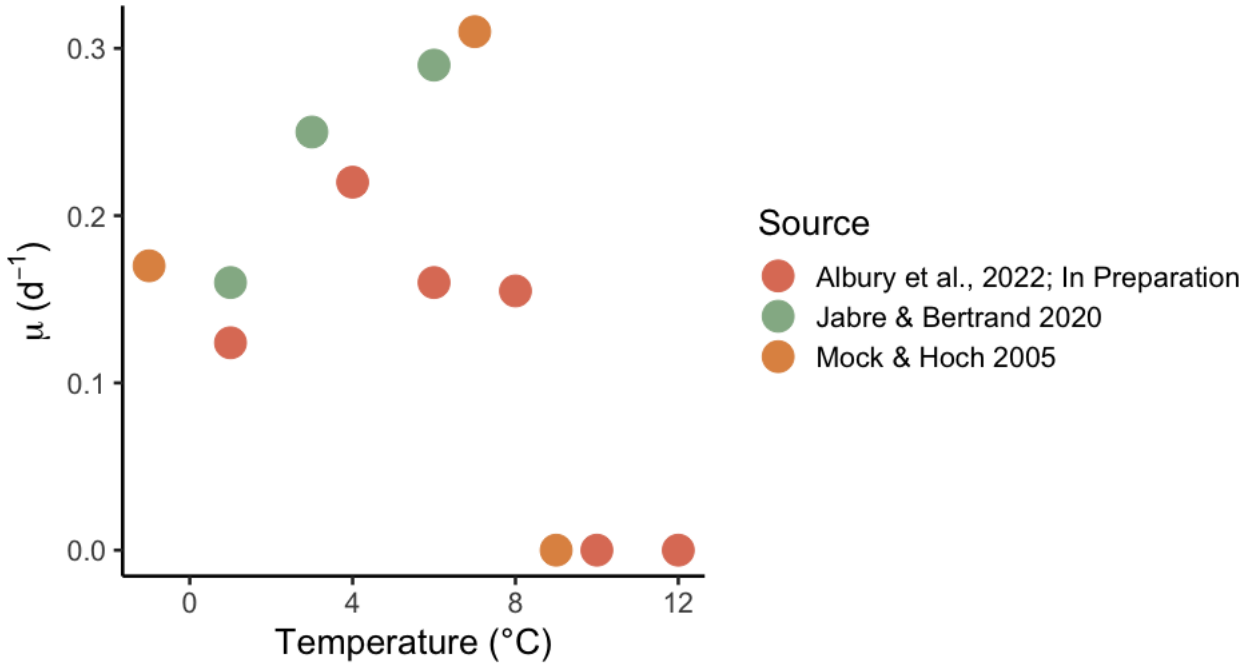

Figure S3.1 A comparison of growth rates (μ; d-1) between preliminary experiments conducted for this dissertation and other published values.

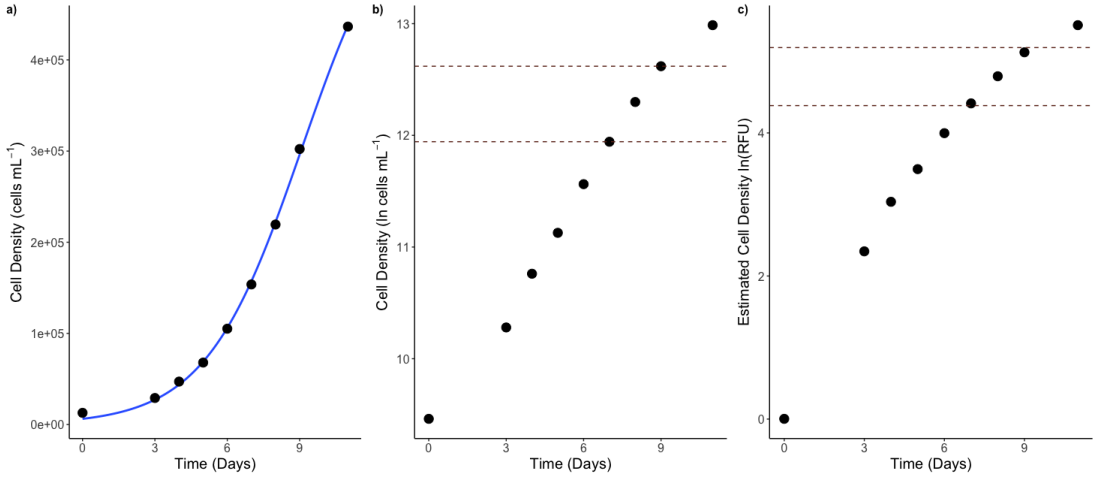

Figure S3.2: Data used to determine cell densities corresponding to late exponential growth phase in *F. cylindrus* cultures grown at 6 °C. Dotted lines correspond to exponential growth. Data collected by Loay Jabre.

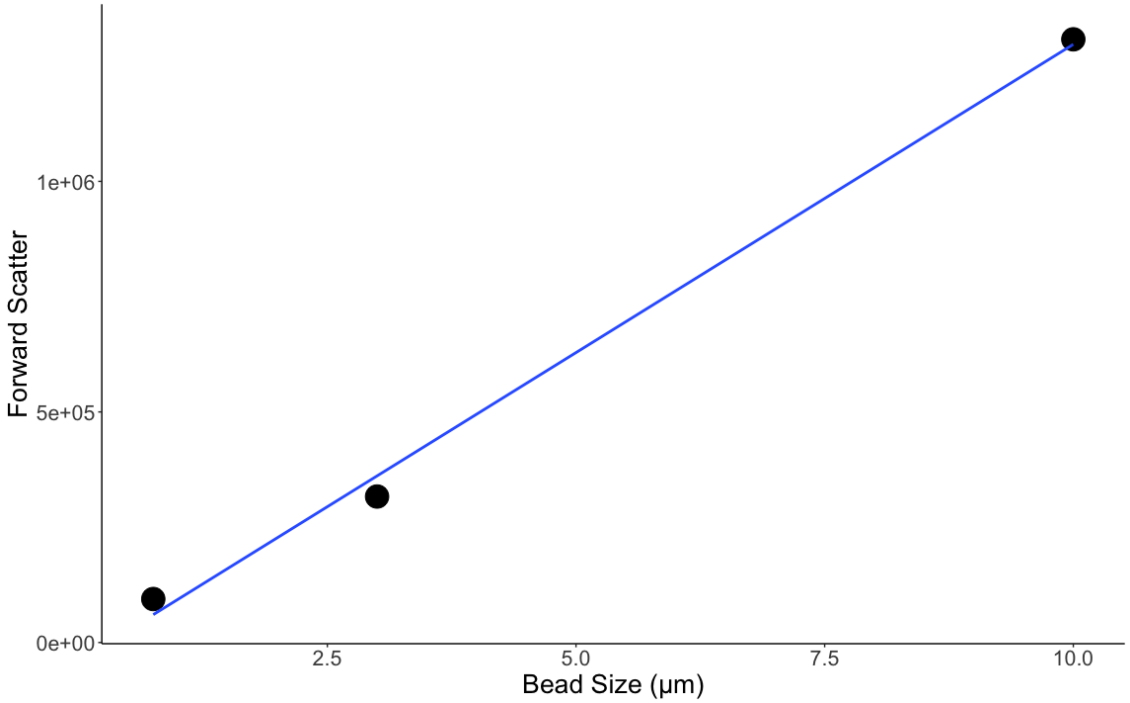

Figure S3.3: Calibration curve for cell size estimation in *F. cylindrus* cultures grown at 6 °C. $R^2 = 0.9961$. Forward scatter = $6x10^{-6}$(bead size) + 0.3145. Data adapted from Jabre and Bertrand 2020.

Table S3.1: A list of monitored metabolite transitions, with precursor and product mass over charge (M/Z), collision energy (volts), and retention time (RT; minutes)

Molecule Name	Precursor M/Z	Product M/Z	Collison Energy (V)	RT (min.)
Heavy B1	268.1	147.1	12.2	2.1
Heavy B1	268.1	122.1	12.8	2.1
Heavy B1	268.1	116.1	40	2.1
Heavy B1	268.1	42.354	37.3	2.1
Heavy B2	383.2	249.1	21.1	5.7
Heavy B2	383.2	204.1	28.3	5.7
Heavy B2	383.2	202.1	35.3	5.7
Heavy B2	383.2	175.1	35.5	5.7
Heavy B12-CN	681.9	366.1	23.7	5.5
Heavy B12-CN	681.9	154.1	38	5.5
B1	265.16	144.2	15.8	2.1
B1	265.16	122.27	16.2	2.1
B2	377.183	243.054	24	5.7
B2	377.183	172.054	37.6	5.7
Homarine	138.122	94.054	20.3	2.1-2.4
Homarine	138.122	78.054	22.8	2.1-2.4
Homarine	138.122	51.125	35.4	2.1-2.4
SAH	386.183	250.054	13.7	2.6
SAH	386.183	136.054	22	2.6
SAH	386.183	88.071	38.1	2.6
SAM	399.209	298.054	13.5	2.1
SAM	399.209	250.04	16.1	2.1
SAM	399.209	136.111	28.3	2.1
B12-OH	665	359.1	24.4	4.2
B12-OH	665	147.1	37.4	4.2
B12-CN	678.4	359.1	22.7	5.5
B12-CN	678.4	147.1	37.8	5.5
B12-Ado	790.9	359.1	29.7	5.2
B12-Ado	790.9	147.1	43.3	5.2
B12-Me	673.5	359.1	26	4.2
B12-Me	673.5	147.1	40.8	4.2
Proline	116.2	70.1	16	5.5
Proline	116.2	43.3		5.5
GBT	118.4	58.1	23	2.1-2.2
GBT	118.4	42.2		2.1-2.2
B3	123.1	80.1	21.3	2.1
B3	123.1	53.1		2.1
HMP	140.1	122.2	12.3	2.1
HMP	140.1	81.3	19.5	2.1
HET	144.1	113.2	24	2.8
HET	144.1	112.2	32	2.8
cHET	188.1	170.1	14.6	3.9
cHET	188.1	140.2	21.1	3.9
B5	220.1	184	13.5	1.2
B5	220.1	90		
B7	245.1	227.1	13.2	5.6
Heavy B7	249.1	231.1	13.2	5.6
B9	295	120		2.6
Glutathione	308.091	162		2.6
TMP	345.2	122.1		2.1

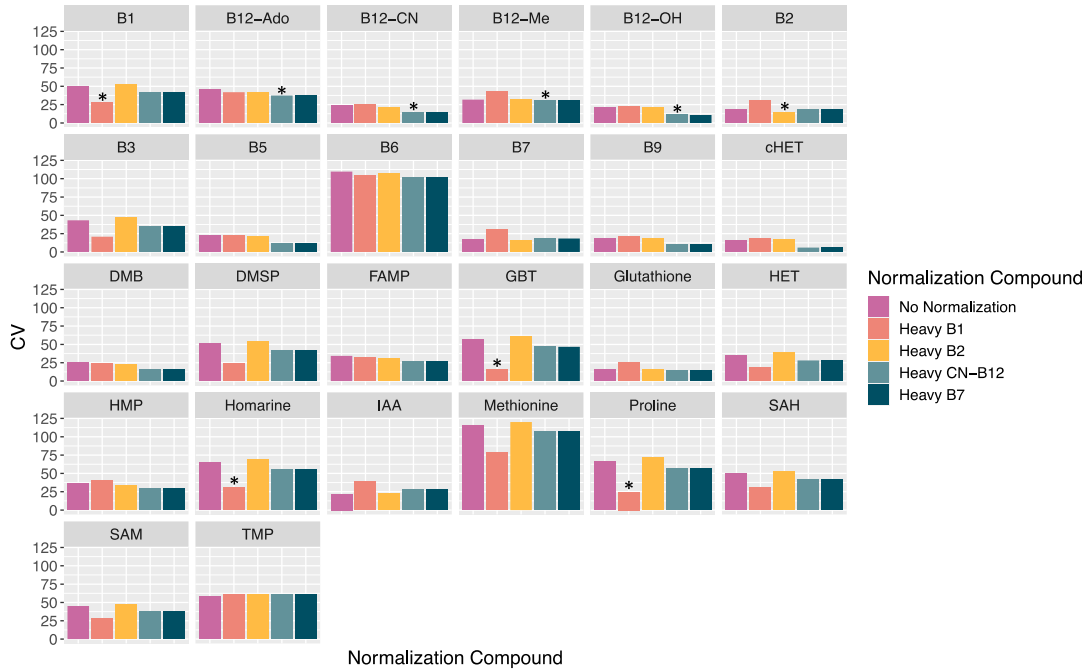

Figure S3.4: The effects of different normalizations on the coefficient of variation (CV) among quality control (QC) samples injected periodically during the metabolite analysis run. Normalizations which reduced QC CV by more than 10% were chosen as the best matched internal standard (BMIS) for that compound. The chosen BMIS is marked for each compound with a star. If no star is included, the compounds was not normalized to a BMIS.

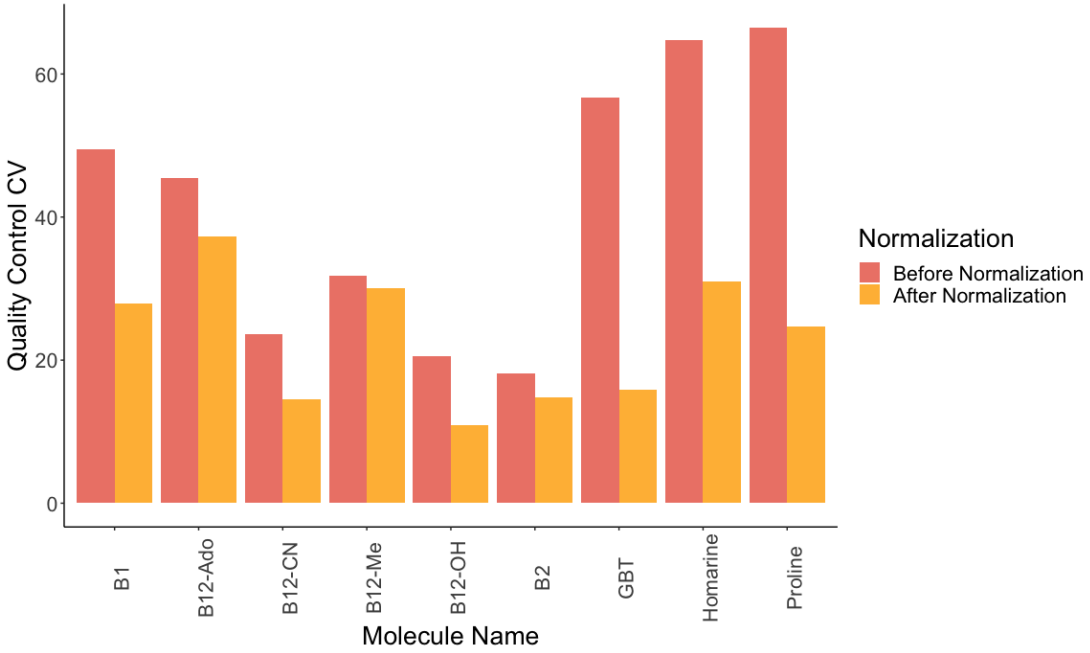

Figure S3.5: The effects of chosen normalizations with BMIS (best matched internal standard) on the coefficient of variation among QC (quality control) samples injected periodically between samples during the metabolite analysis run.

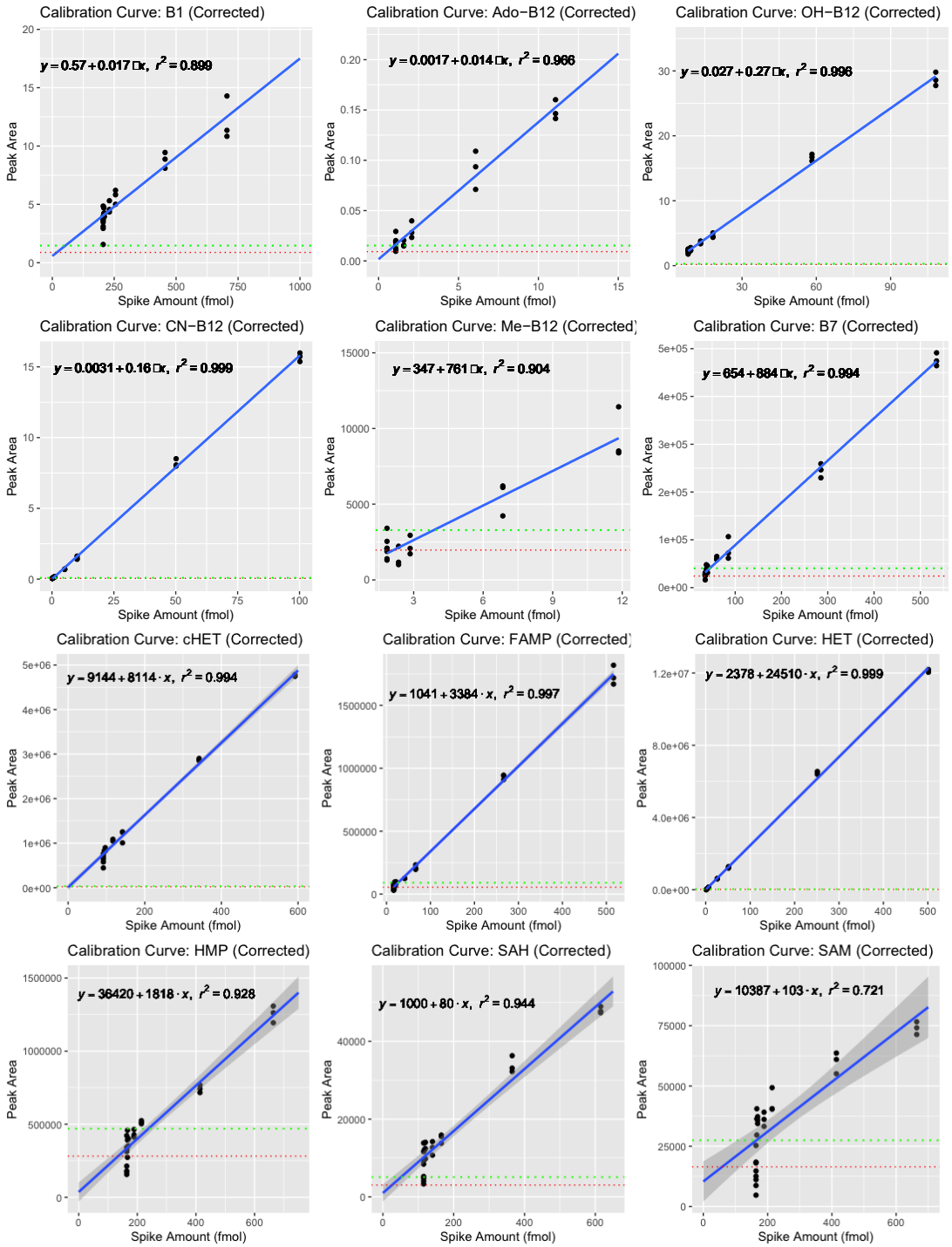

Figure S3.6: Calibration curves used to quantify metabolites of interested in *F. cylindrus* cultures grown at 6 °C. Normalized peak area by spike amount after corrections that estimate the amount of an endogenous metabolite in the QC itself. The Limit of Detection (LOD; 3 x time standard deviation of the QC with no authentic standard added) and Limit of Quantification (LOQ; 5 x time standard deviation of the QC with no authentic standard added) are denoted by a red and green dotted line, respectively for each metabolite of interest. The regression used to quantify each metabolite of interest is annotated, along with an R^2 value in black.

Table S3.2: Fold changes of metabolites that were above detection limit in B_{12} replete and deplete cultures of *F. cylindrus*. For compounds with a calibration curve, biological replicates were considered candidates for absolute quantification if the mean of triplicate injections were above the LOQ (limit of quantification). If the mean of a biological replicate was not above the LOQ, but above the LOD (limit of detection), it is listed as detected in trace amounts. Units for compounds with absolute quantification, are given in Femtomoles cell^{-1}. For compounds without a calibration curve, units are Normalized Peak Area cell^{-1}. p-values are listed in the Significance column, with $p < 0.05$ = *; $p < 0.01$= **; and ns = no significance. Trace amounts of adenosylcobalamin were detected in one replicate of three B_{12} deplete cultures (Figure 6a). nd = not detected. Methionine, Homocystine, HET, Glutathionine, and TMP were below the detection limit. Trace amounts of HMP were only detected in B_{12} replete samples, but not B_{12} deprived samples.

Molecule Name	BMIS Used	Mean Value +B_{12}	Mean Value -B_{12}	Fold Change	Significance	Quantification Type
B1	Heavy B_1	3.54×10^{-3}	5.27×10^{-3}	-0.33	ns	Absolute
Ado-B_{12}	Heavy CN-B_{12}	9.32×10^{-6}	trace	-	-	Absolute
Me-B_{12}	Heavy CN-B_{12}	1.12×10^{-4}	nd	-	-	Absolute
OH-B_{12}	Heavy CN-B_{12}	1.79×10^{-4}	nd	-	-	Absolute
B_2	none	0.72	0.96	-0.25	ns	Relative
B_3	none	10.78	14.74	-0.27	ns	Relative
B_7	none	2.00×10^{-3}	5.04×10^{-3}	-0.60	ns	Absolute
B_9	none	0.95	1.48	-0.36	ns	Relative
cHET	none	2.86×10^{-3}	3.98×10^{-3}	-0.28	*	Absolute
DMSP	none	24.99	35.36	-0.29	*	Relative
GBT	Heavy B_1	2.20×10^{-3}	1.15×10^{-3}	0.91	ns	Relative
Homarine	Heavy B_1	1.01×10^{-2}	1.81×10^{-2}	-0.44	ns	Relative
IAA	none	1.59	1.97	-0.19	ns	Relative
Proline	Heavy B_1	1.09×10^{-2}	1.93×10^{-2}	-0.43	ns	Relative
SAH	none	3.80×10^{-3}	1.73×10^{-2}	-0.78	ns	Absolute
SAM	none	7.38×10^{-3}	1.12×10^{-2}	-0.34	ns	Absolute

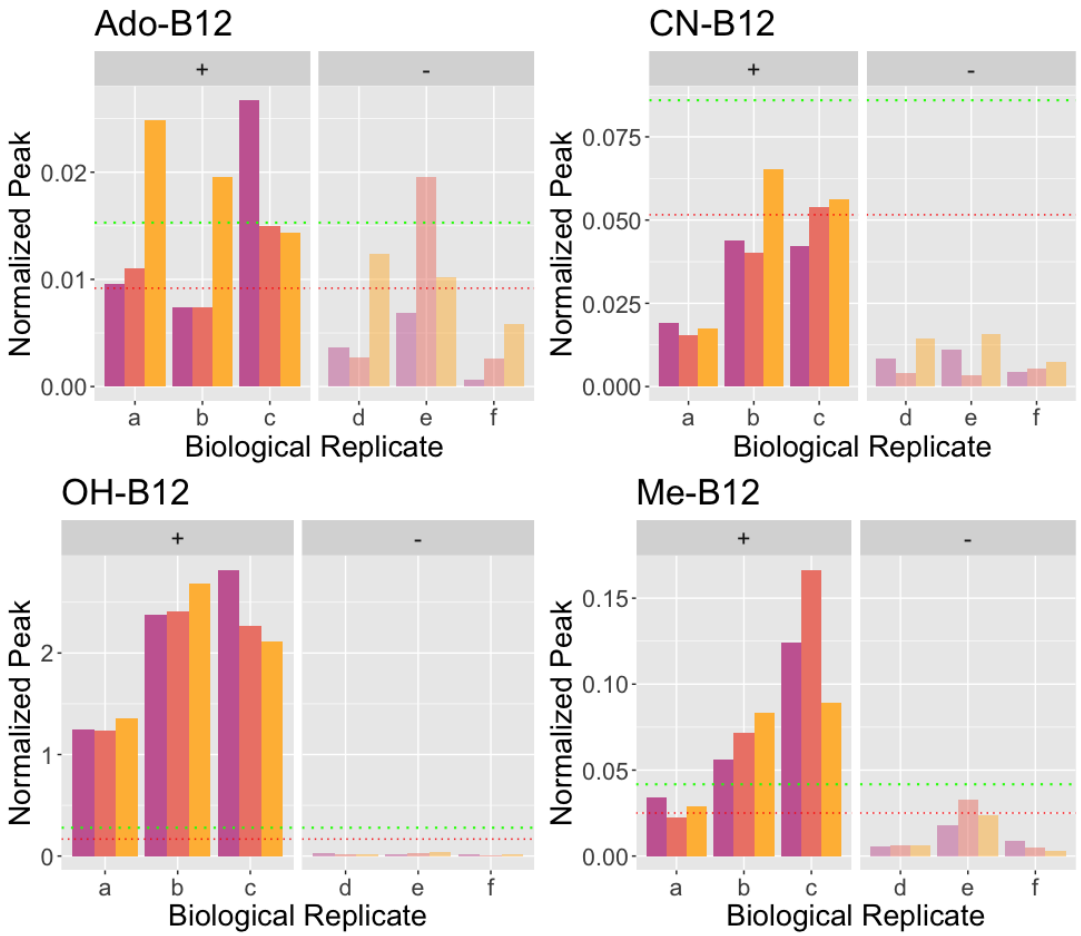

Figure S3.7: The normalized spectral abundance of cobalamin compounds in three technical replicates (purple, orange, yellow), of three biological replicates (a-f) per B_{12} treatment (+ or -) for *F. cylindrus* cultures grown with and without the addition of exogenous B_{12}. The red and green dotted lines represent LOD and LOQ respectively. Any sample with a signal above the LOD but below the LOQ is considered to have trace amounts of the compound. Samples with a mean signal below the LOD are considered "not detected" for the compound. The B_{12}-deplete sample e displayed trace amounts of adenosylcobalamin.